Ana Vanessa Fernandes Ferreira
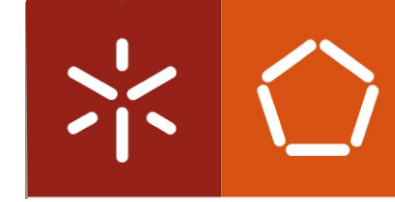
Incorporation of Elastase Inhibitor in Silk Fibroin Nanoparticles for Transdermal Delivery

Ana Vanessa Fernandes Ferreira

Incorporation of Elastase Inhibitor in Silk Fibroin Nanoparticles for Transdermal Delivery
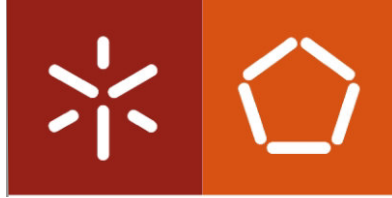
Uminho | 2013

Outubro de 2013

Universidade do Minho
Escola de Engenharia

Ana Vanessa Fernandes Ferreira

Incorporation of Elastase Inhibitor in Silk Fibroin Nanoparticles for Transdermal Delivery

Dissertação de Mestrado
Mestrado em Bioengenharia

Trabalho efetuado sob a orientação do
Professor Doutor Artur Cavaco Paulo
e coorientação de
Doutora Ana Sofia Lemos Machado Abreu

Outubro de 2013

DECLARAÇÃO

Nome: Ana Vanessa Fernandes Ferreira

Endereço eletrónico: pg18774@alunos.uminho.pt

Título da dissertação:

Incorporação de Inibidor de Elastase em Nanopartículas de Fibroína de Seda para Aplicações Transdérmicas

(Incorporation of Elastase Inhibitor in Silk Fibroin Nanoparticles for Transdermal Delivery)

Orientador (es): Professor Artur Cavaco Paulo e Ana Sofia Lemos Machado Abreu

Ano de conclusão: 2013

Designação do Mestrado: Mestrado em Bioengenharia

É AUTORIZADA A REPRODUÇÃO INTEGRAL DESTA TESE/TRABALHO APENAS PARA EFEITOS DE INVESTIGAÇÃO, MEDIANTE DECLARAÇÃO ESCRITA DO INTERESSADO, QUE A TAL SE COMPROMETE.

Universidade do Minho, 29/11/2013

Assinatura: _____

No amount of experimentation can ever prove me right; a single experiment can prove me wrong. - **Albert Einstein**
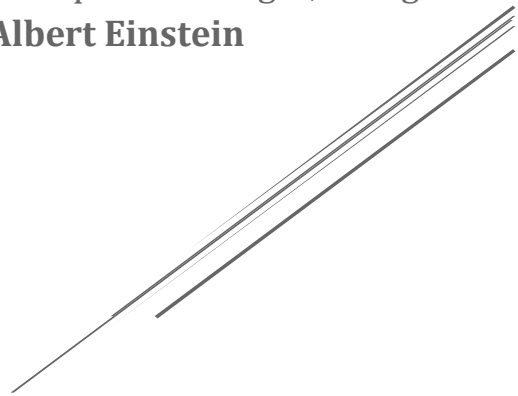
To my beloved family

Agradecimentos / Acknoledgments

Este trabalho não teria sido possível sem a colaboração das pessoas que me ajudaram a concretizá-lo, tanto a nível profissional como pessoal.

Agradeço ao meu orientador, Professor Dr. Artur Cavaco Paulo, pela oportunidade de ingressar no seu grupo de trabalho e neste projeto de investigação, por ter confiado e acreditado nas minhas capacidades e potencial, pelo seu apoio e incentivo nestes últimos dois anos.

À minha coorientadora, Dra. Ana Sofia Abreu, por todo o apoio constante e orientação no trabalho deste projeto, pelos ensinamentos, pela disponibilidade e ajuda. Obrigada pelos conselhos, conversas e partilha de experiências, que decerto me vão ajudar no futuro. Graças ao teu incentivo, estou mais segura do que quero para o meu futuro e fizeste-me entender o "mundo da investigação".

À Dra. Andreia Vasconcelos, pelos conselhos e apoio técnico da sua especialidade, pela valorização dos meus conhecimentos e orientação no início deste trabalho e ainda à Dra. Cláudia Botelho por todo o apoio, incentivo e ajuda na conclusão desta dissertação.

Não podia deixar de agradecer a todas as pessoas do grupo de trabalho de investigação de Bioprocessos do departamento de Engenharia Biológica que me receberam muito bem e sempre contribuíram para um excelente ambiente de trabalho, profissional e empenhado mas também divertido, permitindo-me sempre estar "à vontade" no laboratório.

A todos os meus amigos, pela amizade e apoio durante estes anos. Aos que conheci na licenciatura de Bioquímica e agora no mestrado de Bioengenharia, obrigada pelos momentos divertidos que me fizeram esquecer o trabalho por um pouco, mas também pelo apoio e ajuda, nas nossas sessões de estudo e trabalho.

Ao meu namorado, pelo seu apoio, carinho, amor, dedicação e compreensão. Obrigada por seres um bom ouvinte e aceitares-me tal como sou, sei que por vezes sou muito difícil de lidar mas agradeço que me chames à atenção e resmungues comigo sempre que preciso.

E por fim e muito importante, agradeço imenso à minha família, aos meus maravilhosos pais e à minha querida irmã, por todo o apoio, paciência e amor incondicional. Obrigada por me incentivarem a querer sempre mais e a dar sempre o meu melhor. Vocês são as pessoas mais importantes da minha vida, sempre estiveram do meu lado. Tudo o que que fiz, faço e farei foi graças a vocês, e por essa razão dedico-vos este trabalho.

To all, thank you very much!

Abstract

Human neutrophil elastase, as inflammatory response, has the capacity to degrade collagen and elastin component of extracellular matrix, being extensively involved in wrinkles formation induced by UV radiation damage. In order to develop a cosmetic anti-wrinkling emulsion, we incorporated a potent synthetic HNE inhibitor, sivelestat (IC_{50} = 44 nM, K_i = 0.2 μM), into biopolymeric nanoparticles prepared by high-energy emulsification methods. As nanomaterial was used *Bombyx mori* silk fibroin protein, an FDA approved natural biocompatible and biodegradable polymer.

Silk fibroin nanoparticles (SF-NPs) were produced by two high-energy emulsification methods, ultrasonication and high pressure homogenization (HPH), in oil-in-water (o/w) emulsions using as *n*-dodecane as oil phase. According to optimized results, best formulations were obtained for 10 g/L of SF at 20/80 of o/w ratio at 22 cycles of homogenization by double-stage HPH (APV-2000™). During the NPs production by HPH emulsification process, the secondary SF structure changed from random-coil conformation to a more stable structure, β-sheets.

Stabilizers effect was also studied, namely poloxamer 407, transcutol, tween 80 and sodium dodecyl sulfate (SDS), in which the results suggested that combination of transcutol and SDS would effectively stabilize the SF-NPs over time. To predict the sivelestat incorporation, orange IV was used as a model-drug, being this incorporated into SF-NPs at different concentrations. Release studies of orange IV were evaluated in absence and presence of 0.5 U/mL of HNE. The release of orange IV at 100 μM from SF-NPs (concentration considered as optimal) showed to be controlled at some extent, in which the drug transport mechanism showed to be anomalous (Fickian diffusion and polymer degradation/relaxation) and not affected by 0.5 U/mL of HNE enzyme.

Finally, the incorporation of 100 μM of sivelestat in SF-NPs performed with a formation and encapsulation efficiency of 99% and 50%, respectively, successfully inhibited the HNE enzyme, enhancing the potential of this drug delivery system for topical anti-wrinkling application.

Incorporação de Inibidor de Elastase em
Nanopartículas de Fibroína de Seda
para Aplicações Transdérmicas

Resumo

Elastase de Neutrófilos Humana, como resposta inflamatória, possui a capacidade de degradar os componentes da matriz extracelular, nomeadamente colagénio e elastina, estando envolvida na formação de rugas causadas pela radiação ultravioleta. De forma a desenvolver uma emulsão cosmética antirrugas, decidiu-se incorporar um potente inibidor sintético de elastase, sivelestat (IC_{50} = 44 nM, K_i = 0,2 μM), em nanopartículas biopoliméricas formadas por métodos de emulsificação de elevada energia. Como nanomaterial usou-se a proteína fibroína de seda extraída do bicho-da-seda *Bombyx mori*, que é um polímero natural biocompatível e biodegradável aprovado pela FDA.

As nanopartículas de fibroína de seda foram produzidas por dois métodos de emulsificação, ultrasonicação e homogeneização de elevada pressão, com emulsões óleo-em-água, tendo-se usado *n*-dodecano como fase oleosa. De acordo com os resultados otimizados, a melhor formulação foi obtida com 10 g/L de fibroína de seda numa razão óleo/água de 20/80 a 22 ciclos de homogeneização, através do método de duplo-sistema de homogeneização de elevada pressão (APV-2000™). Nestas condições, durante a produção de nanopartículas nestas condições, a estrutura secundária aleatória da proteína de fibroína de seda sofreu uma alteração conformacional para uma estrutura mais estável, em folhas βeta.

O efeito de estabilizadores na nanoemulsão foi também estudado, nomeadamente poloxamer 407, transcutol, tween 80 e dodecil sulfato de sódio, em que os resultados obtidos sugerem que a combinação de transcutol e dodecil sulfato de sódio estabilizaria eficientemente as nanopartículas de fibroína de seda ao longo do tempo. Para prever a incorporação de sivelestat, o corante orange IV foi utilizado como composto modelo, tendo sido incorporado nas nanopartículas de fibroína de seda a várias concentrações, e tendo-se estudado a sua libertação na ausência e na presença de elastase (0,5 U/mL). A libertação de orange IV das nanopartículas de fibroína de seda, numa concentração de 100 μM (concentração otimizada), exibiu um mecanismo de transporte controlado, tendo este sido definido como anómalo (difusão de Fickian e degradação/relaxamento do polímero) e não mostrou ser influenciada pela elastase (0,5 U/mL).

Finalmente, incorporação de 100 μM de sivelestat nas nanopartículas de fibroína de seda que indicou uma eficiência de formação e de encapsulação de 99% e 50%, respetivamente, inibiu a enzima elastase de forma eficaz, evidenciando o potencial deste nanosistema como cosmético antirrugas para aplicação transdérmica.

Key-words

Anti-wrinkling Agent; Drug Delivery System; Drug Release Profile; Emulsification; Fourier Transform Infrared spectroscopy; High-Pressure Homogenization; Human Neutrophil Elastase; Sivelestat; Kinetic and Inhibition studies; Nanoemulsions; Nanoparticles; Orange IV; Photoaging; Silk Fibroin; Transdermal Delivery; Ultrasonication; Wrinkle Formation.

Palavras-chave

Agente Antirrugas; Elastase de Neutrófilos Humana; Emulsificação; Ensaios de Libertação de Fármacos; Espectroscopia Infravermelha por transformada de Fourier; Fibroína de Seda; Formação de Rugas; Fotoenvelhecimento; Homogeneização de Elevada Pressão; Libertação transdérmica; Nanoemulsões; Nanopartículas; Orange IV; Sistemas de entrega e libertação de fármacos; Sivelestat; Estudos Cinéticos e de Inibição; Ultrasonicação.

Table of Contents

List of Symbols and Abbreviations

%	percent
μ	*Miu (greek symbol)*
3D	Three-dimensional
∞	mathematical representation of infinitive
et al.	*et alia* (and others)
i.e.	*id est* (that is)
per se	*per se* (by itself or in itself)
vs	*versus* (towards)
α	*Alpha (greek symbol)*
β	*Beta (greek symbol)*
ε	*Epsilon (greek symbol)*
ζ	*Zeta (greek symbol)*
η	*Eta (greek symbol)*
π	*Pi (greek symbol)*

A

a.a.	Amino acid
Ala	Alanine (a.a.)
ALI	Acute Lung Injury
ARDS	Acute Respiratory Distress Syndrome
Arg	Arginine (a.a.)
Asp	Aspartic acid (a.a.)
ATR	Attenuated Total Reflectance
α_1-PI	α_1-proteinase inhibitor
α_2-MG	α_2-macroglobulin

B

B. mori	*Bombyx mori*
BSA	Bovine Serum Albumin

C

°C	Centigrade, degree Celsius (temperature unit)
C	Carbon
C=O	Double covalent ligation between Carbon and Oxygen
Ca^{2+}	Calcium ion
$CaCl_2$	Calcium choloride
cm	Centimetre (distance/size unit, 10^{-2} meters)
cm^{-1}	1 per Centimetre (wavenumber measurement)
C-N	Single covalent ligation between Carbon and Nitrogen
Cys	Cysteine (a.a.)

D

D	Diffusion coefficient
d	Diameter of particles
Da	Dalton (SI atomic mass unit)
DD	Drug Delivery
DDS	Drug Delivery System
DLS	Dynamic Light Scattering

E

EC	Enzyme Commission number
ECM	Extra-cellular matrix
EI	Elastase Inhibitor

F

f(Ka)	Role of Henry
FDA	US Food and Drug Administration
FTIR	Fourier Transform Infrared

G

g	gram(s) (mass unit, 10^{-3} Kg)
g	Gravitational force (acceleration measurement)
g/L	gram(s) per litre (mass concentration unit)
Glu	Glutamic acid (a.a.)
Gly	Glycine (a.a.)

H

h	hour(s) (time unit, 60 s)
H	Hydrogen
HCl	Hydrochloric acid
HEPES	4-(2-hydroxyethyl)-1-piperazineethanesulfonic acid
HER2	Human Epithelial growth factor Receptor 2
His	Histidine (a.a.)
HLB	Hydrophilic Lipophilic Balance
HLE	Human Leukocyte Elastase
HNE	Human Neutrophil Elastase
HPH	High-pressure Homogenization
HPLC	High-performance Liquid Chromatography
HSA	Human Serum Albumin

I

IC_{50}	half maximal Inhibitory Concentration
Ile	Isoleucine (a.a.)
IR	Infrared
IRE	Internal Reflection Element

J

K

k	Kilo unit (10^3)
k	Constant of the macromolecular network system
K^+	Potassium ion
kb	Kilo-base
kDa	kiloDalton (atomic mass unit, 10^3 Da)
Kg	Kilograms (SI base mass unit)
K_i	Inhibition Constant
Kpb	Kilo-base pair

L

L	Litre (SI volume unit)
LDA	Laser Doppler Anemometry
Leu	Leucine (a.a.)
LiBr	Lithium Bromide
Lys	Lysine (a.a.)

M

μ	Micro unit (10^{-6})
μ_e	Electrophoretic mobility of the particles
μL	Microliters (volume unit, 10^{-6} liters)
μM	Micrometre (distance/size unit, 10^{-6} meters)
M	Molar unit (SI concentration unit)
m	Mili unit (10^{-3})
m	Meters (SI distance/size unit)
Met	Methionine (a.a.)
mL	Millilitre (volume unit, 10^{-3} liters)
mm	Millimetre (distance/size unit, 10^{-3} meters)
MMP	Matrix Metalloproteins
mol	Mole, SI amount of substance unit
M_t/M_∞	Fractional release of the compound
mV	Milivolts (electrical potential unit, 10^{-3} volts)
MW	Molecular Weight
MWCO	Molecular Weight Cut Off

N

MeOSuc-Ala-Ala-Pro-Val-pNA	N-methoxysuccinyl-Ala-Ala-Pro-Val-p-nitroanilide
n	Nano unit (10^{-9})
n	Replica number
n	Diffusional exponent
N=N	Double covalent ligation between two Nitrogens, known as azo group
Na	Sodium
Na_2CO_3	Sodium carbonate
NADHP	Nicotinamide Adenine Dinucleotide Phosphate
NE	Neutrophil Elastase
N-H	Single covalent ligation between Nitrogen and Hydrogen
nm	Nanometer (distance/size unit, 10^{-9} meters)
NP(s)	Nanoparticle(s)

O

O	Oxygen
o/w	Oil-in-water

P

PCS	Photonic Correlation Spectroscopy
PDB	Protein Data Bank
PDB ID	Protein Data Bank Identification
PEO	Poly(ethylene oxide)
PGA	Poly(glycolic acid)
pH	Potential of hydrogen
Phe	Phenylanine (a.a.)
pI	Isoelectric point
PLA	Poly(lactic acid)
PLGA	Poly(lactide-co-glycolic acid)
PMN	Polymorphonuclear Neutrophils or Leukocytes
Pro	Proline (a.a.)
PVP	Polyvinylpyrrolidone

R

ROS	Reactive Oxygen Species
rpm	Rotation per minute (rotational speed measurement)
RSF	Regenerated Silk Fibroin

S

s	second(s) (SI time unit)
S	Sulphur
S=O	Double covalent ligation between Sulphur and Oxygen, known as sulphonic or sulphonate group
SC	*Stratum Corneum*
SDS	Sodium Dodecyl Sulphate
Ser	Serine (a.a.)
SF	Silk Fibroin
SF-NPs	Silk Fibroin Nanoparticles
SI	International System of Units
SIRS	Systemic Inflammatory Response Syndrome
SLPI	Secretory Leukocyte Peptidase Inhibitor
SLS	Sodium Laury Sulphate
STEM	Scanning Transmission Electron Microscopy
Suc-Ala-Ala-Pro-Phe-pNA	Succinyl-Alanine-Alanine-Proline-Phenylanine-p-nitroanilide

T

T	Temperature
t	Release time
TEM	Transmission Electron Microscopy
Thr	Threonine (a.a.)
Tyr	Tyrosine (a.a.)

U

U	Enzyme Unit (amount of enzyme, 1 µM of substrate per min)
U/mL	Unit per mililiter
US	Ultrasonication
USA	United States of America
UV	Ultraviolet
UV-Vis	Ultraviolet-Visible

V

Val	Valine (a.a.)

W

W/O	Water-in-Oil
W/O/W	Water-Oil-Water
W/O/W/O	Water-Oil-Water-Oil
w/v	Weight per volume (mass concentration unit)

List of Figures

List of Tables

List of Equations

Chapter I.

Introduction

Chapter I. Introduction

1.   **Major Goals and Outline**

The emerging of nanotechnology in association with biotechnology has provided tools for development and innovation of science-based solutions, leading major breakthroughs in science (Morganti, 2010;Reis *et al.*, 2006). In detail, bionanotechnology involves the interface of nanotechnology systems with biological and biochemical applications (Morganti, 2010).

According to the European Commission, the financing for development of nanomaterials and production of innovative nanotechnologies has increased nearly 40% in the last six years, being associated to an increase of about 3.5 billion of euros (Morganti, 2010). In fact, due to their potential uses and benefits, the bionanotechnology methods are already extensively used in medicine and pharmaceutical industry, being also used for cosmetic industry (Morganti, 2010).

More specifically, bionanotechnology in cosmetic industry has been widely used since it improves their ability to penetrate the skin and have shown beneficial to the skin (Buzea *et al.*, 2007;Grebler *et al.*, 2010;Morganti, 2010;Patel *et al.*, 2011;Roy *et al.*, 2012). Additionally, considering the creativity, innovation, competitively and entrepreneurship involved in this area, it is thought to broadly stimulate the economy (Morganti, 2010).

Among nanomaterials for cosmetic use, biopolymeric nanoparticles are of particular interest because they enable high drug loading and release efficiency and controlled size distribution (Reis *et al.*, 2006), and since they are composed of biocompatible and biodegradable polymers they also possess improved safety and stability in biological fluids, (Mohanraj *et al.*, 2006;Nagavarma *et al.*, 2012).

Silk Fibroin (SF) protein is a Food and Drug Administration (FDA) approved natural biopolymer that has been extensively studied for various applications (Cao, Y *et al.*, 2009). SF impressive mechanical properties, good biocompatibility, biodegradability and bioresorbability are the main reasons for this interest (Cao, Y *et al.*, 2009), leading to the development of SF innovative based-materials, such as films, sponges, hydrogels, fibers, tubes and micro or nanoparticles (Rockwood *et al.*, 2011).

Recently, SF based-particles have been proposed as controlled drug delivery systems, (Wang, X *et al.*, 2007;Sharma *et al.*, 2011). This SF nanoparticles can be prepared by emulsification, for example (Lovelyn *et al.*, 2011). These nanoemulsions are formed by mixing of an organic phase (oil) with an aqueous phase (water) (Sundar *et al.*, 2010), using

high-energy methods, like ultrasonication and high pressure homogenization (HPH) (Lovelyn *et al.*, 2011).

Having in consideration that some studies have also suggested that release of organic oils from protein particles can promote inhibition of high levels of Human Neutrophil Elastase (HNE) (Silva *et al.*, 2012), we suggested to combine this ability with the excellent SF properties in nanoparticles for further incorporation with a synthetic HNE inhibitor, sivelestat.

HNE belongs to serine proteinase of the chymotrypsin family (Korkmaz *et al.*, 2008), which is mostly stored in granules of azurophilic neutrophils (Weitz *et al.*, 1986;Woodman *et al.*, 1993). In inflammatory responses, HNE is expressed by neutrophils leading to disruption of collagen and elastin fibers, and consequently damaging ECM in dermis (Imokawa, 2008;Rijken, 2011;Takeuchi *et al.*, 2010).

Therefore, topical application of the new developed nanodevice will allow better control of HNE-induced cell damage and skin diseases, as an anti-wrinkling agent, since HNE is involved in wrinkle formation due to repeated UV irradiation and mild inflammation (Imokawa, 2008;Takeuchi *et al.*, 2010).

Throughout this project it was intended to produce silk fibroin nanoparticles (SF-NPs) for transdermal delivery by two high-energy emulsification methods, ultrasonication and high pressure homogenization (HPH). As a first stage on the various conditions were tested, silk fibroin concentration, oil-in-water ratio and homogenization cycles, using *n*-dodecane as oil phase.

After optimization, various surfactants were added to the best formulations in order to compare their stabilization effect. Then, incorporation of the HNE inhibitor sivelestat in the SF-NPs was assed, however before sivelestat incorporation studies, a model-drug compound was first studied, orange IV, to establish a drug-model of incorporation and release.

Finally, the structure of the formulated nanoparticles was studied by FTIR-ATR, to compare secondary structure and content of β-sheets.

2. Overview

This dissertation research is organized in four parts (excluding references and annexes) containing seven chapters. The contents of each part and chapter are synthetized below:

First part – General introduction

Chapter I: Introduction – In this chapter, the dissertation work is summarized and the thesis contents are introduced, in order to facilitate reading.

Chapter II: Literature Review - This chapter intends to review all the knowledge needed for the development and understanding of this work which goal is to develop silk fibroin nanoparticles for inhibition of wrinkle formation in photoaging by transdermal route. In other words, presents comprehensive overview of nanoparticles for transdermal delivery, silk fibroin protein as a polymeric protein used in biomaterials and finally, wrinkle formation mechanism involving Human Neutrophil Elastase (HNE) and the inhibition mechanism associated.

Second part – Materials and Methods

Chapter III: Materials and Methods – In this chapter, the materials and the experimental procedures used along the work are described in detail. This enables understanding of how the experiments were carried, allowing others to repeat.

Third part – Results and Discussion

Chapter IV: Optimization Production Process of SF-NPs by High-energy Emulsification – In this chapter, silk fibroin nanoparticles (SF-NPs) production is optimized according to two high-energy emulsification methods (ultrasonication and high pressure homogenization). The results on this chapter, besides providing knowledge of how this two emulsification systems work, it also indicates the best parameters and formulations, providing a guideline for further silk fibroin nanoparticles production.

Chapter V: Incorporation in SF-NPs for Transdermal Delivery – In this chapter, first, incorporation studies of various stabilizers in the NPs formulations were evaluated in order to study their potential in silk fibroin nanoparticles stabilization over time. Then, incorporation of a model-drug compound, orange IV, and with the HNE inhibitor, sivelestat,

in optimized silk fibroin nanoparticles was assessed, this enables understanding of the drug release profile and HNE inhibition effect of this developed silk fibroin nanoparticles. This chapter results will allow final design of the silk fibroin nanoparticles, namely their stabilization and application as an anti-wrinkling agent.
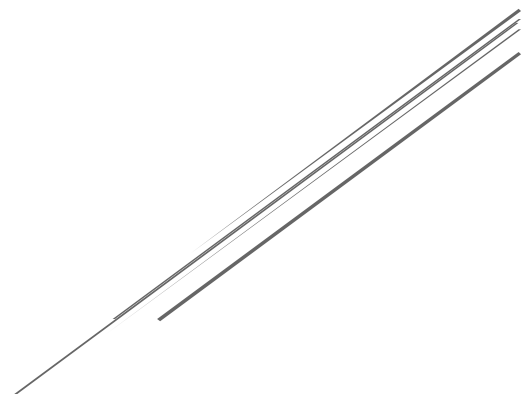
Chapter VI: Structure Analysis of SF-NPs by FTIR Spectroscopy– This chapter reports the silk fibroin structure changes that occur in emulsification using high pressure homogenization, providing a better understanding of this method.

Fourth part – Conclusion

Chapter VII. General Conclusions and Future Perspectives – In this chapter, the final remarks of this research work and the future work than can follow are presented.

Chapter II.

Literature Review

Chapter II. Literature Review

1.   Nanoparticles as Drug Delivery Systems

Nanotechnology concept first emerge in Taniguch article, where it was described as "integrated manufacturing technologies and machine systems which provide ultra-precision machining capacity in the order of 1 nanometre" (Taniguch, 1983); and interest in this "extreme technology" has been growing ever since (Park, 2007), especially for drug delivery systems (DDS) (Reis *et al.*, 2006). Nanotechnology definition has evolved, and currently is defined as research and development in atomic, molecular and macromolecular scales, with the purpose to create and study structures and/or devices at a nanometre scale (Sundar *et al.*, 2010). The considered range for this technology generated some discussion in the scientific community, some authors consider 10-1000nm range (Soppimath *et al.*, 2001), others consider below 100 nm (De Jong *et al.*, 2008), still the exact range is not very relevant.

Studies have reported that nano dimensions present advantages comparing to other technologies, such as high drug loading and release efficiency and controlled size distribution (Reis *et al.*, 2006). Nanoparticles are, by definition, solid drug carriers at a nano range (Reis *et al.*, 2006). For drug delivery (DD) purposes, the drug can be entrapped, encapsulated or attached to the nanoparticle, namely nanocapsules or nanospheres, according to the production method (Soppimath *et al.*, 2001). Briefly, nanocapsules consist in vesicular systems with the drug confined in a cavity surrounded by a membrane; while nanospheres are a matrix system in which the drug may be absorbed at the sphere surface or encapsulated (Mohanraj *et al.*, 2006;Reis *et al.*, 2006). Each type of nanoparticle is represented in Figure II.1 A and B, respectively.
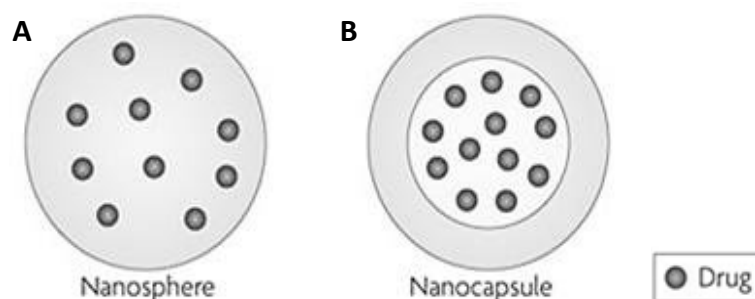
Figure II.1. Schematic representation of nanoparticles: (A) Nanospheres and (B) Nanocapsules, adapted from Orive *et al.*, 2009. Legend: Darker spheres represent the drug molecules.

For nanoparticle (NP) design for drug delivery is important to control particle size, surface properties and drug loading and release profile (Mohanraj *et al.*, 2006). This characteristics will define the drug-action on the desired target at a therapeutically rate and dose (Mohanraj *et al.*, 2006). Summarizing, the NPs as DDS must be safe, biocompatible, non-toxic, stable and with optimal life-span to allow drug targeting and delivery at a therapeutic need (De Jong *et al.*, 2008).

In order to obtain biocompatible and safe nanoparticles for drug delivery, nanoparticles production method cannot involve toxic reagents or if so, these should be easily removed from the final product without affecting its properties (Reis *et al.*, 2006). In addition, the production method must be simple and cheap to allow production at large quantities, *i.e.* scale-up production (Park, 2007), reproducible and efficient (Reis *et al.*, 2006).

Nanoparticles can be produced from various materials, including proteins, polysaccharides and polymers (Sundar *et al.*, 2010). In fact, the NPs material defines their final characteristics, namely size, morphology, surface charge, permeability, life-span, toxicity, drug loading and release efficiency, among others (De Jong *et al.*, 2008;Mohanraj *et al.*, 2006).

1.1. Biopolymeric Nanoparticles

Polymeric nanoparticles, as the name suggests, are nanoparticles produced from polymers, and these are separated in two categories, synthetic polymers and natural polymers, whereas this last one involves polymeric proteins and polysaccharides (Sharma *et al.*, 2011). Initially, synthetic polymers received more attention than natural polymers, because polymers of natural origin often require processing treatment, which could lead to denaturation, and additionally, to different purity levels (Hans *et al.*, 2002). However, synthetic polymeric NPs started to generate some concerns relating to toxicological problems due to non-biodegradable polymers, preventing their use as DDS (Sundar *et al.*, 2010).

To overcome this problem, DD nanoparticles started to be prepared from biocompatible and biodegradable polymers (Nagavarma *et al.*, 2012). These drug carriers feature numerous advantages over the existing systems (Mohanraj *et al.*, 2006), such as improved safety, drug release efficiency and stability in biological fluids (Mohanraj *et al.*, 2006;Nagavarma *et al.*, 2012). However, these biopolymeric nanoparticles may present some instability in liquid and dry form, since smaller size and large surface area particles

can react and aggregate, but this limitation can be overcome by polymers choice and production process optimization (Mohanraj *et al.*, 2006).

Examples of potential DD synthetic biopolymers is poly(lactic acid) (PLA), poly(glycolic acid) (PGA) and poly(lactide-co-glycolic acid) (PLGA) (Hans *et al.*, 2002), but synthetic polymers present difficulty in stabilize the drug within the particle and protect the particle against enzymatic degradation due to their hydrophobic nature, wherein natural polymers like proteins are mainly hydrophilic (Sundar *et al.*, 2010). Hence, natural occurring materials showed to be more promising DDS, where the most widely used polymeric proteins are albumin, gelatin, collagen and silk fibroin, and polymeric polysaccharide are alginate and chitosan (Sundar *et al.*, 2010).

Finally, is important to highlight that all the DDS characteristics, such size, morphology and even drug release profile, are defined along its production process, from the material used to the methodologies used (De Jong *et al.*, 2008;Mohanraj *et al.*, 2006).

1.1.1. Biopolymeric Nanoparticles production methodologies

The most commonly used methods for protein or/and polysaccharide based-nanoparticles are Coacervation/Desolvation and Emulsification (Sundar *et al.*, 2010;Pathak *et al.*, 2009).

Coacervation/Desolvation method uses the differential solubility of proteins in solvents to produce the nanoparticles, and the desired characteristics are obtained by controlling the processing variables such as solvent polarity, pH, ionic strength and/or presence of electrolytes (Pathak *et al.*, 2009). In coacervation, the protein solubility is reduced, using antisolvents like acetone or ethanol, leading to a phase separation (Pathak *et al.*, 2009). Then, a desolvating agent is added causing the protein to change its tertiary structure and forming protein clumps, and finally these clumps are cross-linked with a chemical substance, for example glutaraldehyde or glyoxal, producing the final nanoparticles directly in aqueous solution (Pathak *et al.*, 2009).

The chemical substances used in this process are toxic, so its removal is normally achieved by centrifugation or redispersion (Sundar *et al.*, 2010), but these purification process leads to low yields (Reis *et al.*, 2006). Still, since this process does not use high temperatures, is widely used to produce nanoparticles for delivery heat-sensitive drugs (Reis *et al.*, 2006).

Emulsification method involves formation of an emulsion, in this case in particular, a nanoemulsion (Sundar *et al.*, 2010). An emulsion is defined as colloidal dispersion of liquid droplets in another immiscible liquid phase (Mason *et al.*, 2006;Mason *et al.*, 2006), produced by extreme mixing of an organic phase (oil) with an aqueous phase (water) (Sundar *et al.*, 2010). Briefly, the resulting droplets occur due to hydrophobicity differences between both phases, wherein attraction and repulsion of these two phases leads to an interfacial tension where the oil and water connect (Mason *et al.*, 2006;Mason *et al.*, 2006). The emulsification process is summarized in Figure II.2.
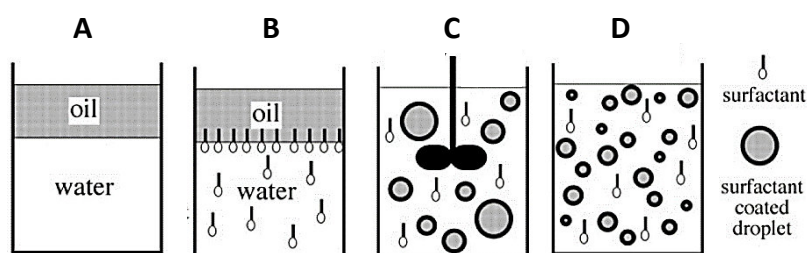
Figure II.2. Schematic representation of emulsification process, adapted from Mason *et al.*, 2006. (A) Initially two immiscible liquids, oil and water, are two separated phases; (B) wherein surfactant can be added to improve formulation stability. (C) Then, applying high-energy, like shear, causes oil to break up into droplets (which are coated with the surfactant), (D) resulting in an emulsion.

Emulsions are generally classified according to its morphology, whereas the oil or water are continuous phase or dispersed phase (Mason *et al.*, 2006;Mason *et al.*, 2006). When continuous phase and dispersed phase are water and oil, respectively, the emulsion is termed by direct, water-based or oil-in-water (o/w) emulsions (Mason *et al.*, 2006;Mason *et al.*, 2006). When water droplets are dispersed in oil, the emulsion is called by inverse, oil-based or water-in-oil (w/o), *i.e.* when continuous phase and dispersed phase are oil and water, respectively (Mason *et al.*, 2006;Mason *et al.*, 2006). Additionally, exists double-emulsions, for example water-oil-water, (w/o/w), and multiple emulsions, such as water-oil-water-oil (w/o/w/o) (Su, 2008).

The nanoemulsion processes are non-equilibrium and non-spontaneous systems, therefore its production requires a large input of energy (Lovelyn *et al.*, 2011) or addiction of surfactants, which reduce significantly the interfacial tension (Mason *et al.*, 2006;Mason *et al.*, 2006).

Consequently, emulsification can be achieved using high-energy methods, where intensely disruptive forces, created by specific mechanical devices, break the oil and water phases leading to nanosized droplets (Lovelyn *et al.*, 2011). Those high-energy mechanical devices can be ultrasonication, high pressure homogenization (HPH) and microfluidization (Lovelyn *et al.*, 2011).

In more detail, when pre-emulsion (oil and water separated phases) are irradiated with ultrasound bubbles are created, due to the alternating expansive and compressive acoustic waves (Bang *et al.*, 2010). This process is termed by cavitation, wherein these bubbles can accumulate ultrasonic energy, and implode to release the stored energy, leading to nanoparticles (Bang *et al.*, 2010). Additionally, ultrasonic irradiation generated free radicals, namely reactive oxygen species (Hofmann *et al.*), still NPs production by this method is FDA approved and findings have suggested that this process does not lead to protein degradation or denaturation (Bang *et al.*, 2010). As disadvantage, this mechanism is mainly used at laboratory scale, so scale-up is difficult (Lovelyn *et al.*, 2011).

Regarding HPH, in this high-energy method more disruptive forces are involved, such as hydraulic shear, intense turbulence and cavitation, which is common to ultrasound (Lovelyn *et al.*, 2011). In HPH, the pre-emulsion is pressed at high pressure through a narrow slit, creating the air bubbles (Grebler *et al.*, 2010). When the liquid emerges from the slit, the bubbles implode and collide, forcing oil to break up in emulsion drops (Grebler *et al.*, 2010). These circuit is repeated in numerous cycles, decreasing the droplets size into to nano range droplets, and consequently forming the nanoparticles (Grebler *et al.*, 2010).

Finally, microfluidizer is an improved mechanism similar to HPH (Lovelyn *et al.*, 2011). It uses a high-pressure positive displacement pump which forces the pre-emulsion to pass through various small channels, called by microchannels (Lovelyn *et al.*, 2011). Following, the bulk emulsion is filtered through a nitrogen filter to remove the large droplets, resulting in more stable and uniform nanoemulsions (Lovelyn *et al.*, 2011).

Surfactants are amphiphilic surface-active molecules, highly soluble in one of the phase, that act as stabilizers of the nanoformulations (Mason *et al.*, 2006;Mason *et al.*, 2006). In fact, presence of surfactants prevents the system to revert to a lower energy configuration at thermodynamic equilibrium (Mason *et al.*, 2006;Mason *et al.*, 2006). The surfactants are classified according to hydrophilic lipophilic balance (HLB), which defines their relative solubility in aqueous and oil liquid phases (Mason *et al.*, 2006;Mason *et al.*, 2006). Surfactants with high and low values of HLB indicate that is more soluble in water and oil, respectively (Su, 2008). Is important to note that HLB values are affected by different parameters like temperature, composition, among others (Lovelyn *et al.*, 2011).

The only disadvantage of this method is the need of an organic phase that has to be removed because it may cause toxic problems (Sundar *et al.*, 2010). Still most organic solvent can be removed by simple evaporation (Sundar *et al.*, 2010), and may affect the produced nanoparticle characteristics (Mason *et al.*, 2006;Mason *et al.*, 2006).

2. Transdermal Delivery

Drug delivery through the skin to the systemic circulation is very useful for several clinical conditions (Lovelyn *et al.*, 2011), and has been used as an alternative to oral, intravascular, subcutaneous and transmucosal routes (Kumar *et al.*, 2010).

Comparing to the conventional modes of drug administration, transdermal delivery avoids gastrointestinal absorption preventing enzymatic and pH inactivation of the DDS, therefore reduces the dosage (Pankaj *et al.*, 2011), preventing the potential side effects (Kumar *et al.*, 2010). Besides, steady absorption of drug over hours or days is rather desirable than the blood level spikes produced by oral dosage forms (Kumar *et al.*, 2010). Additionally, transdermal DDS is also more convenient to administer drugs and administration interruption is more flexible, being more comfortable, painless and simple to the patient (Kumar *et al.*, 2010).

Conversely, it possesses some disadvantages including, possible local irritation in application site and inflammatory responses can be trigged, like erythema, itching and local edema, and production is more expensive than other alternative routes for DDS (Kumar *et al.*, 2010).

Transdermal drug delivery allows medicines to be delivered via the skin over an extended period of time, at a predetermined and maintained rate of an effective drug concentration (Pankaj *et al.*, 2011). However, the transdermal route presents a major barrier within the skin, the *stratum corneum* (SC) (Kumar *et al.*, 2010), which is localized in the top layer of the dermis, within the bilayer lipid matrix (Prow *et al.*, 2011).

The following figure II.3 represents various epidermal layers in a cross-section image of skin, edited by Mikael Häggström, from Wbensmith work and published in Wikimedia in 2010. Being the most relevant in this work the *stratum corneum*.

Figure II.3. Cross-section of the skin with the epidermal layers represented, image adapted from Häggström, 2010. The keratynocytes maturity and differentiation increases with the deep of the skin. From exterior to dermis, the epidermal layers are *stratum corneum* (cornified layer), *stratum lucidum* (translucent layer), *stratum granulosum* (granular layer), *stratum spinosum* (spinous layer) and *stratum basale* (basal or germinal layer) (Weedon, 2002).
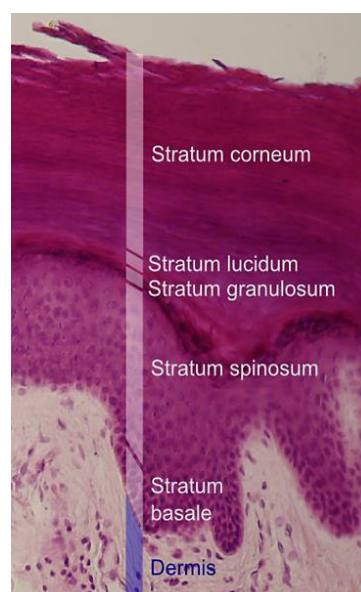
The *stratum corneum* (SC) consists of a 10-20 µm protect layer (Buzea *et al.*, 2007) of flattened and anuclear dead cells, composed with keratin fibers (corneocytes) (Prow *et al.*, 2011). To be noted, these dead cells were fragments of once active dividing epidermal cells (Kumar *et al.*, 2010) and the corneocytes integrity is maintained by corneodesmosomes (Prow *et al.*, 2011). The SC arrangement is often called by "brick and mortar", in this analogy corneodesmosomes are the mortar and the corneocytes are the bricks (Prow *et al.*, 2011).

The drug delivery through the SC can occur by passive diffusion and/or by three possible routes, intercellular, transcellular and appendageal (Prow *et al.*, 2011). Initially, delivery across SC of polar and non-polar solutes were thought to occur via transcellular and intercellular route, respectively (Prow *et al.*, 2011). But studies showed that most solutes diffuse through intercellular pathway, in fact between this two, intercellular route is considered the most favourable (Prow *et al.*, 2011).

Even so, small molecules can cross freely between the intercellular spaces, the macromolecules or larger particles are physically constrained, indeed the diffusion rated through this route depend on molecular weight, the capability to establish interactions and forces, solubility and lipophilicity of the crossing material (Prow *et al.*, 2011).

Hence, the appendageal route is considered as a realistic alternative, where the crossing is focused in the hair follicles, called by transfollicular route, or through sweat glands (Prow *et al.*, 2011). Since the hair follicles are deeply extended in the skin and connected to a capillary blood supply, the diffusion out of the follicle of the DDS through the skin is possible (Prow *et al.*, 2011). In fact, Toll and co-workers studies shown that spherical particles with 750nm - 6µm of diameter were able to penetrate selectively through hair follicles at 2.4 mm of depth (Toll *et al.*, 2004;Buzea *et al.*, 2007).

Furthermore, if the skin is damaged and the normal barrier disrupted, entry of DDS through SC may be significantly increased (Patel *et al.*, 2011), such as Monteiro-Riviere findings have suggested that larger particles of 500 nm – 7 µm of diameter can penetrate broken skin (Monteiro-Riviere *et al.*, 2005;Buzea *et al.*, 2007).

2.1. Nanoparticles in cosmetic applications

Currently, engineered nanosystems are applied in several areas, including cosmetic industry (Morganti, 2010). Several cosmetics and personal care products use nanomaterials (Buzea *et al.*, 2007;Morganti, 2010), which are mostly produced by nanoemulsion, since it produces transparent and pleasant products to touch (Patel *et al.*, 2011). In fact, nanoemulsions are used in deodorants, sunscreens, shampoos and skin and hair care products, because nanoemulsions increase stabilization of the nanomaterials and are more suitable for drug delivery (Grebler *et al.*, 2010).

Nanomaterials are capable to deeply penetrate the skin with improved efficiency than the previous cosmetics (Buzea *et al.*, 2007), allowing nanoparticles encapsulated nanoparticles with active cosmetics to be delivered through the skin (Morganti, 2010).

Cosmetic products are used to enhance beauty, magnificence and attractiveness of the skin and protect it against exogenous and endogenous harmful and damaging agents (Morganti, 2010;Roy *et al.*, 2012).

Ever since, use of nanomaterials and nanoparticles in cosmetic industry has able fragrances to last longer, sunscreens to be more effective allowing better UV protection (Patel *et al.*, 2011), development of anti-ageing creams by concealing wrinkles with nanoparticles (Buzea *et al.*, 2007), maintenance of hair properties, among others (Morganti, 2010;Patel *et al.*, 2011).

In conclusion, cosmetic products are the best solution to develop attractive external appearance of the skin and reduce or prevent skin disorders, such as hyper pigmentation, aging, wrinkles, rough texture, and others (Morganti, 2010;Roy *et al.*, 2012).

3. Silk Fibroin, a biopolymeric protein

Silk fibroin (SF) is a natural protein polymer, produced by some lepidoptera larvae, like silkworms and spiders (Altman *et al.*, 2003). Depending on its source, the silk composition, structure and properties differ extensively, according to its biological function and need (Altman *et al.*, 2003)**.** These fibers are involved in cocoon formation for protection of eggs and larvae, web formation and support for spiders, and in insect traps for predation (Kearns *et al.*, 2008;Nagarkar, 2010).

One of the most characterized silks comes from the silkworm *Bombyx mori* due to its long history of domestication (Kaplan, 1994) and use in textile fibers and in medicine, as sutures and artificial ligaments (Sah *et al.*, 2010). Due to its biocompatible and mechanical properties, its use has been increasing dramatically in biotechnology and biomedical areas (Altman *et al.*, 2003).

Native Silk fiber from *B. mori* consists in two different proteins: sericin, a glue-like protein that binds the structural fibrous protein, fibroin, into fibers (Kaplan, 1994). This Silk fibroin as a polymer consists in a repetitive primary polypeptide sequences of amino acids (-Gly-Ala-Gly-Ala-Gly-Ser-), that leads to antiparallel β-sheets (Cao, Z *et al.*, 2007) due to the hydrophobic domain predominance as result of homogeneity in secondary structure (Vepari *et al.*, 2007).

B. mori silk secreted into the posterior silk gland is composed of a three protein components: Heavy (H) chain of 350 kDa, Light (L) chain of 25 kDa and Glycoprotein P25 of 30 kDa, in a molar ratio of 6:6:1, respectively (Mondal *et al.*, 2007). The light chain that is linked to the heavy chain by a single disulphide bond has 262 amino acid (a.a.) residues and a nonrepetitive sequence (Zhou *et al.*, 2001). While the heavy chain has 5263 residues and is composed of 45.9% of glycine (Gly), 30.3% of alanine (Ala), 12.1% of serine (Ser), 5.3% of tyrosine (Tyr), 1.8% of valine (Val) and 4.7% of the other 15 a.a. types (Zhou *et al.*, 2001). Beside**s** the heavy chain has a low-complexity repetitive sequence, in fact most of the sequence forms 2377 repetitions of a Gly-X dipeptide motif, with X being Ala, Ser, Tyr and Val (Zhou *et al.*, 2001).

For better elucidation, the quantitative amino acid composition for silk fibroin, published in Vasconcelos *et al.*, 2008, is presented in a table (Table Annex.1) in Annex I.

Since 1953 there is some discrepancy regarding the silk fibroin molecular weight (MW), in fact various studies present large differences on the SF MW values, being this differences influenced by the silk fibroin process (Hyde *et al.*, 1962). The most accepted SF MW value is 391 367 Da (Zhou *et al.*, 2000).

A number of *B. mori* silk fibroin crystalline structures have been reported, the glandular state (Silk I), the crystalline silk structure (Silk II) and an air/water interface orientation (Silk III) (Vepari *et al.*, 2007).

The structure of Silk I is the water-soluble state (Vepari *et al.*, 2007) that ordinarily occurs in the silkworm glands (Malay, 2005) and it contains random-coil and amorphous regions (Cao, Y *et al.*, 2009). Also is unstable to mechanical deformation (Kaplan, 1994) since upon heat exposure or physical spinning converts to antiparallel β-sheet, the Silk II structure (Vepari *et al.*, 2007). In addition, Iizuka *et al.* studies have shown that Silk II structure can also dissolve without precipitation in mixed solvents of water and methanol or dioxane (Iizuka *et al.*, 1968;Vepari *et al.*, 2007).

Regarding the β-sheet silk structure (Silk II), Takahashi *et al.* proposed an antiparallel hydrogen bonded sheets, *i.e.* adjacent strands oriented in opposite directions, with one side occupied with hydrogen side chains from glycines and the other with methyl side chains from alanines (Kaplan, 1994;Vepari *et al.*, 2007;Takeuchi *et al.*, 2010). As mentioned above, this crystalline conformation establishes strong intermolecular hydrogen bonding and van der Waals forces that lead to a thermodynamically stable structure, preventing the separation of molecules (Kaplan, 1994;Malay, 2005) and the water dissolution, including in mild acid and alkaline conditions, and several chaotropes (disruption agents, they increase the entropy and interfere with the protein interactions) (Vepari *et al.*, 2007).

This crystalline structure is schematized in Figure II.4, where grey dashed represents the hydrogen bounds and grey line shows stabilization between C-terminal and N-terminal of two SF chains in an antiparallel direction, which forms the secondary structure β-turns and consequently the β-sheets. This β-sheets and β-turns in *Bombyx mori* SF structure are highlighted in Figure II.5 (yellow and violet colours, respectively). To be noted the deduced molecular structure of silk fibroin presented in Figure II.5 was obtained by expression in *Escherichia coli*.
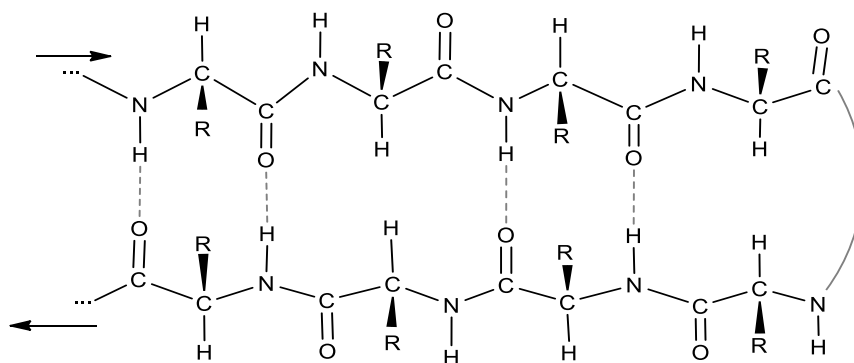
Figure II.4. Schematic representation of β-sheet antiparallel structure of silk fibroin protein, stabilized with hydrogen and van der Waals bonds. Legend: grey dashed line represents intra-chain hydrogen bonds and grey line represents stabilization of C and N-terminal between two SF chains.

Figure II.5. Molecular representation of N-terminal domain of *Bombyx mori* silk fibroin secondary structure, expressed in *Escherichia coli*. Modulation performed in jmol and stored in protein data bank (PDB) by PDB identification (PDB ID) of 3UA0. Legend: yellow represents β-strands; violet represents β-turns; and white represents none assigned or defined structure.

Finally, the crystal Silk III structure involves a hexagonal arrangement of silk molecules in a threefold helical chain conformation caused by the serine and alanine residues separation (Valluzzi *et al.*, 1999). This structure was first observed in films taken from the air-water interface of aqueous fibroin solutions in Valluzzi *et al.* previous experiments (Valluzzi *et al.*, 1999).

The silk fibers stability and β-sheets structure provides SF unique strength, toughness and elasticity, which is much desired in biomaterials industry (Altman *et al.*, 2003). In fact, currently silk fibroin protein has been extendedly applied in films, membranes, sponges, three-dimensional scaffolds, hydrogels, powders, electrospun fibers and microspheres (Kundu *et al.*, 2010;Cao, Y *et al.*, 2009). Besides, the crystallinity levels of silk fibroin and morphology can be applied in drug release control (Mandal, BB *et al.*, 2009).

3.1. Silk Fibroin processing

For many years, silk has been used as sutures in medicine in spite that this material had to be treated with waxes or silicone, since untreated silk was considered a potential allergen, leading to type I allergic responses (immediate hypersensitivity) (Altman *et al.*, 2003). Findings of Wen and co-workers have reported that sericin protein was responsible for the allergenic responses, and when removed from silk, leaving only silk fibroin, the material was considered safe (Wen *et al.*, 1990;Altman *et al.*, 2003).

Therefore, in order to use silk fibroin protein as a biomaterial, silkworm silk requires removal of contaminating sericin to avoid biocompatibility problems and then, dissolution

of structure Silk II of silk fibroin, which contains β-sheets, in aqueous solution since is insoluble in water.

Sericin removal is obtained by alkali salt heat treatment, called degumming process (Malay, 2005). Briefly, the original silk (*Bombyx mori* cocoons) is dissolved in Na_2CO_3 or $NaHCO_3$ solution at 100 °C, resulting in cotton-like fluffy mass of sericin-free silk, *i.e.* silk fibroin fibers (Wray *et al.*, 2011;Sah *et al.*, 2010).

The degumming process affects the silk fibroin produced material, namely mechanical properties like elasticity, molecular weight and cell viability (Wray *et al.*, 2011). Wherein mechanical changes are caused by disruption of hydrogen and van der Waals bonds (Wray *et al.*, 2011) but these changes were considered insignificant when compared to dissolution process of the degummed silk (Kearns *et al.*, 2008); and molecular weight and cell viability decreases when increasing degumming time because the treatment can lead to degradation of silk fibroin into lower molecular weight fragments, that can affect cell function (Wray *et al.*, 2011). Therefore the process conditions needs to be controlled to ensure complete removal of sericin, without degradation of silk fibroin, in which the optimized process involves boiling *Bombyx mori* cocoons in 0.05-0.01M of sodium carbonate (Na_2CO_3) for 20-30 minutes, which maximal concentration of cocoons to total solution volume, w/v (g/L), is 5:1 (Sah *et al.*, 2010;Wray *et al.*, 2011).

Following, the degummed material is dissolved in an heated organic-aqueous concentrated solution of salts, such as calcium chloride ($CaCl_2$) or lithium bromide (LiBr), (Sah *et al.*, 2010) since SF protein is destabilized and its solubility is increased in high ionic-strength of chaotropic salts (Sah *et al.*, 2010). In general, this process is performed with 9-9.3M concentration of LiBr at 60-70°C, until complete dissolution, 3-5 hours (Sah *et al.*, 2010). Finally, dissolved silk fibroin is dialyzed against double distilled water to prepare an aqueous silk fibroin solution without salts (Wray *et al.*, 2011), called regenerated silk fibroin (RSF).

For a better elucidation, silk fibroin processing is schematized in Figure II.6.
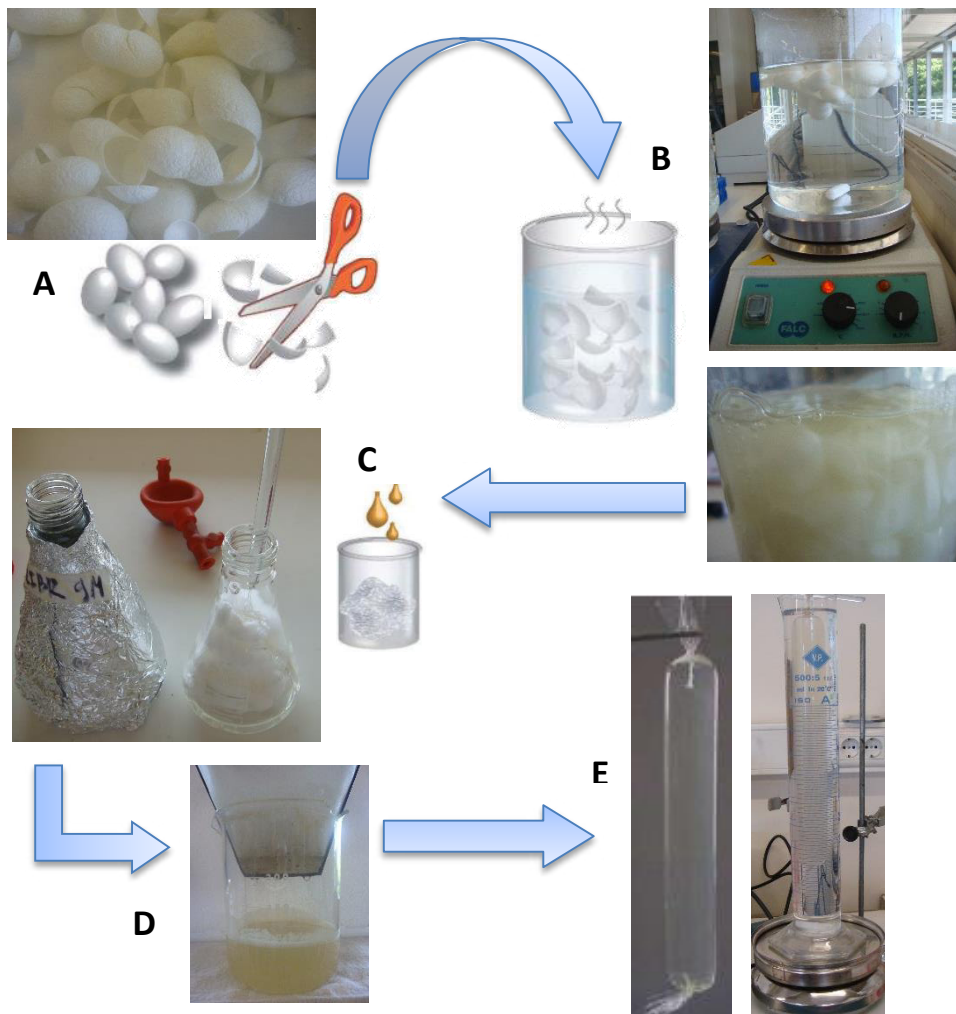
Figure II.6. Schematic representation of silk fibroin extraction process, images adapted from Malay, 2005 and (Rockwood *et al.*, 2011). Legend: (A) original silk material of silkworm *Bombyx mori* cocoons, (B) degumming process, (C) dissolution of degummed silk in LiBr, (D) filtration process, (E). Dialysis process, resulting in RSF solution.

3.2. Silk Fibroin as a biomaterial

Silk Fibroin protein as a natural biopolymer presents advantages over synthetic polymers, including favourable mechanical properties, good biocompatibility, biodegradability and bioresorbability (Cao, Y *et al.*, 2009), which makes it an environment-friendly solution (Malay, 2005), suitable for biomedical applications.

As already mentioned, silk fibroin is a safe material since it does not triggers inflammatory or toxic responses *in vitro* and *in vivo,* as long as sericin protein is removed in the degumming process. In fact, this material is approved by FDA (Cao, Y *et al.*, 2009). Additionally it possesses high permeability to oxygen and water-vapour, as demonstrated in Minoura *et al.* studies of silk fibroin membranes, which is promising in applying silk fibroin as skin dressings, like wound dressing artificial skin, contact lenses or even as scaffolds such as artificial corneas or bone (Malay, 2005).

Indeed, SF process is very versatile, making it possible to produce silk fibroin films, scaffolds, delivery particles or hydrogels (Rockwood *et al.*, 2011). In which the desired characteristics can be obtained by simply change the processing conditions or by additional treatment (Malay, 2005;Cao, Y *et al.*, 2009).

In addition, silk fibroin protein is very environment stable when comparing to globular proteins (Vepari *et al.*, 2007) because hydrogen bonds, high hydrophobic proportion and crystallinity features enhance its stability (Altman *et al.*, 2003).

Another important property in biomaterials is its biodegradation because the material must maintain its characteristics till reach the target and then be degraded by organism, therefore should have acceptable life-span (Cao, Y *et al.*, 2009).

Silk Fibroin is defined as non-degradable by United States Pharmacopeia however this classification is set only for 60 days, and SF is degradable after this time, actually Ethicon, Inc. in patent US 4014973 (Darrell, 1973) claims that SF fibers maintain tensile strength for one year (Altman *et al.*, 2003).

SF degradation results of proteolytic enzymes mediated by a foreign body response (Cao, Y *et al.*, 2009), where studies report protease as major responsible (Kearns *et al.*, 2008). Since low molecular weight and non-compact structures are more easily hydrolysed by proteases, silk fibroin biomaterials should be designed according to the desired degradation rate (Cao, Y *et al.*, 2009), and this can be accomplished by changing crystal content, porosity including pore size and molecular weight distribution (Vepari *et al.*, 2007). Additionally, implantation site, size, geometry and surface properties also influence degradation behaviour (Altman *et al.*, 2003).

3.2.1.Silk Fibroin based-materials

The silk fibroin protein can be further processed into different materials, films, sponges, hydrogels, fibers, tubes and micro or nanoparticles (Rockwood *et al.*, 2011;Sharma *et al.*, 2011).

Currently, silk fibroin has been proposed as a material for tissue engineering, since its mechanical properties, biocompatibility and biodegradability, would enable its use *in vivo* and the degradation rate would be similar to the new tissue growth (Yang *et al.*, 2012). In fact, Inouye *et al.* findings in use of silk fibroin film in several culturing animal cells as a substratum, concluded that silk fibroin are able to support cell attachment, physiological morphology and growth (Altman *et al.*, 2003). In addition, Altman, 2003 studies concluded that SF films induced bone tissue growth *in vitro* and Sugihara, 2000 studies shown that they heal full thickness skin wounds in rats faster than traditional porcine-based wound dressings (Vasconcelos *et al.*, 2012;Sugihara *et al.*, 2000;Altman *et al.*, 2003). Besides, SF films can also be applied for DD by encapsulating bioactive molecules within the film (Mandal, BB *et al.*, 2009).

SF use as three-dimensional (3D) porous scaffolds provides a microenvironment for cell attachment, proliferation, differentiations and tissue neogenesis (Zhang, Q *et al.*, 2009), and have been used in a number of studies for connective tissue regeneration (Vepari *et al.*, 2007). As reported in Meinel *et al.*, 2005, this structures have been reported to regenerate and heal femur deficiencies in rats (Vepari *et al.*, 2007).

Hydrogels, by definition, are 3D polymer networks non-dissolving and physically durable to swelling in aqueous solutions (Vepari *et al.*, 2007). This structures when constituted by a biocompatible material, like silk fibroin, can be applied in biomedical applications, for example in soft tissue regeneration (Rockwood *et al.*, 2011) and drug delivery for wound healing.

SF hydrogels structure is mainly dependent on β-sheets content (Vepari *et al.*, 2007), indeed during gelation process, increase of hydrophobic interactions, van der Waals forces and hydrogen bonds, lead to structural transition of random-coil to β-sheets (Zhang, Q *et al.*, 2009). To better understand, SF hydrogel formation is further detailed in Annex II, in Annexes section.

Silk fibroin fibers possess the unique ability to be weaved into a wipe-rope geometry, and since it design can be controlled, is possible to achieve the desired final mechanical properties (Altman *et al.*, 2003). Their high functionality, surface area and porosity; and their ability to improve cell migration and proliferation, also allows its use in tissue regeneration and as DDS (Zhang, X *et al.*, 2011). In effect, SF wipe-rope with mechanical properties similar to the human anterior cruciate ligament (ACL) are used as biomaterial replacements for ligaments in tissue regeneration (Vepari *et al.*, 2007).

Currently, silk fibroin based-particles have been proposed as controlled drug release and delivery system, since is a biocompatible material and presents a well-defined model for degradation and drug release (Wang, X *et al.*, 2007) due to the control of the β-sheets formation (Hofmann *et al.*, 2006).

The micro and nanospheres have been produced by various methods, like emulsification (already discussed in section II. 1.1.1) spray-drying, lipid vesicles, and others. In detail, production using spray-drying method enables formation of 100 μm particles, yet in this process high temperatures are involved, limiting its use for SF drug release (Wang, X *et al.*, 2007). In addition, preparation of SF micro and nanoparticles under mild processing conditions recommends lipid vesicles methodology, which uses lipid templates to shape the microspheres however it uses toxic compounds, such as methanol (Wang, X *et al.*, 2007).

Interestingly, Silk has been developed as a microneedles system (500 μm of height and 10 μm of tip radii) to deliver precise amounts of drugs over time by Biomedical Engineering department of Tufts University (Tsioris *et al.*, 2012). This silk-based microneedle system presents the following advantages: no-need of refrigeration, easy production process, painless, environmental-friendly material, biodegradable and biocompatible (Tsioris *et al.*, 2012).

4. Photoaging and Wrinkle Formation

Photoaging, also known as extrinsic aging, refers to skin histology alterations caused by ultraviolet (UV) radiation exposure (Rijken, 2011). In general, the most prominent characteristic of skin ageing is wrinkles formation (Imokawa, 2008), yet is also characterized by dryness, rough texture, loss of skin tone and deep creases (Rijken, 2011).

Is important to note that tissues are not solely composed by cells, it exists extra-cellular space, termed as extra-cellular matrix (ECM) (Satardekar *et al.*, 2010). By definition, ECM surrounds connective tissue cells and is composed of glycosaminoglycans connected with fibrous matrix proteins like collagen, elastin and fibronectin, providing structural support to the tissues (Satardekar *et al.*, 2010).

Normal dermis skin consists in a complex network of collagen and elastic fibers that provide elasticity and resistance to the skin, maintaining its shape and texture (Rijken, 2011). These fibers are connected by mucopolysaccharide gel (Weedon, 2002), and are both produced by fibroblast, the main cells of connective tissues (Rijken, 2011).

Collagen fibers, which constitute ~70-80% of skin, are composed by collagen molecules connected in triple helices structures and responsible for skin strength and toughness (Rijken, 2011;Weedon, 2002).

Elastic fibers are protein bundles localized parallel or radially to the epidermis composed by elastin, main component of elastic fibers (~90%) that provides skin elasticity, and microfibril, which includes fibrilin and glycoproteins (Rijken, 2011). Degeneration of these elastic fibers results in accumulation of elastotic material, mainly abnormal elastin, also called Actinic Elastosis when caused by solar damage (Rijken, 2011).

Studies reported that loss of skin elasticity leads to wrinkle formation, which is induced by age and cumulative exposure to sunlight (Imokawa, 2008). The physicochemical and biological mechanisms involved in wrinkle formation are not entirely understood, as a result various mechanisms have been proposed for this process (Imokawa, 2008). In fact, elastotic material hypothesised to be caused by degradation of elastic fibers and/or collagen fibers, and/or by abnormal stimulation of fibroblasts (Rijken, 2011). Furthermore, UV radiation easily affects the skin, entering through different skin chromophores (like melanin, DNA, RNA, proteins, lipids, water, aromatic amino acids, among others) and leading to photochemical reactions, production of reactive species of oxygen (Hofmann *et al.*), and consequently to harmful effects and skin damage (Roy *et al.*, 2012).

The most plausible mechanism suggests that cellular damage caused by UV exposure leads to production of basement membrane-permeable biological factors that induce dermal fibroblasts (Imokawa, 2008). These cells rapidly induce inflammatory responses, including neutrophils migration, which directly express elastases and indirectly produce matrix metalloproteins (MMPs), that degrade elastic and break collagen fibers, respectively (Imokawa, 2008;Rijken, 2011;Takeuchi *et al.*, 2010). These mechanism is supported by Imokawa findings, in which they observed that: UV radiation *in vivo* studies significantly reduced elastic properties of skin, resulting in wrinkles; and *in vitro* studies of cultured human fibroblasts secreted cytokines, which stimulated elastase and leaded to wrinkle formation too (Imokawa, 2008). For better elucidation, the mechanism that causes aging and wrinkle formation disorders is represented in Figure II.7.

Additionally, UV radiation in skin also affects antioxidation, decreasing levels of antioxidants and inactivating of antioxidant enzymes, and increasing markers of lipid peroxidation in skin, leading to other skin disorders, such as hyper pigmentation (Roy *et al.*, 2012).
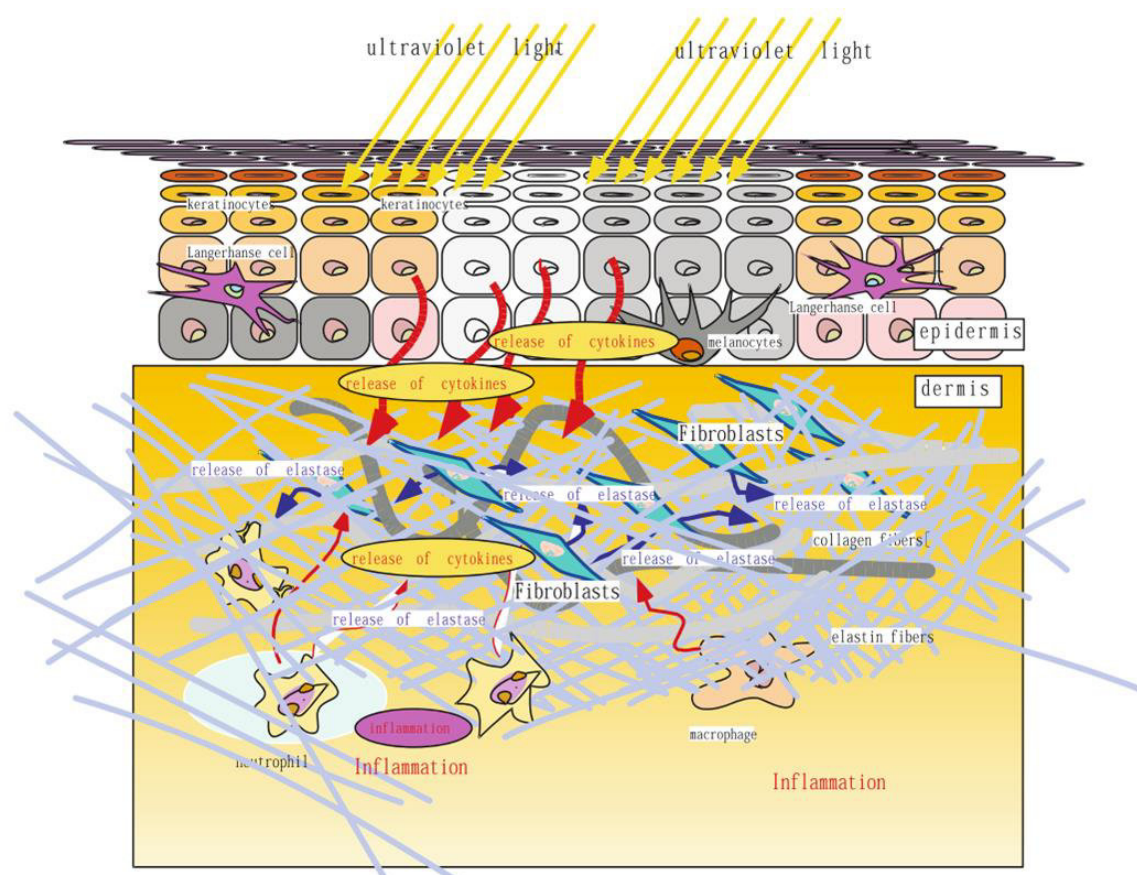
Figure II.7. Schematic diagram of the current hypothetical model for photoaging adapted from Imokawa, 2008, where UV radiation induces release of biologic factors, namely cytokines and proteolytic enzymes from neutrophils like elastases capable of disrupt collagen and elastin proteins of ECM in dermis.

Neutrophil-derivated proteolytic enzymes, like Neutrophil Elastase (NE) are also capable of producing ROS by the membrane-associated nicotinamide adenine dinucleotide phosphate (NADHP) oxidase enzyme complex (Rijken, 2011). These oxidase-derived oxygen metabolites, ROS, can lead to overwhelming responses that ultimately damage the ECM proteins, like collagen and elastin (Rijken, 2011), and consequently producing histochemical changes in skin, such as thickening of stratum spinosum (epidermal layer, deeper than SC) and flatting of dermoepidermal junction (Roy *et al.*, 2012).

To be noted, solar UV (wavelengths 100-400 nm) is classified into UVA, UVB and UVC, which only UVA and UVB are capable of reaching earth's surface though UVB is mostly blocked by stratospheric ozone layer (Rijken, 2011). Regarding to UV skin damage, UVA penetrates deeply into skin than UVB and is the main inducer of ROS however UVB is more energetic and considered as more harmful (Rijken, 2011).

4.1. Human Neutrophil Elastase

Polymorphonuclear Neutrophils or Leukocytes (PMNs), the most abundant type of phagocyte, acts in inflammation and immune responses as protection against pathogenic organisms and cell(s) damage by healing or destroying tissues (Rijken, 2011). In fact, PMNs cells provide a primary line of defence against bacterial infection, being the first cells to arrive to the site of inflammation (Korkmaz *et al.*, 2008).

The oxidative and proteolytic potential of neutrophils enables ECM degradation (Wagner *et al.*, 1999), allowing them to rapidly migrate between tissues, but also to participate in tissue remodelling/repair, wound healing, coagulation and fibrinolysis (process that prevents blood clots) (Owen *et al.*, 1999). In spite of this capability, when excessive, can lead to various diseases or abnormalities (Owen *et al.*, 1999).

PMNs proteolytic depends of proteinases, which cleave peptide bonds in the central regions of polypeptides of proteins (Owen *et al.*, 1999). One of the most abundant neutral proteinases present in PMNs is Elastase (EC 3.4.21.11) (Weitz *et al.*, 1986).

Human neutrophil elastase (HNE), also called Human leukocyte elastase (HLE), belongs to serine proteinase of the chymotrypsin family (Korkmaz *et al.*, 2008), presenting a catalytically essential serine residue in the enzyme (Owen *et al.*, 1999), which are mostly stored in granules of azurophilic neutrophils (Weitz *et al.*, 1986;Woodman *et al.*, 1993) but are also found in monocytes (Hajjar *et al.*, 2010). Is extremely cationic and possess an isoelectric point (pI) of pH 10-11 and demonstrates optimal activity at neutral pH (pH 7-9) (Owen *et al.*, 1999).

Structurally, HNE is a glycoprotein composed by 218 a.a. in a single polypeptide chain and two asparagine-linked carbohydrate side chains and its active-site is on catalytic triad Asp[102], His[57] and Ser[195] residues (Owen *et al.*, 1999), which is separated in the primary structure but joined in their tertiary structure (Korkmaz *et al.*, 2008). In the 3D HNE secondary structure (Figure II.8), the active-site residues are established between two fold β-barrels domains composed by six anti-parallel β-sheets, each, typical to all chymotrypsin-like serine proteins (Hajjar *et al.*, 2010;Korkmaz *et al.*, 2008). Besides, it possesses a carboxyl-terminal segment disposed in α-helix (Korkmaz *et al.*, 2008).
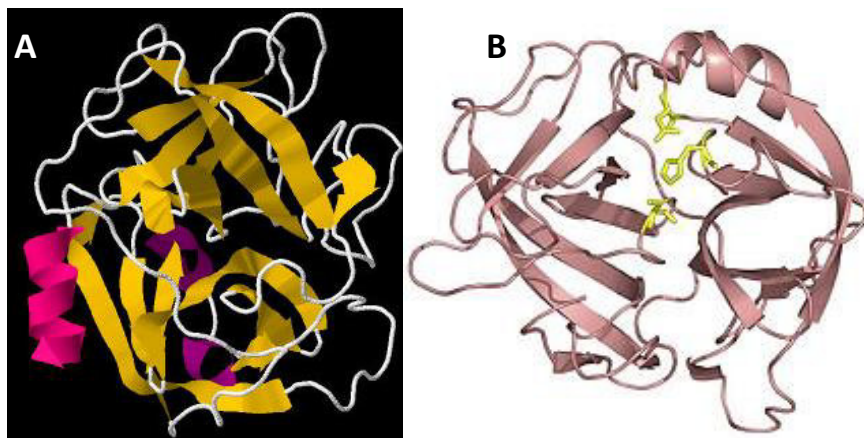
Figure II.8. Ribbon representation of uncomplexed secondary structure of Human Neutrophil Elastase. Legend: (A) Image performed in jmol, stored in PDB with ID 3Q76, where yellow represents β-strands; pink represents α-helix; violet represents β-turns; and white does not represents any defined structure; (B) Image adapted from Korkmaz *et al.*, 2008, which PDB ID is 1PPF, where yellow represents the catalytic triad and pink represents the rest of the structure.

4.1.1. Human Neutrophil Elastase inhibition

Under normal physiological conditions, HNE activity is mostly regulated by natural endogenous serine protease inhibitors (serpins) (Siedle *et al.*, 2007), such as α_1-proteinase inhibitor (α_1-PI), α_2-macroglobulin (α_2-MG), elastase inhibitor (EI), secretory leukocyte peptidase inhibitor (SLPI), elafin, and others (Siedle *et al.*, 2007;Winiarski *et al.*, 2012). In fact, serpins account for ~2% of the total protein in human plasma, where ~70% is α_1-PI (Krowarsch *et al.*, 2003).

In more detail, serpins are larger proteins, typically composed by 350-500 a.a, and capable to adopt different conformations (Krowarsch *et al.*, 2003)**.** These type of inhibitors, (serpins) interact in a substrate-like manner, forming exposed binding loops (composed of ~17 a.a.), preventing the enzyme to act in other subtracts, and consequently inhibiting it (Krowarsch *et al.*, 2003;Moreau *et al.*, 2008).

According to literature, natural inhibitors with high MW, like α_1-PI (52 kDa), α_2-MG (~190 kDa) and EI (42 kDa), were considered more potent and powerful, but they are less effective in contact with other substrates since they are excluded at close contact, whereas low MW HNE inhibitors, like SLPI (11.7 kDa) and elafin (6 kDa), can achieve close contacts, suggesting advantage of low MW inhibitors (Kawabata *et al.*, 1991;Krowarsch *et al.*, 2003).

As previously mentioned, HNE contributes to ECM degradation in tissue damage, being the cause for various inflammatory diseases. Also, as stated in Imokawa, 2008 and Takeuchi, 2010 studies, HNE acts in wrinkle formation by repeated UV irradiation and mild inflammation (Imokawa, 2008;Takeuchi *et al.*, 2010). Thus, for HNE proteolytic activity regulation, various inhibitors have been developed. Whereas inhibitors development requires high specificity, low MW, systemic activity and FDA approval (Kawabata *et al.*, 1991).

In 1991, Kawabata and co-workers have discovered a potent and specific NE inhibitor with low MW, *N*-[2-[4-(2,2-dimethylpropionyloxy)phenylsulfonylamino]benzoyl] aminoacetic acid, termed as ONO-5046 (Kawabata *et al.*, 1991), which was further developed by Ono Pharmaceutical Co. Ltd (Osaka, Japan) as N-{2-[({4-[2,2-Dimethylpropanoyl)oxy]phenyl}sulfonylamino]benzoyl} glycine sodium, and named as sivelestat (Aikawa *et al.*, 2011).

The following figure II.9 represents the chemical structure of this HNE inhibitor, in pure state (A) and when associated with sodium, in salt form (B).
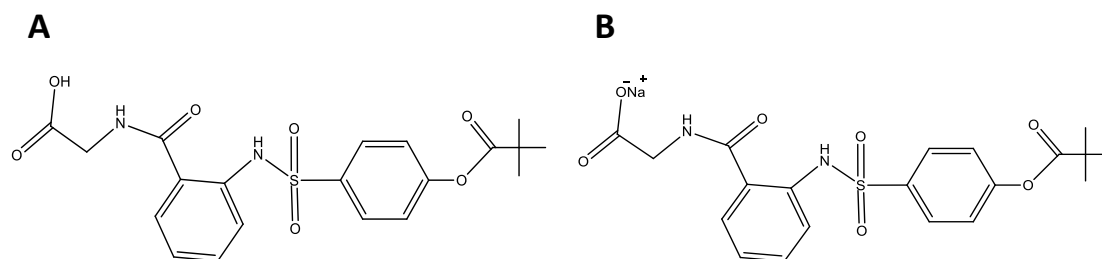
Figure II.9. Chemical structure of HNE inhibitor, ONO-5046, also named as sivelestat, in pure state (A) and in sodium (Na) salt form (B), wherein the molecular weight is 434.5 and 528.5, respectively.

In Kawabata, 1991 studies, ONO-5046 potently inhibit HNE with an half maximal inhibitory concentration (IC$_{50}$) of 0.044 ± 0.003 μM and inhibition constant (K$_i$) of 0.20 ± 0.02 μM, using succinyl-Alanine-Alanine-proline-phenylanine-p-nitroanilide (suc-Ala-Ala-Pro-Phe-pNA) as substrate; and additionally intravenous administration in guinea pigs significantly suppressed NE action in capillary permeability (Kawabata *et al.*, 1991). According to Lineweaver-Burk plot analysis of this studies, ONO-5046 inhibition showed to be competitive (Kawabata *et al.*, 1991).

Miyazaki, 1998 findings also suggested that ONO-5046 could attenuate acute lung injury (ALI) in acute respiratory distress syndrome (Edwards *et al.*), which is thought to be caused by microvascular endothelial cell damaging triggered by HNE (Miyazaki *et al.*, 1998). Miyazaki and colleagues showed that ONO-5046 attenuated the neutrophil-dependent pulmonary edema in isolated perfused rabbit lungs by inhibiting the alveolar epithelial and vascular endothelial injury caused by activated neutrophils and by reduced the shedding of thrombomodulin on the endothelium (Miyazaki *et al.*, 1998). In fact, this inhibitor (sivelestat) shown to be effective in treatment of patients with ALI associated with systemic inflammatory response syndrome (SIRS). As a result was the first drug approved for treatment of this disease, being marketed as Elaspol by Ono Pharmaceutical Co. Ltd, and approved by FDA in Japan in 2002 (Kitamura *et al.*, 2003;Takada *et al.*, 2003).

Recently, Nawa *et al.* studies suggested combinatorial use of this inhibitor (sivelestat) and trastuzumab as a therapeutically strategy for human epithelial growth factor receptor 2 (HER2)-positive breast cancer (Nawa *et al.*, 2012). In this therapy, sivelestat prevents the effect of HNE in cell growth through HER2 signalling pathway, and in combination with trastuzumab, which is a monoclonal antibody against HER2, improves the prognosis of patients with HER2-positive breast cancer (Nawa *et al.*, 2012).
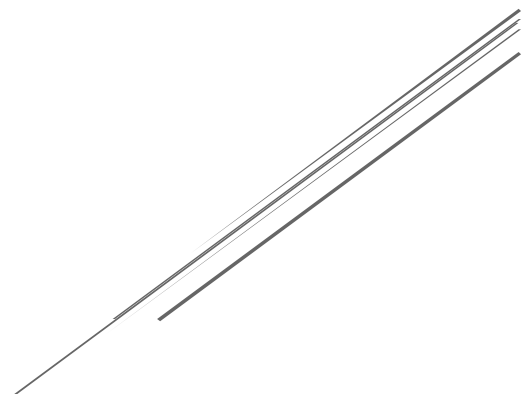
Regarding HNE inhibition for anti-wrinkling therapy, Imokawa and co-workers suggested that application of inhibitors of skin fibroblast elastase would reduce wrinkle formation (Imokawa, 2008). They also showed that N-phenetylphosphonyl-L-leucyl-L-tryptophane (NPLT) and *Zingiber officinale (L.) Rose* extract act as anti-wrinkling agents by inhibiting fibroblast elastase (Imokawa, 2008), where NPLT presented IC_{50} of 0.050 µM, using N-succinyl-tri-alanyl-p-nitroanilide (STANA) as substrate (Tsuji *et al.*, 2001).

Nonetheless, others elastase inhibitors can be suggested as anti-wrinkle agents, for example, hyperoside (IC_{50} of 0.3 µM), fukinolic acid (IC_{50} of 0.23 µM) (Siedle *et al.*, 2007), oleic acid albumin (IC_{50} of 0.26-0,42 µM, depending on formulation) (Edwards *et al.*, 2004) and other organic oils (Silva *et al.*, 2012), etc.

In conclusion, photoaging process and wrinkle formation can be significantly prevented and/or reduced by topical application of elastase inhibitors. For example, sivelestat, a potent, selective and FDA approved HNE inhibitor has been shown impressive results to control HNE-induced cell damage and consequential associated anomalies and diseases, therefore its use as anti-wrinkling agent is promising.

Chapter III.

Materials and Methods

Chapter III. Materials and Methods

Materials

Cocoons of *Bombyx mori* silkworms were kindly supplied by the CRA-APi: Unitá di Ricerca di Apicoltura e Bachicoltura (Padova, Italy). In this experimental work we used two different batches of *B. mori* cocoons due to material depletion.

Taking in consideration that environmental factors (like temperature, humidity, light, air and feed) can influence silkworm growth and development, and consequently may affect the cocoons' silk production (Rahmathulla *et al.*, 2004), the final properties of the silk fibroin solutions produced from the different batches may differ. However, the CRA-API supplier states that the silkworm breed was preserved and the feed was always maintained, preventing differences between batches. Even so, to minimize experimental error we decided to separate their use as following: the first batch was used in optimization process (being prepared as stated in section III.2 and respective results were presented in chapter IV) while the second batch was used in further nanoparticles development (being used in section III.3 and respective results in chapter V and VI).

The dialysis tubing cellulose membrane of molecular-weight cut off (MWCO) 12-14 kDa (21 mm of diameter and 33 mm of width) were purchased from Sigma-Aldrich (Spain).

The centrifugal filters devices Amicon Ultra-15 of 3kDa MWCO (volume capacity of 15 mL, 29.7 mm of diameter and 122 mm of length) used to calculate encapsulation efficiencies were purchased from Milipore Corporation (Ireland).

The kinetic assays were performed in microplate format, using 96 wells microplates (F96) from Nunc™ (Denmark).

The absorbance of orange IV assay was performed in one milliter Bio-Cell™ quartz vessels (108-000-10-40) from 230-700nm and were supplied Izasa, Werfen Group (Portugal).

Reagents

In general, all the chemicals were purchased from Sigma-Aldrich (Spain), namely, lithium bromide (LiBr, purity ≥ 99%), n-dodecane oil ($CH_3(CH_2)_{10}CH_3$, purity ≥ 99 %), poloxamer 407 (impurity ≤ 1.0% water), di(ethylene glycol) ethyl ether (termed as transcutol, purity ≥ 99 %), sodium dodecyl sulfate (SDS, purity ≥ 99 %), orange IV (sodium 4-{(E)-[4-(phenylamino)phenyl]diazenyl}benzenesulfonate; purity ≥ 99 %), elastase from human leukocytes (*i.e* HNE enzyme, purity ≥ 50 U/mg determined by Bradford), synthetic substrate *N*-methoxysuccinyl-Ala-Ala-Pro-Val-p-nitroanilide (*i.e.* HNE substrate), sivelestat sodium salt hydrate (*i.e.* HNE synthetic inhibitor, purity ≥ 98 % determined by HPLC).

While, the reagent sodium carbonate (Na_2CO_3) was purchased from Riedel-de-Haën (Germany) and Tween 80 was purchased by Merck-Schuchardt.

To be noted, all chemicals and materials used along this work were stored and manipulated according to the manufacturer's instructions and safety practices. In addition, all chemicals were used as supplied without any further purification.

Equipment

Various equipment's were used along this experimental work. To facilitate, a list of the used equipment's with their specific use in this work and supplier is summarized in a table (Table Annex. 2) in Annex III.

Methods

1. Preparation of Regenerated Silk Fibroin (RSF) Solution

Silk fibroin stock solutions were prepared as previously described (Sah *et al.*, 2010;Wray *et al.*, 2011). Initially, the cocoons were cut and cleaned from debris. Then, raw silk of the Cocoons *Bombyx mori* silkworms were boiled 3 times in an aqueous solution of Na_2CO_3 (0.05 %) during 30 minutes and washed several times with deionized water for sericin removal.

The dried degummed silk was then dissolved in 9 M LiBr for 3 hours at 60 °C and after filtration, the resulting SF solution was dialyzed in cellulose tubing (MWCO of 12-14 kDa) against double-deionized water for at least 3 days at room temperature to remove the neutral salts and LiBr.

Final solution of regenerated silk fibroin (RSF) was quantified by Bradford method for further nanoparticle formation studies, and stored at 4ºC for a maximal period of 2 weeks. Bradford method was performed according to protocol from Sigma-Aldrich technical bulletin of the Bradford Reagent. This procedure involves Bio-Rad protein assay (Bio-Rad Laboratories, GmbH) based on the shift of absorbance maximum for an acidic solution of Coomassie Brilliant Blue G-2SO at 595 nm when binding to protein occurred, and using RSF as a standard protein. Absorbance measurements were performed by Ultraviolet-Visible (UV-Vis) spectrophotometry using SynergyM with Gen5 ™ Microplate Data Collector and Analysis Software (Bio-Tek Instruments, Inc., Vermont, USA). The calibration curve of RSF used for Bradford quantification is presented in Figure Annex.1, in Annex IV.

2. Process optimization of Silk Fibroin Nanoemulsions

In order to optimize the nanoparticles formation, SF nanoemulsions were produced by an oil-in-water (o/w) emulsification using two high-energy methods, ultrasonication and high pressure homogenization (HPH). RSF solutions were emulsified in different concentrations and oil-in-water (o/w) emulsion ratios, using *n*-dodecane as oil organic phase and RSF protein dissolved in the water phase.

According to this initial optimization, a silk fibroin nanoparticles production guideline was established for further studies, since results enable method, parameters and conditions selection.

2.1. Optimization by Ultrasonic Emulsification method

Nanoemulsions by ultrasonic emulsification, to further obtain nanoparticles, were prepared by an adaptation of Bang and Suslick method (Bang *et al.*, 2010), according to previous studies conducted by our research group (Silva *et al.*, 2012;Silva *et al.*, 2012;Silva *et al.*, 2012).

The ultrasonic emulsification method was carried in a thermo-stated bath at 4ºC, for 3 minutes with percentage amplitude of 40 % as power delivery. Samples (16 mL) were placed for reaction in an open glass cell (diameter 19 mm and height 75 mm). The equipment was composed of a probe type ultrasound source (20 kHz Sonics and Materials Vibrocell ™ CV 33) fitted with a 3 mm diameter titanium micro-tip. For temperature control, the sonochemical reactor was controlled via a thermo-stated water bath with a freezer exchanger placed within a thermo jacket cell. Temperature was monitored throughout using K type thermocouples. Pictures of this equipment are presented in Figure III.1.

The volume of RSF (silk fibroin solution, water phase) at specific concentration was first added to the ultrasonic flask, and the *n*-dodecane (oil phase) was added for last. Then, the bottom of the high intensity ultrasonic horn was positioned at the interface of this two phases and the sonochemical treatment was initiated.

After emulsification, the flasks were kept at 4ºC for at least 24h until phase separation was established. Then, the *n*-dodecane oil phase (at the top of the flask) was gently removed with a micropipette. The removed *n*-dodecane oil was measured, verifying that almost the volume of oil used was recovered (up to 91 % of oil recover). Samples were closed with a rubber cap and stored at 4ºC for further characterization.

The ultrasonic emulsification was tested for 3, 5 and 10 g/L of RSF concentration and for 10/90, 20/80 and 40/60 of o/w emulsion ratios.

Figure III.1. Pictures of the Ultrasonic equipment used along this work for silk fibroin nanoparticles production. The samples placed in ultrasonic flasks were putted in contact with an ultrasound probe.

2.2. Optimization by High Pressure Homogenization (HPH) method

Production of nanoparticles by high pressure homogenization was based in previous works of our research group (Gonçalves *et al.*, 2013;Nogueira *et al.*, 2013).

SF-NPs production by high pressure homogenization (HPH) method was evaluated in two different operating systems, a single-stage and a double-stage system. The following equipment's are presented in Figure III.2.

The single-stage HPH equipment (Figure III.2-A), an Emulsiflex™-C3 (supplied from Avestin, Inc., Canada), where homogenization of 20 mL of sample was carried at 2000 bar for 12, 18, 24, 30 and 36 homogenization cycles. By this single-stage method, the following conditions were tested: 3, 5 and 10 g/L of RSF concentration and for 10/90, 20/80 and 40/60 of o/w emulsion ratios.

The double-stage HPH equipment (Figure III.2-B), an APV-2000™ (supplied from SPX Flow Technology, APV Manufacturing, Poland) and 100 mL samples passed through two homogenizing devices connected in series, the first stage at 580-600 bar and second stage at 240-250 bar, for 2, 4, 6, 8, 10, 12, 14, 16, 18, 20, 22, 24, 26 and 28 homogenization cycles. Samples by HPH emulsification using double-stage equipment were tested for 5 and 10 g/L of RSF concentration and for 10/90, 20/80 and 40/60 of o/w emulsion ratios.

In both systems, the *n*-dodecane oil phase was removed from the HPH emulsified samples according to the same procedure applied for ultrasonic method (section 2.1 of chapter III). Again, the samples were closed and stored at 4°C for further studies.
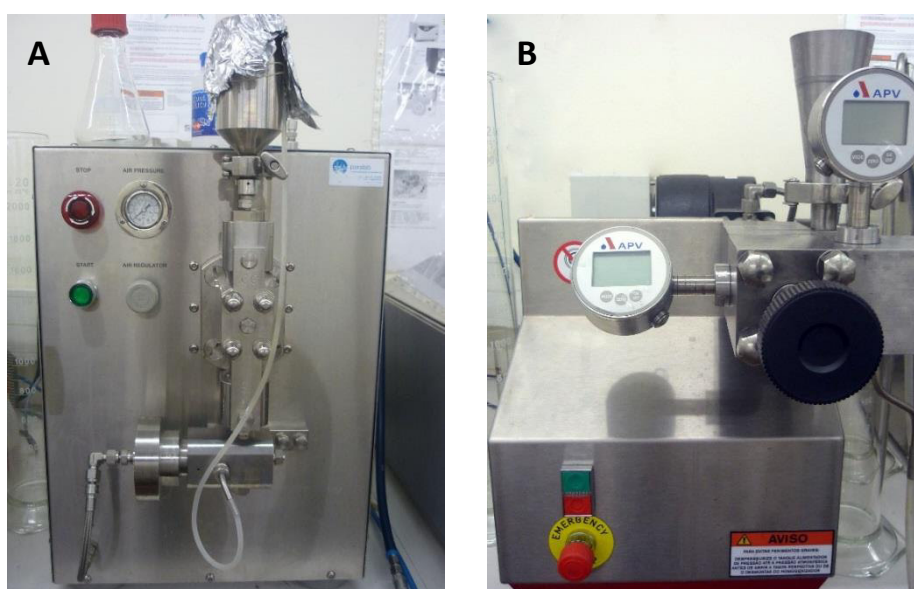
Figure III.2. Pictures of the High-pressure homogenization (HPH) equipment's used along this work for silk fibroin nanoparticles production, single-stage HPH Emulsiflex™-C3 (A) and double-stage HPH APV-2000™ (B).

3.   Preparation of Silk Fibroin Nanoemulsions and Nanoparticles

SF nanoemulsions for further studies (after optimization) were produced by double-stage HPH using an APV-2000™ homogenizer. Briefly, 80 mL of 10 g/L of RSF solution were emulsified with 20 mL of *n*-dodecane (20/80 ratio of o/w) by double-stage HPH for 22 homogenization cycles, at 580-600 bar and 240-250 bar of first and second stage of pressure, respectively. Being these conditions considered as standard/optimized.

The reproducibility of this method was assessed by repeating the SF-NPs production process at the same optimized conditions. Then, they were statistically analyzed (n=3) according to mean and standard deviation.

All compounds to add or incorporate into the silk fibroin formulations were dissolved in the water phase, as performed in previous works of our research group (Nogueira *et al.*, 2013;Silva *et al.*, 2012;Silva *et al.*, 2012).

3.1. Stabilizers incorporation in silk fibroin nanoemulsions formulation

Stability studies of silk fibroin nanoparticles was performed by combining several stabilizers with RSF solution and then, emulsified at the optimized production conditions. The tested stabilizers were poly(ethylene glycol)-*block*-poly(propylene glycol)-*block*-poly(ethylene glycol) (often termed as poloxamer 407), di(ethylene glycol) ethyl ether (commonly called by transcutol), polyoxyethylene 80 sorbitan monooleate (usually referred as tween 80) and sodium dodecyl sulfate (SDS). The respective molecular weight, molecular formula and structure of the tested stabilizers are summarized in Annex V.

Briefly, each of these stabilizers was completely dissolved in 1% of concentration in the RSF solutions (80 mL) and then, emulsified with 20 mL of *n*-dodecane at the optimized conditions (22 homogenization cycles and 580-600 bar and 240-250 bar of first and second stage of pressure, respectively).

3.2. Loading Compounds in Silk Fibroin Nanoemulsions

Incorporation of a model-drug, orange IV, and HNE inhibitor, sivelestat, in silk fibroin nanoparticles was also tested. Their chemical information is presented in Annex VI.

Orange IV at 50 µM, 75 µM and 100 µM and sivelestat at 100 µM were individually added to 80 mL of RSF solution (10g/L of concentration). After complete dissolution, these solutions were placed in the double-stage homogenizer, layered with 20 mL of *n*-dodecane (20/80 of o/w ratio), and emulsified at the standard conditions.

In addition, their stability effect in the SF-NPs was also assessed.

4. Human Neutrophil Elastase (HNE) studies

This dissertation intends to produce a human neutrophil elastase (HNE) enzyme inhibition system, in order to apply it as an anti-wrinkling agent. Therefore is important to first conduct a control of this enzyme normal behaviour, *i.e.* evaluate the HNE kinetic without inhibition, and then with an inhibitor, in this case, sivelestat.

4.1. HNE activity determination and Inhibition by Sivelestat

The human neutrophil elastase (HNE) activity was assayed with the chromogenic synthetic substrate *N*-methoxysuccinyl-Ala-Ala-Pro-Val-*p*-nitroanilide (MeOSuc-Ala-Ala-Pro-Val-pNA), in accordance with the protocol supplied by Sigma-Aldrich. In this assay, the enzymatic hydrolysis of the substrate is followed by *p*-nitroaniline release, allowing it detection by the increase of absorbance.

The normal HNE activity assay consisted in mixing 15 μL of HNE enzyme at 0.5 U/mL with MeOSuc-Ala-Ala-Pro-Val-pNA substrate at various concentration (25, 50, 100, 200, 400, 600, 800 and 1000 μM), then the final volume was completed with the reaction buffer 0.1M HEPES + 0.5M NaCl, pH 7.5. The assay control (blank) consisted only in buffer and substrate mixture, without HNE.

The HNE Inhibition assays with synthetic inhibitor sivelestat consisted in incubating 15 μL of HNE (0.5 U/mL) and 15 μL of sivelestat at various concentration (0.1, 0.25, 0.5, 1, 1.5, 2, 2.5 and 5 μM) for 5 minutes. Then, the mixture was added to the microplates, which already contain the reaction buffer and various concentration of MeOSuc-AAPV-pNA substrate (25, 50, 100, 200, 400, 600, 800 and 1000 μM).

All enzyme assays were conducted at 37°C for 10 minutes in microplates of 300 μL and absorbance were measured in triplicate (n=3) at 405 nm by UV-Vis spectrophotometry.

5. Characterization of developed Silk Fibroin Nanoparticles

The SF nanoemulsions were further characterized in order to determinate the produced NPs properties.

In optimization process, initial characterization consisted in mean diameter and heterogeneity of the produced nanoparticles using dynamic light scattering (DLS) in ZetaSizer Nano ZS equipment. Then, in a second phase, the nanoparticles yield through formation efficiency was determined by Bradford method using UV-Vis spectrophotometry.

SF-NPs further developed with the optimized parameters were characterized as referred above but also, according to surface charge using laser Doppler anemometry (LDA) in ZetaSizer Nano ZS equipment.

For NPs incorporated with orange IV and sivelestat, encapsulation efficiency was determined for both, drug release studies of incorporated orange IV were performed by dialysis bag method and HNE inhibition studies for incorporation with sivelestat was performed by kinetic HNE studies.

Then, secondary structure conformation changes were evaluated by Fourier Transform Infrared (FTIR) Spectroscopy, before and after emulsification, being also studied the differences between non-encapsulated and encapsulated nanoparticles.

5.1. Yield of Silk Fibroin Nanoparticles

In nanoemulsification process, not all SF protein used in formulation forms nanoparticles. Therefore is important to determinate the yield (%) of nanoparticle production, which can be determined by Formation efficiency, presented in the following equation (Equation III.1).

$$Formation\ Efficiency\ (\%) = \frac{[\text{Protein}]\text{initial} - [\text{Protein}]\text{final}}{[\text{Protein}]\text{final}} \times 100$$

Equation III.1. Determination of efficiency of nanoparticles formation, also referred as yield of nanoparticles.

Formation efficiency of SF-NPs was performed by ultracentrifugation using Allegra® X-15R Centrifuge with an FX6100 rotor (Beckman Coulter, Inc., California, EUA), at 10,000 rpm (10,976 g) for 60 minutes, in order to separate the free SF protein of the nanoparticles.

The supernatant of each sample was collected and quantified by Bradford method in UV-Vis spectrophotometry. RSF protein was used as calibration, calibration curve presented in Annex IV. The determination was conducted in triplicate (n=3).

5.2.   Size and PDI by Dynamic Light Scattering (DLS)

The produced SF-NPs were first characterized according to size by mean diameter values and size distribution by polydispersity index (PDI) values. These measurements were conducted immediately after the emulsification process and over time (up to 2-5 weeks) in order to study their stability, being the samples stored at 4ºC.

These characterization was determined by dynamic light scattering (DLS), also known as photonic correlation spectroscopy (PCS), being this technique further detailed in Annex VII.

These measurement were evaluated in ZetaSizer Nano ZS, a Malvern Zetasizer equipment (Worcestershire, United Kingdom), where 800 µL of sample were placed in disposable low volume polystyrene cells (ZEN0112) and analyzed at 25°C using a He-Ne laser of 633 nm and a detector angle of 173°. In addition, the Malvern dispersion technology software version 7.01 (DTS) (Worcestershire, UK) was used with multiple narrow mode (high-resolution) data processing, and mean size (nanometer), and error values were considered, being analyzed in triplicate (n = 3).

5.3. Surface charge by Laser Doppler Anemometry (LDA)

Nanoparticles were further characterized according to their surface charge, for that the zeta-potential (ζ) value of the samples was determined by laser Doppler anemometry (LDA) using ZetaSizer Nano ZS (same equipment used for size and PDI determination, section III.5.2). The LDA method is further detailed in Annex VIII.

The zeta-potential measurements were evaluated in the same conditions as in size and PDI determinations (section III.5.2), with the difference that samples were placed in folded capillary cells (DTS1060).

5.4. Stability studies

To evaluate the stabilizers, orange IV and sivelestat effect in silk fibroin nanoparticles, measurements of mean diameter and polydispersity index were performed at time of production and over time, once a week, from 2-4 weeks. Evaluation of these results consisted in statistical determination of standard deviation.

5.5. Encapsulation efficiency of Orange IV in Silk Fibroin Nanoparticles

Orange IV was used through this experimental work as a model-drug compound in order to predict and define a drug release profile.

This compound was loaded in the silk fibroin nanoparticles during high-pressure homogenization (HPH) process, as described in loading Compounds in silk fibroin nanoemulsions (section III.3.2).

After emulsification process, samples were placed in centricon tubes (MWCO of 3 kDa) and ultracentrifuged at 5,000 x g (6,749 rpm) for 45 minutes. According to this method, the free (non-encapsulated) orange dye passed through the tube filter since its molecular weight is lower than 3 kDa, whereas when orange IV is loaded in the nanoparticles, their molecular weight is higher, limiting their passing thought the filter.

Then, the orange IV concentration of the supernatant (liquid that passed thought the filter) was measured in triplicate (n=3) at 240 nm by UV-Vis spectrophotometry. This quantification was performed using a standard calibration curve of orange IV, presented in Figure Annex.1, in Annex IX.

Finally, the encapsulation efficiency of orange IV-loaded SF nanoparticles was determined in triplicate, according to Equation III.2.

$$Encapsulation\ Efficiency\ (\%) = \frac{[\text{orange IV}]\text{initial} - [\text{orange IV}]\text{final}}{[\text{orange IV}]\text{final}} \times 100$$

Equation III.2. Determination of encapsulation efficiency of orange IV-loaded in nanoparticles.

5.6. *In vitro* Orange IV Release Studies by Dialysis bag method

Before loading the drug sivelestat in the SF-NPs, studies with a model-drug compound orange IV were first conducted to establish a model of incorporation and drug release. For that, i*n vitro* release behaviour of SF-NPs loaded with 100 μM of orange IV were assessed in dialysis bag method, according to the procedure used in various studies (D'Souza *et al.*, 2006;Nounou *et al.*, 2006;Shazly *et al.*, 2008;Silva *et al.*, 2012). Briefly, samples (total volume of 2 mL) were placed in dialysis bag (cellulose membrane, MWCO 12-14 kDa), sealed and immersed in 10 mL of deionized water, with continuous magnetic stirring (200 rpm) at room temperature for 140 hours.

Release studies were performed in triplicate (n=3) for the following conditions: SF-NPs incorporating orange IV, free orange IV (87 μM) dissolved in 10g/L of RSF solution and solution of orange IV (87 μM), with and without HNE enzyme (0.5 U/mL).

To be noted, the used sample of SF-NPs incorporated with orange IV was retrieved from the top of the tube after ultracentrifugation applied in encapsulation efficiency of orange IV in SF-NPs determination (section III.5.5), so this sample only possessed the incorporated orange IV.

Then, at predetermined time intervals, dialysis volume were withdrawn and replaced again with deionized water. Orange IV concentration was measured in triplicate at 240 nm by UV-Vis spectrophotometry, using a standard calibration curve of orange IV, presented in Annex IX.

To better understand the orange IV release behavior, the orange IV release kinetics was evaluated by fitting the release data in a mathematical empirical relationship defined by the Ritger-Peppas equation (Ritger *et al.*, 1987), presented above in Equation III.3.

$$\frac{M_t}{M_\infty} = k \times t^n$$

Equation III.3. Ritger-Peppas equation used to define release behaviour of compounds from polymeric systems, where M_t/M_∞, k, t and n represent the fractional release of the compound, constant incorporating characteristics of the macromolecular network system, release time and diffusional exponent characteristic of the release mechanism, respectively. Based in Ritger *et al.*, 1987 publication.

The diffusional exponent, *n* value, indicates the mechanism of transport of the released compound to the exterior medium, in this case the orange IV release (Ritger *et al.*, 1987). Considering Silva *et al.* method, this value can be determined by transforming the Ritger-Peppas equation in a linear function, where *n* is the slope value of the plot log (% released) *versus* log (t), as described in Equation III.4 (Silva *et al.*, 2012).

$$log\left(\frac{M_t}{M_\infty}\right) = log\,(\% \text{ released}) = log\,(t) \times n + log(k)$$

Equation III.4. Ritger-Peppas modified equation used to determinate *n* value, where M_t/M_∞, % released, *k*, *t* and *n* represent the fractional release of the compound, the percentage of compound released, constant incorporating characteristics of the macromolecular network system, release time and diffusional exponent characteristic of the release mechanism, respectively. Based in Ritger *et al.*, 1987 and Silva *et al.*, 2012 publications.

5.7. Encapsulation efficiency of Sivelestat in Silk Fibroin Nanoparticles

Sivelestat was also loaded in the silk fibroin nanoparticles during emulsification by high-pressure homogenization (HPH), as stated in section III.3.2. This method is similar to the one applied for orange IV (section III.5.5) differing in the quantification assay since sivelestat could not be individually detected by UV-Vis Spectrometry.

Emulsified sample of sivelestat 100 µM loaded in silk fibroin nanoparticles were placed in centricon tubes (MWCO of 3 kDa) and ultracentrifuged for 45 minutes at 5,000 x g (6,749 rpm). The encapsulated sivelestat was confined in the top of the tube while the free (non-encapsulated) sivelestat passed through the tube filter (supernatant).

Sivelestat concentration in the supernatant was further submitted to kinetic assays at 405 nm in microplates of 300 µL by UV-Vis spectrophotometry. In this kinetic assay, the enzyme used was human neutrophil elastase (HNE) at 0.5 U/mL and *N*-methoxysuccinyl-Ala-Ala-Pro-Val-p-nitroanilide (MeOSuc-Ala-Ala-Pro-Val-pNA) as substrate. Quantification was performed in triplicate (n=3) using a standard calibration assay of the HNE inhibition studies (section III.4.1) by extrapolation.

5.8. HNE inhibition studies of silk fibroin Nanoparticles

The HNE inhibition effect of the developed SF-NPs loaded with sivelestat was assessed as described in section III.4.1.

Briefly, 15 µL of HNE (0.5 U/mL) was incubated with 15 µL of SF-NPs loaded with 100 µM of sivelestat sample for 5 minutes. Then, the incubation mixture was added to the microplates, previously set with the reaction buffer 0.1M HEPES + 0.5M NaCl, pH 7.5 volume and MeOSuc-Ala-Ala-Pro-Val-pNA substrate at different concentrations (25, 50, 100, 200, 400, 600, 800 and 1000 µM). The kinetic assays at 37°C for 10 minutes and absorbance were measured in triplicate at 405 nm by UV-Vis spectrophotometry.

The control (blank) of the assay, *i.e.* without inhibitor sivelestat, consisted in the following: a control without enzyme HNE using only buffer and substrate mixture; a control to establish the normal kinetic behaviour of the HNE enzyme using buffer, substrate and HNE enzyme mixture; and a control to evaluate the SF effect in HNE activity using buffer, substrate, HNE and RSF solution.

In this assay, we used the silk fibroin and sivelestat nanoemulsion sample retrieved from the top of the tube after ultracentrifugation applied in encapsulation efficiency of sivelestat in SF-NPs determination (section III.5.6). This way, the sample used does not possess residual (non-encapsulated) sivelestat, *i.e.* only possess the incorporated sivelestat.

5.9. Structural analysis by Fourier Transform Infrared (FTIR) Spectroscopy

Silk fibroin nanoparticles were analyzed by Fourier transform infrared (FTIR) spectroscopy to quantitatively assess their protein secondary structure, namely the differences that emulsification process may cause (Yampolskaya *et al.*, 2005). This method was applied for the following samples: silk fibroin solution at 10g/L of concentration, SF nanoparticles, SF nanoparticles loaded with 100 μM of orange IV and SF nanoparticles loaded with 100 μM of sivelestat.

The FTIR spectra of the lyophilized silk fibroin solution and produced nanoparticles were recorder in transmission mode between wavenumber 600 and 4000 cm^{-1} using Jasco FT/IR 4100 spectrometer equipped with attenuated total reflectance (ATR) accessory (JASCO, Inc., Easton, USA), with 128 scans and a resolution of 8 cm^{-1}. The resulting spectra were further carbon dioxide (CO_2) removed according to Jasco software, and in addition to the fact that samples were lyophilized, it allows a more accurate analysis.

Gaussian deconvolution of Amide I band region (wavenumber between 1600 and 1700 cm^{-1}) was analyzed using OriginPro 8.5 software (OriginLab Corporation, MA, USA). In deconvolution analyze, a linear baseline was fitted; the number of components and their peak position were determined according to the second derivative spectrum of this same region; and the secondary structure content was calculated from the areas of the assigned peak as percentage fraction of the total area of the Amide I range. Using Gaussian function, all data were treated manually in three fitting modes: first, the base line was held fixed and fitted while intensity and bandwidth was allowed to vary, then, the base line and bandwidth were fixed and fitted again, and finally, the base line and center peaks were fixed and fitted once more. The deconvulated frequencies were then assigned to the respective secondary structure (β-sheet, β-turns, random-coil, α-helix and 3_{10}-helix) according to Kong *et al.,* 2007 and Dong *et al.*, 1992 publications (Dong *et al.*, 1992;Dong *et al.*, 1992;Kong *et al.*, 2007)**.**

Chapter IV:

Optimization Production Process of SF-NPs

by High-energy Emulsification Methods

Chapter IV: Optimization Production Process of SF-NPs by High-energy Emulsification Methods

In order to develop SF-NPs for HNE inhibitor incorporation it is important to optimize the nanoparticles production process. Since the emulsification process are extensively applied in biopolymeric nanoparticles for cosmetic nanoparticles, we decided to use this method (Buzea *et al.*, 2007;Patel *et al.*, 2011;Pathak *et al.*, 2009;Sundar *et al.*, 2010). Briefly, emulsification method involves mixture of an oil and water phases into emulsions, that can consequently lead to emulsions at a nano range and to nanoparticle formation when extreme high shear stress is applied (Mason *et al.*, 2006;Mason *et al.*, 2006). Therefore, we used two high-energy methods, ultrasonication and high pressure homogenization (HPH). Besides, since the NPs production method delineates the final SF-NPs characteristics, we tested various conditions of production, namely SF concentration and emulsion ratio.

In this work, the selection of the oil phase and the optimization variables were based on the previous works of our research group (Gonçalves *et al.*, 2013;Nogueira *et al.*, 2013;Silva *et al.*, 2012;Silva *et al.*, 2012). In detail, choice of oil *n*-dodecane was based in Silva and co-workers studies, in which they produced Bovine Serum Albumin (BSA), Human Serum Albumin (HSA) and Silk Fibroin (SF) nanoparticles with this oil and obtained great NPs yield, diameter and PDI by sonochemical treatment and also showed that release of this oil from the nanoparticles reduced the activity of human neutrophil elastase (HNE) (Silva *et al.*, 2012).

This optimization will enable us to design the best possible method and respective conditions to produce silk fibroin nanoparticles with the desirable characteristics at the less possible resources.

In this optimization step, the produced nanoparticles were first characterized by simple measurement of mean diameter and polydispersity index (PDI), in which we intended to obtain the smallest possible values, namely ideal nanoparticle diameter would be less than 200 nm and ideal PDI would be below 0.1. To be noted, PDI value features the NPs size distribution and ranges from 0 to 1, being 1 indicative of large variation of size and 0 of absent variation (Schiffelers *et al.*, 2005).

Then, the best considered formulations were further characterized by formation efficiency determination, in which the purpose was to obtain the highest possible nanoparticles yield values.

The results for nanoparticles production by ultrasonic emulsification and by high-pressure homogenization are presented in distinct sections below. This separation will enable a better selection of the optimized conditions.

1.   SF-NPs production by Ultrasonic Emulsification

The ultrasonication method is extensively used for nanoemulsions generation and further nanoparticles production (Anton *et al.*, 2008;Bang *et al.*, 2010;Lovelyn *et al.*, 2011;Naik *et al.*, 2012). In this process, the high-energy involved is created by the ultrasound waves, produced by the sonifier probe device (Bang *et al.*, 2010). These ultrasound waves generate mechanical depressions and compressions, which lead to formation of cavitation bubbles that tend to implode (Anton *et al.*, 2008;Bang *et al.*, 2010;Naik *et al.*, 2012). When the bubbles implode, the accumulated energy is released leading to entropy and instability (Bang *et al.*, 2010). Since the cavitational implosion is localized and the horn was positioned in the interface of *n*-dodecane and silk fibroin solution, the oil/water interface becomes unstable, causing oil droplet eruption into the water phase (Anton *et al.*, 2008;Bang *et al.*, 2010;Naik *et al.*, 2012). The intensification of the shock events will consequently lead to disruption of the droplets into nano range, resulting in nanoparticles production (Anton *et al.*, 2008;Bang *et al.*, 2010;Naik *et al.*, 2012).

The efficiency of the nanoparticles produced by ultrasonic emulsification depends on the emulsion composition, namely the composition of the both oil and water phases and their oil-in-water ratio, and the method parameters, such power input (amplitude) and duration time (Anton *et al.*, 2008;Naik *et al.*, 2012).

In this experimental work, silk fibroin nanoparticles were produced with *n*-dodecane as oil phase and regenerated silk fibroin (RSF) solution as water phase, at various oil/water ratio (10/90, 20/80 and 40/60) and using various concentrations of RSF (3, 5 and 10 g/L), being then characterized according to mean diameter and polydispersity index (PDI) . The results of ultrasonic optimization are presented in Figure IV.1, being the mean diameter and PDI represented in columns and points, respectively.
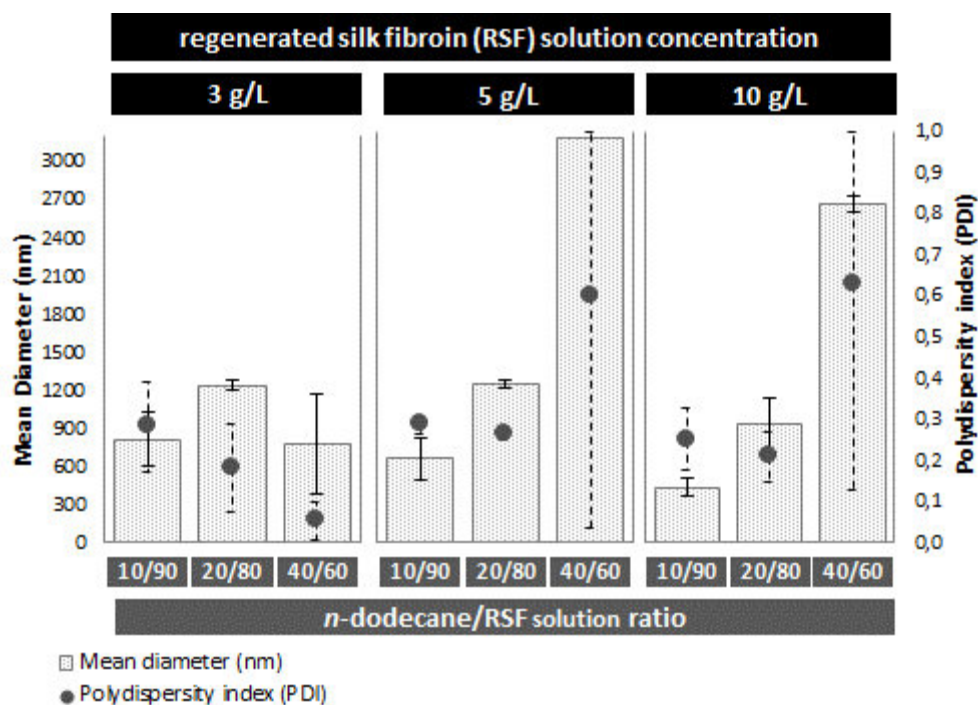
Figure IV.1. Effect of ultrasonic emulsification on silk fibroin nanoparticles production at different RSF concentrations and *n*-dodecane/RSF solution ratios. Being mean diameter in nanometers (nm) and polydispersity index value (PDI) presented in columns and points, respectively.

According to Figure IV.1, it is possible to observe some tendency that increase of SF concentration leads to smaller nanoparticles for oil/water ratio of 10/90 and 20/80, but not for 40/60. In emulsions, proteins form a macromolecular layer surrounding the dispersed particles, consequently stabilizing the nanoemulsions and the formed nanoparticles (Floury *et al.*, 2000). Therefore, an increase of concentration of protein SF promotes cover of the formed particles more easily, allowing a better control of the nanoparticles structure, namely their size, since it prevents them from losing their form (Silva *et al.*, 2012;Silva *et al.*, 2012). In addition, silk fibroin used in nanoemulsions also decreases the surface tension between the oil/water interface, facilitating the emulsification process (Floury *et al.*, 2000), hence increasing of SF concentration lead to increases the nanoemulsion formation.

Regarding the oil content, we verified that almost all samples present larger nanoparticles when the *n*-dodecane quantity is increased. This agrees with other studies that report an increase in mean diameter when the oil content in oil-in-water emulsions was increased (Floury *et al.*, 2000). According to Pandolfe *et al.*, 1995 studies, the increase of oil content decreases the interaction of the agents present in the aqueous solution (Floury *et al.*, 2000;Pandolfe, 1995). Therefore, the increase of *n*-dodecane limits the silk fibroin protein stabilizing benefits referred above, which increases the droplets size, leading to larger mean diameter particles (Floury *et al.*, 2000).

Giving this facts, higher SF concentration and lower content of organic phase enables production of smaller nanoparticles with a consistent distribution, *i.e.* smaller mean size diameter and PDI values.

In conclusion, by ultrasonic emulsification method we obtained the smaller nanoparticles (~430 nm) using 10 g/L of RSF and 10/90 of o/w ratio, wherein the respective polydispersity index (PDI) value was 0.251. Regarding this production method, we considered this formulation as the best, even so the obtained characteristics were not ideal, being necessary to evaluate the effect of high-pressure homogenization process in nanoparticles production.

2.   SF-NPs production by High-pressure homogenization (HPH)

Emulsification by high-pressure homogenization was conducted by two types of homogenization, a single and a double-stage system. A single-stage homogenization system contains only one homogenization device, being one stage of pressure involved, whereas a double-stage system possesses two homogenization devices connected in series.

2.1.   Production using HPH single-stage system

Nanoemulsions of *n*-dodecane and RSF were tested at the following conditions: oil/water ratio of 10/90, 20/80 and 40/60 and at RSF concentrations of 3, 5 and 10 g/L. The nanoparticles were characterized according to mean diameter and polydispersity index (PDI), being this measurements mainly performed in 6 cycles, from 6 to 36 cycles of homogenization. The results for silk fibroin nanoparticles production by HPH single-stage are above, in Figure IV.2, in which (A), (B) and (C) present the values obtained for RSF at 3, 5 and 10 g/L, respectively.
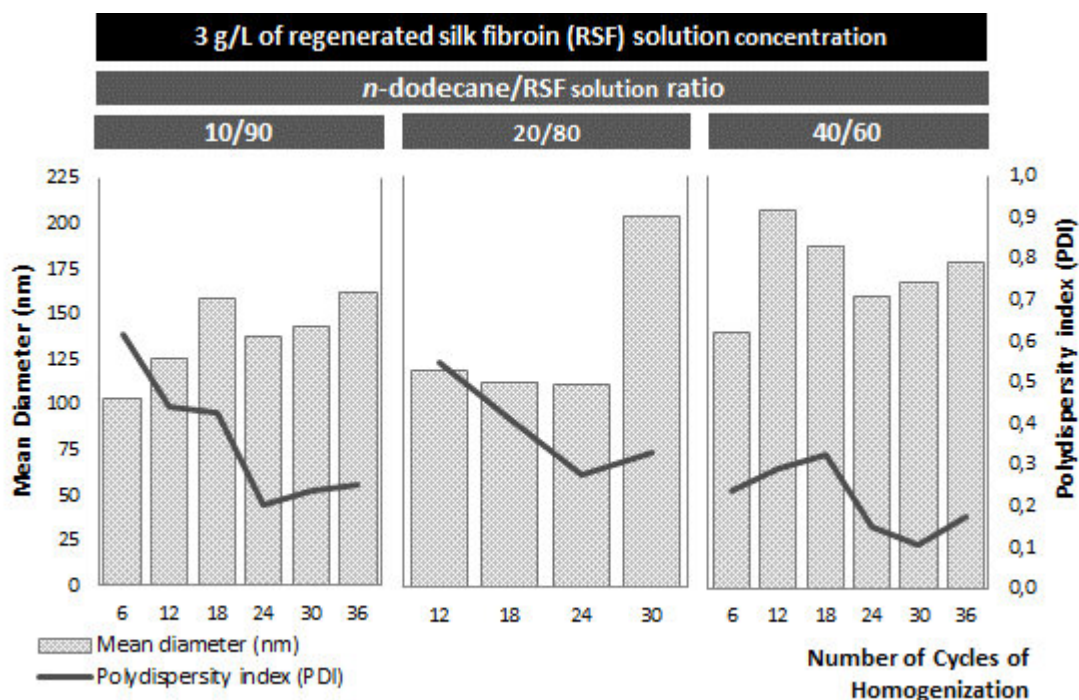
Figure IV.2. (A) Effect of emulsification by single-stage HPH (EmulsiFlex™-C3) on silk fibroin nanoparticles production for 3 g/L of RSF concentration at various *n*-dodecane/RSF solution ratios, along several homogenization cycles. Being mean diameter in nanometers (nm) and polydispersity index value (PDI) presented in columns and lines, respectively.
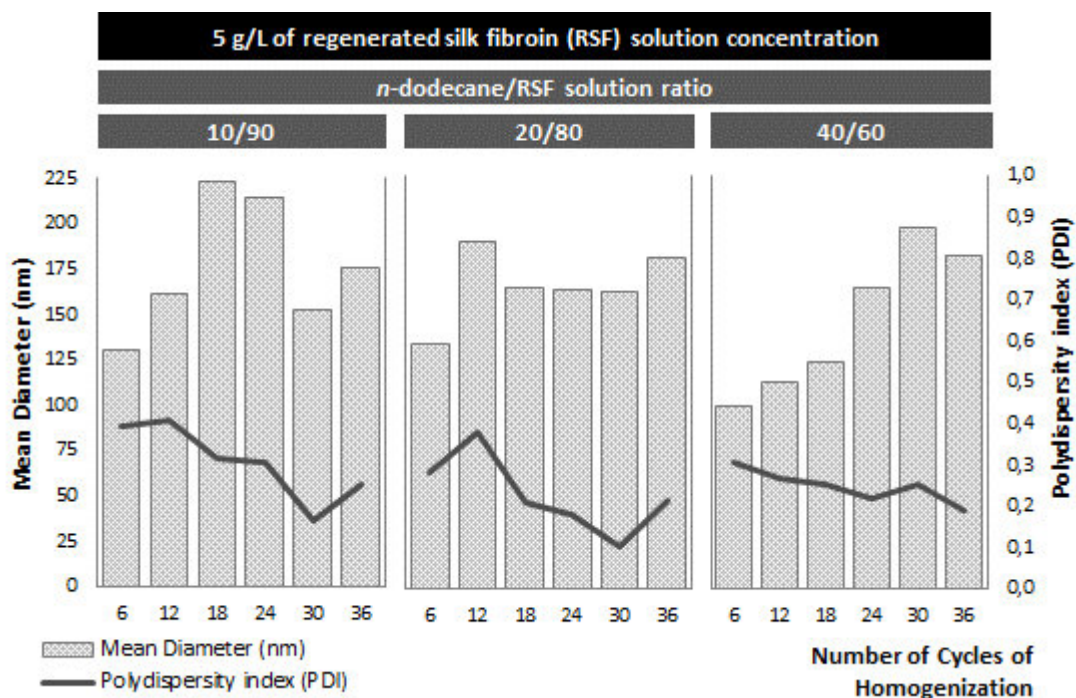
Figure IV.2. (B) Effect of emulsification by single-stage HPH (EmulsiFlex™-C3) on silk fibroin nanoparticles production for 5 g/L of RSF concentration at various *n*-dodecane/RSF solution ratios, along several homogenization cycles. Being mean diameter in nanometers (nm) and polydispersity index value (PDI) presented in columns and lines, respectively.
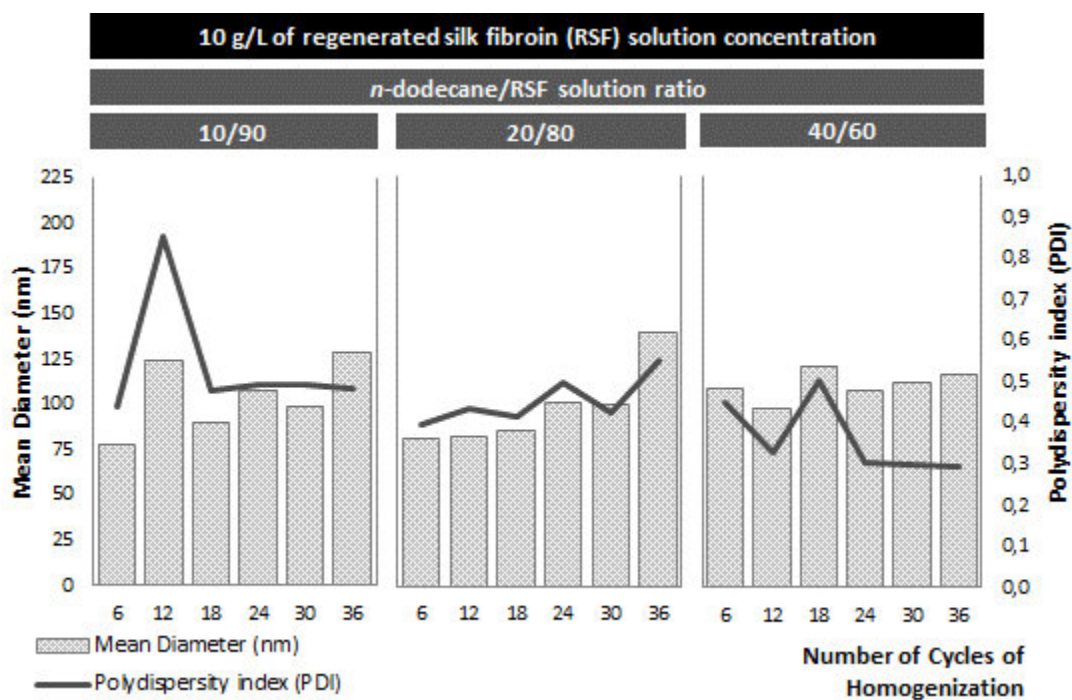
Figure IV.2. (C) Effect of emulsification by single-stage HPH (EmulsiFlex™-C3) on silk fibroin nanoparticles production for 10 g/L of RSF concentration at various *n*-dodecane/RSF solution ratio s, along several homogenization cycles. Being mean diameter in nanometers (nm) and polydispersity index value (PDI) presented in columns and lines, respectively.

In general, Figure IV.2 shows that almost all obtained nanoparticles possess a mean diameter lower than 200 nm, which was better than the previous studies performed with ultrasonic emulsification. As already mentioned, nanoparticles are formed due to involvement of the disruptive forces, and since more disruptive forces are involved in high-pressure homogenization than in ultrasound (Lovelyn *et al.*, 2011), it is expected that homogenization process can give better results.

The forces involved in HPH are hydraulic shear, intense turbulence, shear stress, cavitation, impingement and increase of temperature, in which turbulence is thought to be the dominant mechanism (Floury *et al.*, 2000;Lovelyn *et al.*, 2011). Briefly, in turbulence the dispersed phase break-up leads to small droplets and the fluid motion results in droplets collision, leading to coalescence (droplets are combined into one) but also to breakage (Floury *et al.*, 2000). The equilibrium between this two effects consequently increases nanoparticle formation (Floury *et al.*, 2000). In addition, this method involves large variations of pressure and fluid velocity, causing significant energy release, allowing droplet size reduction of the produced emulsions and it may also improve their stability over time (Floury *et al.*, 2000).

Finally, the high temperature involved in HPH method also influences the size of the droplets by affecting the viscosity of the oil and aqueous phase (Floury *et al.*, 2000). Along

the homogenization process, the energy involved is partially dissipated as heat, increasing the fluid temperature, which then causes decreases the fluid viscosity and reduces the interfacial tension between oil/aqueous phases, facilitating the droplets formation at small range (Floury *et al.*, 2000). Even so, it is important to highlight above a critical temperature that proteins can be significantly affected, they can unfold and aggregate (Floury *et al.*, 2000). For example, the protein secondary structure can lose their repeated motifs, leading to conformational changes of stable structures to the unstable random-coil configuration, which will be further discussed in chapter VI.

According to other studies, it is expected the decrease of the mean diameter of the nanoparticles along the homogenization process, *i.e.* with the increase of the homogenization cycles since this prolongation leads to more intensive disruptive forces, causing droplets disruption into even smaller droplets (Anton *et al.*, 2008;Bang *et al.*, 2010;Floury *et al.*, 2000;Naik *et al.*, 2012). In our experimental work, this behaviour was not observed, in fact correlation between size and number of cycles is controversial since it suggests that increase in number of cycles produces larger nanoparticles. This may suggest the method instability, wherein the formed nanoemulsions are very unstable and silk fibroin protein cannot stabilize the formed nanoparticles (Silva *et al.*, 2012;Silva *et al.*, 2012).

We also observed that increase of homogenization cycles causes PDI values to decrease, suggesting that the developed emulsions become more homogenous along the prolongation of the HPH emulsification, narrowing the NPs size distribution. However, as Figure IV.2 (C) shows, this tendency does not occur when using 10 g/L of RSF, which disagrees with previous reports that state higher concentration of protein stabilized the nanoparticles, leading to a more uniform size distribution (Floury *et al.*, 2000;Silva *et al.*, 2012;Silva *et al.*, 2012).

Taking into account that this method is unstable, we suggest it to be unable to control the formulation and the nanoparticles formation, probably because more energy is required. This behaviour is well-described by Floury and co-workers, in which they showed that at low rates of HPH, cluster and aggregates of droplets are formed (Floury *et al.*, 2000). In this case, the hydrodynamic forces involved are insufficient, and incapable to disrupt this flocs structures, this causes viscosity to increase and consequently of leads to larger size droplets at a dispersed range (Floury *et al.*, 2000).

Therefore, we suggest that an increase of the hydrodynamic forces involved in the emulsification process may enable the flocs disruption, leading to production of smaller nanoparticles (Floury *et al.*, 2000). Taking this into account, we decided to increase the

pressure involved in HPH emulsification, namely by applying two stages of pressure in the homogenization process.

Even so, in HPH single-stage optimization, we considered the formulation using 10 g/L to be the best since the formed nanoparticles possess a mean diameter variation between 75 and 125 nm, while others vary from 100 to 225 nm.

2.2.   Production using HPH double-stage system

Since the previous methods, ultrasonic and single-stage HPH emulsification, were not able to produce optimal silk fibroin nanoparticles, we decided to test a double-stage HPH, because according to the manufacture company APV, most emulsions when applied in a double-stage system show improvement in droplet size reduction, allowing the production of smaller nanoparticles.

For that, we tested 5 and 10 g/L of RSF solution at 10/90, 20/80 and 40/60 of organic/aqueous phase, using as oil phase *n*-dodecane and aqueous phase the SF solution. The homogenization process was conducted for 28 cycles, wherein nanoparticles characterization was performed every 2 in 2 cycles.

The obtained measurements of mean diameter and PDI values using 5 and 10 g/L of silk fibroin solution are presented in Figure IV.3 (A) and (B), respectively.

In this experimental work, we did not test 3 g/L of RSF concentration because HPH singles-stage results showed that this condition was less stable than the others since it presented a more significant size variation, but mainly due to the knowledge that protein higher concentration leads to smaller nanoparticles (Floury *et al.*, 2000;Silva *et al.*, 2012;Silva *et al.*, 2012).
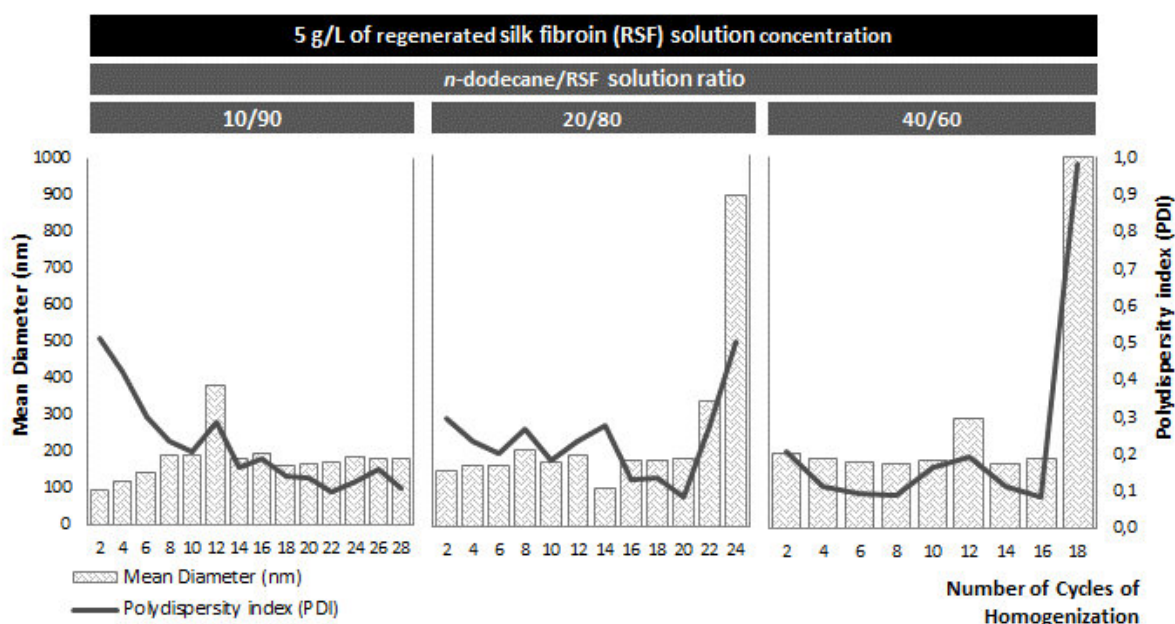
Figure IV.3. (A) Effect of emulsification by double-stage HPH (APV-2000™) on silk fibroin nanoparticles production for 5 g/L of RSF concentration at various *n*-dodecane/RSF solution ratio s, along several homogenization cycles. Being mean diameter in nanometers (nm) and polydispersity index value (PDI) presented in columns and lines, respectively.
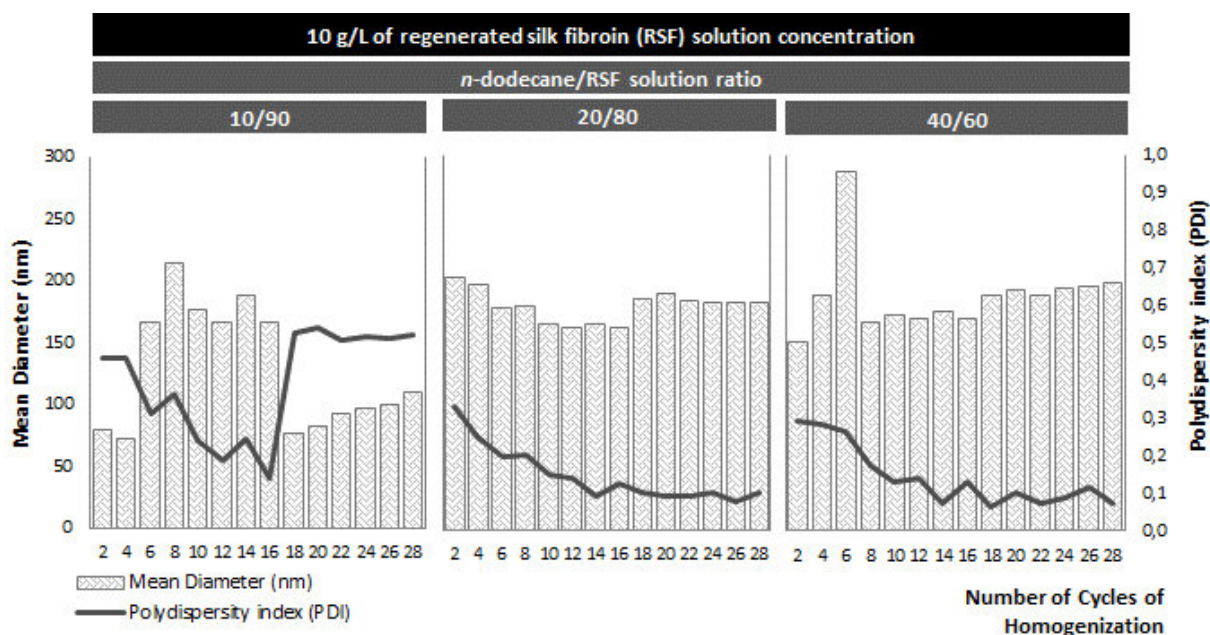
Figure IV.3. (B) Effect of emulsification by double-stage HPH (APV-2000™) on silk fibroin nanoparticles production for 10 g/L of RSF concentration at various *n*-dodecane/RSF solution ratio s, along several homogenization cycles. Being mean diameter in nanometers (nm) and polydispersity index value (PDI) presented in columns and lines, respectively.

During the homogenization process, the pre-emulsion characteristics are improved along the increase of number of homogenization cycles, and consequently the nanoparticles that forms (Anton *et al.*, 2008;Bang *et al.*, 2010;Floury *et al.*, 2000;Naik *et al.*, 2012). This nanoparticles improvement is mainly observed by the decrease of the droplets mean diameter and reduction of their distribution size (Anton *et al.*, 2008;Bang *et al.*, 2010;Floury *et al.*, 2000;Naik *et al.*, 2012).

Studies have suggest that the mean diameter evaluation along the homogenization process consists in two main trends (Floury *et al.*, 2000).

In the first trend, the mean diameter and size distribution of the nanoparticles decreases with the increase of the number of cycles (Floury *et al.*, 2000). This behaviour is a result of the intensification of the pressure that allows an increase of the energy input, leading to disruptive forces intensification which disrupt and decrease the larger droplets into smaller sizes (Floury *et al.*, 2000). Even so, as we already mentioned, this behaviour is only achieved when the energy and pressure involved are large enough to cause the disruptive forces (Floury *et al.*, 2000).

However, when the homogenization pressure and energy involved is too high it shows a saturation-like behaviour (Barnadas-Rodríguez *et al.*, 2001;Floury *et al.*, 2000). Indeed, at a given pressure, the increase of number cycles over a critical value does not result in mean diameter and size distribution decrease (Barnadas-Rodríguez *et al.*, 2001).

In this second phase, the involved high pressure negatively affects the emulsion formation and the produced nanoparticles. According to Brandl *et al.* studies with liposomes, this behaviour is due to the instability of the formed droplets which rapidly fuse with one another, leading to larger droplets, known as coalescence effect (Barnadas-Rodríguez *et al.*, 2001;Brandl *et al.*, 1990). The authors also suggest that the decrease of the droplets beyond the cycle's critical value would require a larger pressure and energy input (Barnadas-Rodríguez *et al.*, 2001;Brandl *et al.*, 1990). Pandolfe and others studies also emphasises this idea (Barnadas-Rodríguez *et al.*, 2001;Floury *et al.*, 2000;Pandolfe, 1995).

In addition, studies have shown that severe processing involved in this method can lead to deterioration of the involved protein (Floury *et al.*, 2000), therefore we suggest that increase of the involved forces, namely the increase of the cycles, could lead to instability of the silk fibroin protein and further destabilization, preventing their action in facilitating and stabilizing the nanoparticles formation into smaller sizes.

The cycle critical value depends on the emulsion composition, namely the oil and water phase composition (Barnadas-Rodríguez *et al.*, 2001). In fact, the protein used in the emulsion extensively affects this behaviour since the protein facilitates and stabilizes the

nanoparticles formation, and therefore the protein characteristics (such as molecular weight, conformational structure, properties and others) influence the emulsification process (Floury *et al.*, 2000).

This mentioned behaviours were observed in our experiment. For some cases, we only observed the first trend (decrease of the diameter and size distribution with the increase of number of cycles), namely in Figure IV.3 (A) for 10/90 and in Figure IV.3 (B) for 20/80 and 40/60. In this cases, we did not observed the second trend because the increase of cycles need to be further evaluated, *i.e.* more cycles had to be tested.

For Figure IV.3 (A) 20/80 and 40/60 and Figure IV.3 (B) 10/90, the second trend was observed since the diameter and size distribution over a specific cycle started to increase. For this conditions, we observed that the critical cycle value was 16 and 20.

As we mentioned above, higher silk fibroin concentrations enable a better emulsification process (Floury *et al.*, 2000), hence we evaluated the formation efficiency for 10g/L of RSF at 10/90, 20/80 and 40/60 of *n*-dodecane/SF solution ratio. The nanoparticles yield values are presented in the following table.

Table IV.1. Silk Fibroin Nanoparticles yield production (formation efficiency) for 10 g/L of RSF concentration at various *n*-dodecane/RSF solution ratio for 28 cycles of homogenization, using double-stage HPH (APV-2000™) emulsification.

Sample	SF-NPs Yield Formation Efficiency (%)
SF-NPs 10/90 of *n*-dodecane/RSF	74.802 ± 2.462
SF-NPs 20/80 of *n*-dodecane/RSF	79.134 ± 0.715
SF-NPs 40/60 of *n*-dodecane/RSF	76.159 ± 0.814

According to Table IV.1, the formulation 10g/L at 20/80 of *n*-dodecane/SF solution ratio obtained higher nanoparticles yield, which is due to the fact that high oil contents allow production of more stable nanoparticles (Floury *et al.*, 2000) and in this condition we did not observe a saturation-like behaviour, therefore the formed nanoparticles were more stable at 20/80 than 10/90 of *n*-dodecane/SF solution ratio. Additionally, we observed that 10/90 formulation possess a high deviation standard, emphasizing it instability due to this saturation effect (Barnadas-Rodríguez *et al.*, 2001;Brandl *et al.*, 1990;Floury *et al.*, 2000;Pandolfe, 1995).

Comparing this results with the Figure IV.3 (B), we conclude that the best formulation was obtained for 10g/L at 20/80 of n-dodecane/SF solution ratio, at 22 cycles, in which we obtained silk fibroin nanoparticles with 183 nm of mean diameter and polydispersity index (PDI) of 0.089. We considered this cycle as the lower possible cycle that allowed to achieve lower values of mean diameter and polydispersity index (PDI), besides it also enables prevention of the saturation-like since for further cycles the size is maintained constant.

In conclusion, we will use these optimization results, namely the optimized conditions (double-stage HPH, formulation 10g/L at 20/80 of n-dodecane/SF solution ratio, at 22 cycles) to further develop nanoparticles for elastase inhibitor incorporation.

Chapter V:

Incorporation in SF-NPs for

Transdermal Delivery

Chapter V: Incorporation in SF-NPs for Transdermal Delivery

After optimization and selection of the best parameters for silk fibroin nanoparticles, we proceeded to the main purpose of this dissertation work, incorporation of the HNE inhibitor sivelestat into the developed silk fibroin nanoparticles to act as an anti-wrinkling agent. However, we also performed stabilization studies in order to evaluate their potential application as a cosmetic.

This chapter comprehends three main incorporations into the developed SF-NPs at the established optimized conditions: incorporation of various stabilizers to evaluate their potential in stabilizing the cosmetic formulation; incorporation of a model-drug, orange IV, to establish a model of incorporation and drug release profile; and finally, incorporation of the HNE inhibitor, sivelestat,. In order to better elucidate, results of this chapter were divided in three main sections, being these present ahead.

However, before presenting and discussing the results for these sections, we will clarify some issues, namely differences between *Bombyx mori* SF material and the double-stage high-pressure homogenization method reproducibility.

As referred in materials and reagents section of chapter III, due to material depletion, we had to use two different batches of *Bombyx mori* cocoons in optimization process and in the following of the experimental work. Since we used a different batch for optimization process and another for the further studies, the optimization results obtained with the first batch, which were presented in chapter IV, may vary from the ones obtained with the second batch. Hence, in Table V.1, we present the size diameter, PDI, zeta-potential and formation efficiency values for the optimized conditions, and also the initial values according to optimization of chapter IV, for comparison.

Table V.1. Characteristics of the silk fibroin nanoparticles produced during the initial optimization process (presented in chapter IV) and after optimization with the optimized conditions, by double-stage high-pressure homogenization for 10 g/L of RSF at 20/80 o/w ratio, being the homogenization cycle presented in parentheses.

Characterization	SF-NPs produced during the initial optimization	SF-NPs produced with the optimized conditions
Mean Diameter (nm)	183.1 (22 cycles)	140.7 ± 1.852 (22 cycles)
Polydispersity index (PDI)	0.089 (22 cycles)	0.249 ± 0.004 (22 cycles)
Zeta-Potential (mV)	-21.2 ± 1.674 (28 cycles)	-33.3 ± 0.473 (22 cycles)
SF-NPs Yield Formation Efficiency (%)	79.134 ± 0.715 (28 cycles)	60.097 ± 3.033 (22 cycles)

According to Table V.1, we observe some differences between the results obtained by the two batches of cocoons of *B. mori* silkworms. However, in further analysis we observed that these differences were constant for all conditions, in fact the tendency observed in optimization results maintained. In other words, the parameters selected as optimal remained the same, differing only in the obtained values. In conclusion, although these differences are significant, we do not consider them relevant since the only purpose of optimization process was to help design and select the best parameters for silk fibroin nanoparticles production, and these "optimal parameters" did not change.

Furthermore, we suggest that the differences of mean diameter and PDI values may be due to the usage mode of the homogenization equipment. During the optimization process of HPH, the equipment was stopped for sample measurements and again started, at every 2 in 2 cycles. While, after optimization, the equipment was only stopped at the 22nd cycle, since this was the optimized parameter. According to this, we suggest that the stop/start action could influence the emulsification process. For example, we suggest that these interruptions may lead to energy loss, which could affect the involved disruptive forces, or on the contrary, could increase the energy involved since it could lead to a malfunction on controlling the pressure. Indeed, as mentioned above extensive variables are involved along the HPH process, so process interruption could affect these variables and consequently affect the nanoparticles characteristics. Even so, Middelberg studies highlight the importance that the homogenizer process is maintained without interruption (Middelberg, 2000).

In addition, differences of zeta-potential and formation efficiency cannot be comparable since they were evaluated for different cycles.

Finally, we also assessed the double-stage high pressure homogenization reproducibility by comparison of mean diameter and PDI values. For that, we repeated the silk fibroin nanoparticles production process at the optimized condition (10 g/L of silk fibroin at 20/80 of *n*-dodecane/RSF solution ratio at 22 cycles of homogenization) by double-stage HPH APV-2000™ and then determinate the statistical parameter of standard deviation. The results showed a low standard deviation of NPs mean diameter and PDI values, 9.683 nm and 0.015, respectively, therefore we concluded that this SF-NPs production method was reproducible.

1.   Stabilizers effect in Silk Fibroin Nanoparticles

This experimental work consisted, first, in incorporation of various stabilizers into the optimized SF-NPs formulation, namely poly(ethylene glycol)-*block*-poly(propylene glycol)-*block*-poly(ethylene glycol) (often named by poloxamer 407), polyoxyethylene 80 sorbitan monooleate (usually referred as tween 80), di(ethylene glycol) ethyl ether (commonly termed as transcutol) and sodium dodecyl sulphate (SDS).

As referred above, surfactants are amphiphilic surface-active molecules, which highly solubilize in one of the phases and stabilize the formed conformation, namely the nanoparticles (Mason *et al.*, 2006;Mason *et al.*, 2006).

Polymeric surfactants are one of the most effective stabilizers, since they control and prevent flocculation and coalescence effects (Tadros, 2011). In fact, these types of stabilizers are extensively used in cosmetic and personal care preparations, nanoemulsions (Tadros, 2011).

In detail, poloxamer 407, also known as pluronic F127, is a non-ionic polymeric surfactant of the A-B-A *block* graft type, where A is poly(ethylene glycol), the "stabilizing" chain and B is poly(propylene glycol), the "anchor" chain (Dumortier *et al.*, 2006;Tadros, 2011). The hydrophilic lipophilic balance (HLB) of poloxamer 407 is 22 at 22°C, being considered as a solubilizer of hydrophobic compounds (Dumortier *et al.*, 2006).

Other non-ionic surfactant is tween 80 derived from polyethoxylated sorbitan and oleic acid (Kim, S *et al.*, 2013;Kloet *et al.*, 2002). This compound is also called by polysorbate 80 and is a detergent and a solubilizing agent, presenting HLB value of 15 (Kloet *et al.*, 2002).

Transcutol is a powerful stabilizer agent since it possesses great optimal solubilizing properties, and is consider as a skin penetration enhancer since it increases significantly percutaneous penetration (Mura *et al.*, 2000). This short-chain alcohol is mainly used as additive due to their weakly amphiphilic character. Transcutol, like many other alcohols molecules are considered as a co-surfactant, being frequently used in combination with surfactants or others stabilizing molecules. Several authors suggest that this co-surfactant molecules are capable of concentrating and aggregating the surfactant molecules in the particles interphase layer, improving the surfactant self-assembly around the particles, and their stabilizer effect. To be noted, transcutol possesses a HLB value of 4, being considered as lipid soluble (Mandal, S *et al.*, 2011;Solanki *et al.*, 2012).

SDS, also known as sodium lauryl sulphate (SLS), is a small-molecule anionic surfactant capable of adsorbing the oil droplets surfaces within homogenizers (Qiang *et al.*, 2011). Similar to poloxamer 407, SDS acts as a gelling agent since it causes SF molecules to self-assembly into stable β-sheets structures, and to associate in nanoparticles by stronger hydrophobic and electrostatic interactions (Wu, X *et al.*, 2012). In addition, SDS presents and HLB value of 40, and also possesses an amphipathic structure, being also considered as a detergent, like tween 80 (Lo, 2003).

As mentioned, the stabilizers were incorporated in the formulation by dissolution in the RSF solution (water phase) before the emulsification process at the optimized conditions (10 g/L of RSF at 20/80 o/w ratio, for 22 cycles of homogenization). These stabilizers were added only in 1% of concentration because their use should be limited to a minimum possible level, to prevent any toxic and hypersensitivity reactions (Stevanovic *et al.*, 2009).

Then, their effect was evaluated by measuring the mean diameter and PDI values over time, once a week, for 2-4 weeks. As control, we used silk fibroin nanoparticles without any stabilizer. These results are presented in the following Figure V.1, where the mean diameter is presented in columns and PDI values in lines.

Figure V.1. Stability evaluation of silk fibroin nanoparticles incorporated with various stabilizers, namely tween 80, transcutol, SDS and poloxamer 407, on mean diameter in nanometres (nm) and polydispersity index value (PDI) along several weeks.

According to Figure V.1, the size and size distribution of SF-NPs without any stabilizer (control) was considered stable only for 2 weeks, since the mean diameter and PDI increases significantly at the 2nd week (∼200 nm) and it kept increasing. This shows the need to incorporate a stabilizer in the formulation.

Regarding the studied stabilizers, we considered that the most efficient stabilizer was transcutol because the mean diameter and PDI values variation over the weeks was smaller than the others stabilizers. In fact, for transcutol we obtained smaller standard deviation value for mean diameter values. According to other studies, this effect may be due to transcutol co-surfactant action. In which, we suggested that transcutol improves SF protein stabilization activity in the nanoparticles by helping adsorption of SF molecules around the nanoparticles (Mandal, S *et al.*, 2011;Solanki *et al.*, 2012). Besides, transcutol possesses a great potential use in cosmetic application, especially, for this work, in the development of an anti-wrinkling agent, since it can be used as a drug permeation enhancer due to their solubilizing properties and ability in drug cutaneous retention (Mura *et al.*, 2000).

Even so, stabilizers tween 80 and SDS also showed great stability for PDI values, in which, SDS presented the lower standard deviation for PDI values. SDS ability in stabilizing nanoparticles size and size distribution over time may be due to the fact that it is a gelling agent, since it causes SF protein to be orientated around the nanoparticles in a more stable and strong conformation (Wu, X *et al.*, 2012), preventing the coalescence and flocculation effect.

Tween 80 showed mean diameter values higher than the others but after the 1st week, size and size distribution stabilized, and the standard deviation between this period was smaller than for others stabilizers. The tween 80 effect in particles size agrees with Asasutjarit *et al.*, 2013 studies, in which they suggest that tween 80 acts as amphiphilic molecules, being deposited in the particles, and preventing them from interact with others, thus, controlling the size and size distribution (Asasutjarit *et al.*, 2013). In fact, some reports state that detergents, like tween 80 and SDS, are capable of enhancing proteins conformational stability, preventing them from unfolding and protecting from aggregation (Arakama *et al.*, 2000). So, silk fibroin protein, and consequently silk fibroin nanoparticles are stabilized by these detergent molecules due to their amphiphilic structure.

However, it is important to highlight that their ability to modify proteins structure due to their amphiphilic nature, can also cause downsize effects, namely protein denaturation (Caligur, 2008). In fact, tween 80 is considered as a "mild" detergent because it is less likely to denature proteins while SDS is considered a "harsh" detergent (Caligur, 2008). Even so, in this case, SF is not likely to denature since the compounds were added to the formulations at a very low concentration, 1% (Caligur, 2008).

Poloxamer 407 was not able to stabilize the SF-NPs since it presented higher values of mean diameter higher than the control condition, being the mean diameter and PDI increased over time. In fact, this condition did not present any nanoparticles formation since the mean diameter was higher than 1 µm and the sample was too disperse (PDI value of 1). This behaviour can be explained by the fact that the propylene oxide chain are not strong enough to ideally absorb in the particle, therefore they cannot influence the particle stability like the others stabilizers (Tadros, 2011). We, then, predict that increase of poloxamer 407 concentration would increase their effect and improve the particles stability (Tadros, 2011).

To better understand these results, we evaluated the surface charge of the formed nanoparticles by zeta-potential determination. In detail, zeta-potential is the electrical potential of the surface of hydrodynamic shear, which is around the colloidal particles (Bunjes, 2005). According to this, is possible to measure indirectly the surface potential of these nanoparticles by the zeta-potential values (Bunjes, 2005).

The particle surface charge is mainly responsible for the stability of this particle in a dispersion or solution, in fact, this charge depends on the concentration and type of ions involved in the surround medium of this particle (Malvern, 2005). Taking all this into account, it is possible to evaluate the stability of a particle in a specific environment by zeta potential determination (Greenwood *et al.*, 1999;Hanaor *et al.*, 2012;Malvern, 2005).

In various studies, it is shown that high absolute values of zeta-potential indicate more stable dispersion since high charge (positive and negative) increase the electrostatic repulsion of other molecules, and consequently inhibit agglomeration and flocculation (Greenwood *et al.*, 1999;Hanaor *et al.*, 2012).

In general, stabilizers are deposited in the surface of the particles and change the electrical potential around the interface of the particle and medium, hence, incorporation of stabilizers in these formulation will affect the zeta potential values (Stevanovic *et al.*, 2009). Considering this, zeta potential measurements were performed after production of the silk fibroin nanoparticles for the tested stabilizers, being this presented in Figure V.2. As control conditions, we used regenerated silk fibroin solution without stabilizer before being emulsified and after.

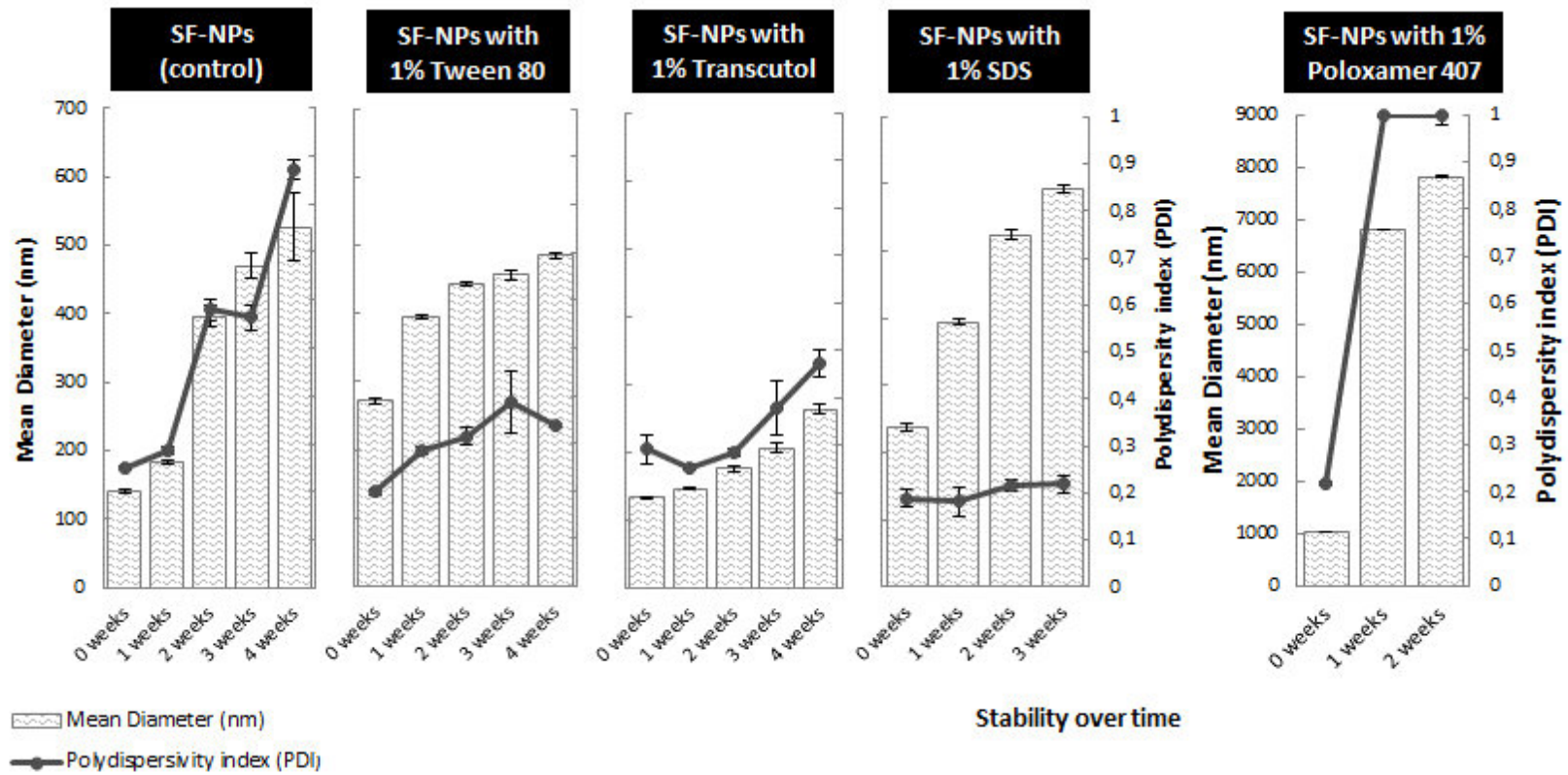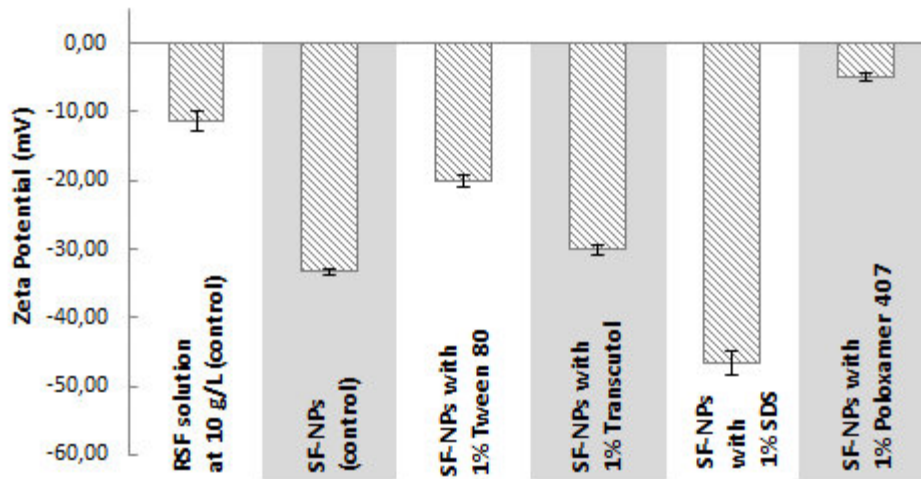**Figure V.2.** Surface charge evaluation of silk fibroin nanoparticles incorporated with various stabilizers, namely tween 80, transcutol, SDS and poloxamer 407, by zeta-potential determination in millivolts (mV) at time of production.

The results of the Figure V.2 highlight the previous discussion. In which, mean diameter and PDI stabilization over time is related to the zeta-potential values, namely the high values of zeta-potential indicate stable emulsion, as established by other studies (Greenwood *et al.*, 1999;Hanaor *et al.*, 2012).

According to Figure V.2, incorporation with transcutol and SDS showed better stability results since results for these conditions presented larger magnitude of the zeta-potential values.

In addition, as predicted, poloxamer 407 showed lower zeta-potential values, which allow us to conclude that this stabilizer was the less effective in SF-NPs stabilization.

Finally, comparison of zeta-potential values of RSF solution and SF-NPs showed that the nanoparticles formation increases stability, which goes according to the literature (Silva *et al.*, 2012;Silva *et al.*, 2012;Zhao *et al.*, 2013). Since it is thought that HPH process may lead to conformational changes from unstable random-coil to stable β-sheets (Silva *et al.*, 2012;Silva *et al.*, 2012), we considered that this result might be due to this effect, which will be further discussed in the next chapter (chapter VI).

Finally, we measured the nanoparticle yield for the stabilizers tween 80, transcutol and SDS, since poloxamer 407 was considered as a non-efficient stabilizer. As control, we used SF-NPs without any stabilizer. The obtained formation efficiency values are presented in Table V.2.

Table V.2. Silk Fibroin Nanoparticles yield production for various stabilizers by determination of formation efficiency.

Sample	SF-NPs Yield Formation Efficiency (%)
SF-NPs (control)	60.097 ± 3.033
SF-NPs with 1% Tween 80	26.450 ± 4.822
SF-NPs with 1% Transcutol	60.943 ± 3.277
SF-NPs with 1% SDS	76.259 ± 2.001

Higher formation efficiency was obtained for SDS, however according to the previous results their stability effect was not optimal, whereas transcutol showed a better stability over time and their formation efficiency value was considered acceptable.

In conclusion, we considered transcutol as the most efficient stabilizer since it presented good mean diameter and PDI stability, large magnitude of zeta-potential value and acceptable nanoparticles yield (~61%). In addition, transcutol possesses the advantage of being a drug permeation enhancer (Mura *et al.*, 2000).

Even so, since the formation efficiency value of transcutol was not ideal and for SDS we obtained a better yield, we suggest a combination of these two stabilizers. We predict that combination of the co-surfactant transcutol and surfactant SDS, would increase the SF-NPs stability since transcutol would increase SDS effect (Mandal, S *et al.*, 2011;Solanki *et al.*, 2012) and improve the SF-NPs further permeation in the skin (Mura *et al.*, 2000).

2.   Incorporation of a model-drug, orange IV, in SF-NPs

In this second step, incorporation of a model-drug compound, orange IV, was conducted to establish a model of incorporation and drug release profile. The obtained results will allow selection of the best concentration of drug to incorporate and to predict the drug release from the nanoparticles at different conditions, namely in absence and presence of HNE enzyme.

Briefly, orange IV (4-{(E)-[4-(phenylamino)phenyl]diazenyl}benzenesulfonate) is an orange dye, also named as tropaeolin 00, benzenesulfonic acid or acid orange 5, with $C_{18}H_{14}N_3NaO_3S$ as molecular formula (Uddin *et al.*, 2010;Wang, HY *et al.*, 2006). Due to the azo group, this compound is extensively used in textile industry as a dye, being also used to in silk dyeing (Uddin *et al.*, 2010).

Several studies have reported dyes as models for incorporation in various devices, mainly because dyes enable simple evaluation of the incorporation process, in a quantitative way but also by visual detection (DeLauder *et al.*, 2000;Shu *et al.*, 2000;Teichmann *et al.*, 2007;Wu, BM *et al.*, 1996). Considering this, we decided to use the dye orange IV as a model-drug, since it quantification is simply detected by UV-Vis at 240 nm and is possible to visually detect it exit from the nanoparticles.

In addition, orange IV possesses sulphonic groups (S=O) and aromatic rings (Uddin *et al.*, 2010) and a smaller structure like sivelestat, in fact their molecular weight is very similar to sivelestat. To be noted, in the dye selection, we had to take into account their availability in our research lab.

First characterization of the SF-NPs incorporated with model-drug orange IV consisted in evaluation of this compound effect in the developed nanoparticles, namely in their size and size distribution and this parameters stability over time. For that, the developed nanoparticles loaded with orange IV at various concentrations were evaluated by measuring mean diameter, PDI and zeta-potential. In addition, determination of the formation and encapsulation efficiency for the considered best concentrations of orange IV was also performed.

The results of size and size distribution stability along time are presented in Figure V.3 and zeta-potential measurement at time of production are presented in Figure V.4.

Figure V.3. Stability evaluation of silk fibroin nanoparticles incorporated with various concentrations of the model-drug orange IV (50, 75, 100 and 1000 µM), on mean diameter in nanometres (nm) and polydispersity index value (PDI) along several weeks.

Figure V.3 suggests improvement of the size and size distribution of the developed nanoparticles stability when incorporating the model-drug orange IV, since the mean diameter and PDI values of the SF-NPs incorporated with orange IV show some persistence over time while the values for SF-NPs without incorporation tended to increase over time.

This results may suggest that orange IV possesses the ability to stabilize the nanoparticles, probably due to establishment of hydrophobic interactions and van der Waals forces with the SF structure by the azo (N=N) and sulphonic groups (S=O) (Uddin *et al.*, 2010). In addition, this stabilization effect might also be related to the orange IV ability to increase gelation in silk fibroin, since gelation increases the emulsion stability (Matsumoto *et al.*, 2006). Since orange IV is an acid dye, dissolution of orange IV decreases the pH and causes SF protonation, which decreases the repulsions and leads to the mentioned interactions, enabling the SF-NPs with orange IV stabilization and size and size distribution control (Matsumoto *et al.*, 2006).

This behaviour was proved visually. After dissolution of orange IV in silk fibroin, we observed that the consistency of the solution increased slightly, in which this increase showed to be related to the increase of orange IV concentration. Also, when carrying the HPH emulsification with incorporation of 1 mM of orange IV, the sample showed some increase in their viscosity and along cycles it turned into a gel.

In order to better understand this stabilization process, SF secondary structure will be further evaluated by FTIR, in chapter VI.

Regarding the size and size distribution results, we considered that incorporation of 100 µM of orange IV enable to obtain smaller SF-NPs and allowed better stabilization of the mean diameter and PDI values since the standard deviation of size and size distribution was smaller (~25 nm and 0.06, respectively). Even so, incorporation of 50 and 75 µM of orange IV also showed stability along time, since the standard deviation values for size and size distribution was also smaller, being only higher than for 100 µM due to the slightly increase of mean diameter and PDI values at week 4.

In addition, incorporation of 1 mM of orange IV showed larger SF-NPs and a higher size distribution than the others concentrations of orange IV, however it showed good stabilization of the size and size distribution over time.

According to this, determination of zeta-potential at time of production and along the weeks were conducted to help us select the best concentration of orange IV to incorporate, being these present in the following Figure V.4.

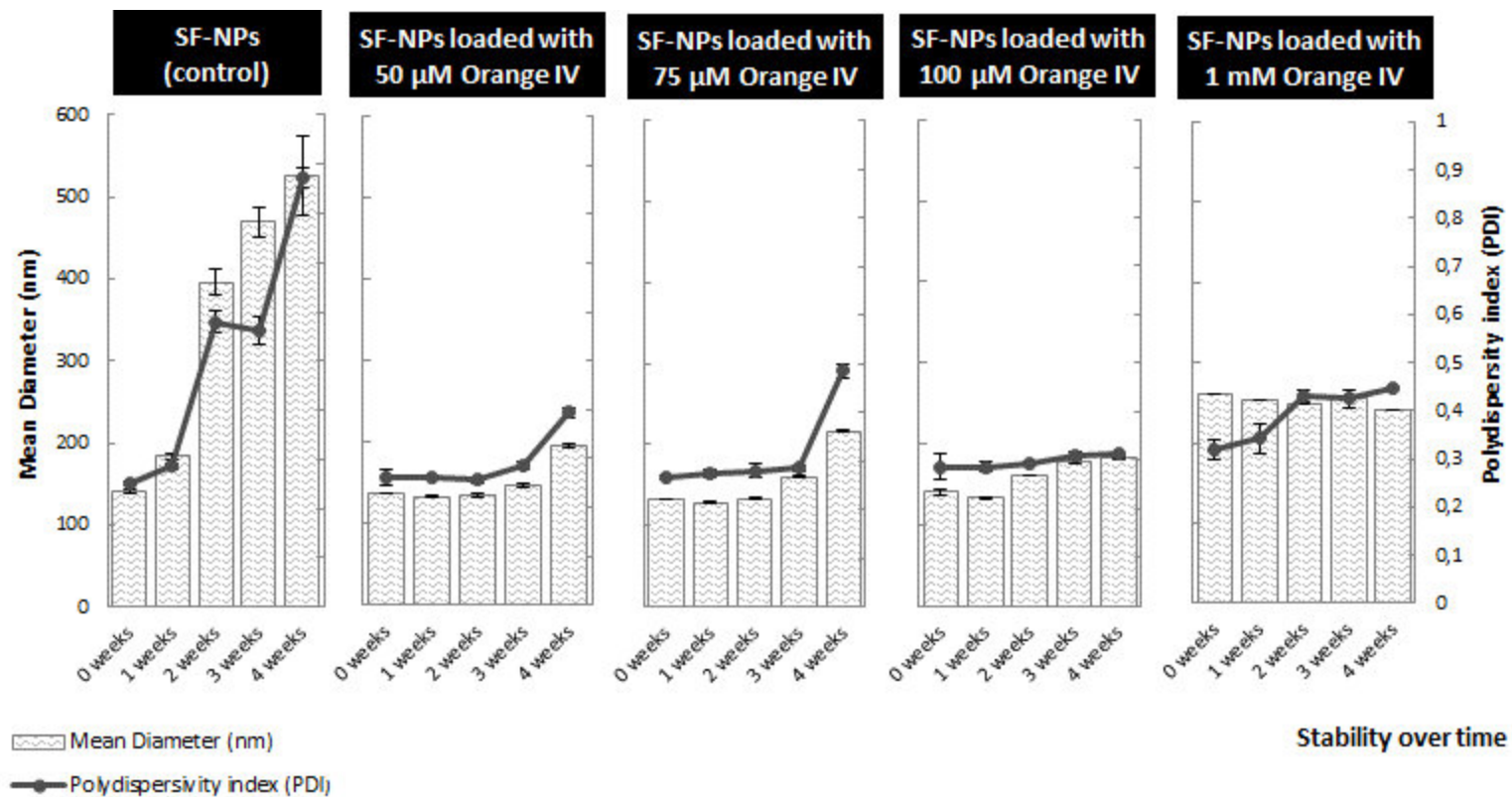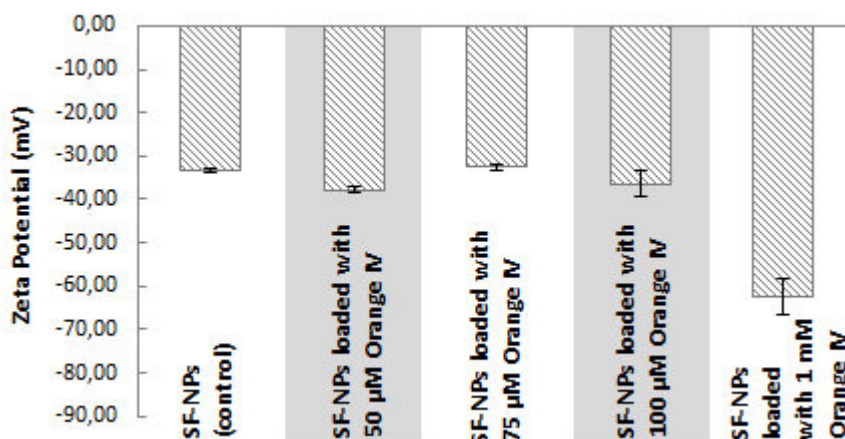**Figure V.4.** Surface charge evaluation of silk fibroin nanoparticles incorporated with various concentrations of the model-drug orange IV (50, 75, 100 and 1000 µM) by zeta-potential determination in millivolts (mV) at time of production.

As mentioned above, incorporation with 1 mM of orange IV showed increase in the SF gelation, being this proven by their higher zeta-potential value (-62.5 mV) in Figure V.4. Since the gelation process occurred during the HPH emulsification, we considered this condition as non-optimal because it could lead to HPH equipment malfunction.

Considering the rest of incorporation with orange IV samples, we observed that 50, 75 and 100 µM showed high zeta-potential values and excellent stability of the surface charge over time.

Finally, the formation and encapsulation efficiency were determined to help us selecting the ideal concentration to incorporate. Since we eliminated incorporation of 1mM of orange IV, we only determined these parameters for incorporation with 50, 75 and 100 µM of orange IV, being these results presented in the following table, Table V.3.

Table V.3. Silk Fibroin Nanoparticles yield production (formation efficiency) and encapsulation efficiency for incorporation of various concentrations of the model-drug orange IV (50, 75, 100 and 1000 µM).

Sample	SF-NPs Yield Formation Efficiency (%)	SF-NPs Encapsulation Efficiency (%)
SF-NPs (control)	60.097 ± 3.033	-
SF-NPs loaded with 50 µM Orange IV	74.930 ± 3.522	26.518 ± 0.705
SF-NPs loaded with 75 µM Orange IV	72.289 ± 2.065	83.096 ± 1.355
SF-NPs loaded with 100 µM Orange IV	66.879 ± 2.147	91.446 ± 0.082

As it is possible to observe in Table V.3, higher formation and encapsulation efficiency was obtained for incorporation of 50 and 100 µM of orange IV, respectively. In general, all conditions showed an increase of the formation efficiency when incorporating orange IV. This results, as already discussed, may be due to the stabilization effect of orange IV in SF protein, which further stabilizes the nanoparticles production.

Considering the previous results and Table V.3, we considered that the best concentration to incorporate in SF-NPs is 100 µM, since allow us to obtain smaller nanoparticles (140 nm) at an acceptable size distribution (PDI of 0.3), with a high absolute zeta-potential value and presented good formation and encapsulation efficiency (~67 and 91 %).

Hence, we selected this condition as optimal concentration to incorporate in SF-NPs and in the following studies we will use this value.

2.1. *In vitro* Orange IV Release Studies

In a second characterization, the model-drug orange IV release from the SF-NPs with 100 µM of orange IV was evaluate over time, in absence and presence of human neutrophil elastase (HNE) enzyme (0.5 U/mL). This results will enable us to predict the sivelestat release profile from the nanoparticles in control conditions (absence of HNE enzyme) and when applied to the skin as anti-wrinkling agent (presence of HNE enzyme).

The release of drug from proteinaceous nanoparticles was studied by dialysis bag diffusion technique since it is considered as the most popular method to study the drug release (D'Souza *et al.*, 2006;Nounou *et al.*, 2006;Shazly *et al.*, 2008;Silva *et al.*, 2012).

The result from the orange IV release studies is presented in the following Figure V.5, where dashed and filled lines represent absence and presence of HNE enzyme, respectively. In order to better elucidate the orange IV release at initial time, we emphasis this initial behaviour in a smaller graph.
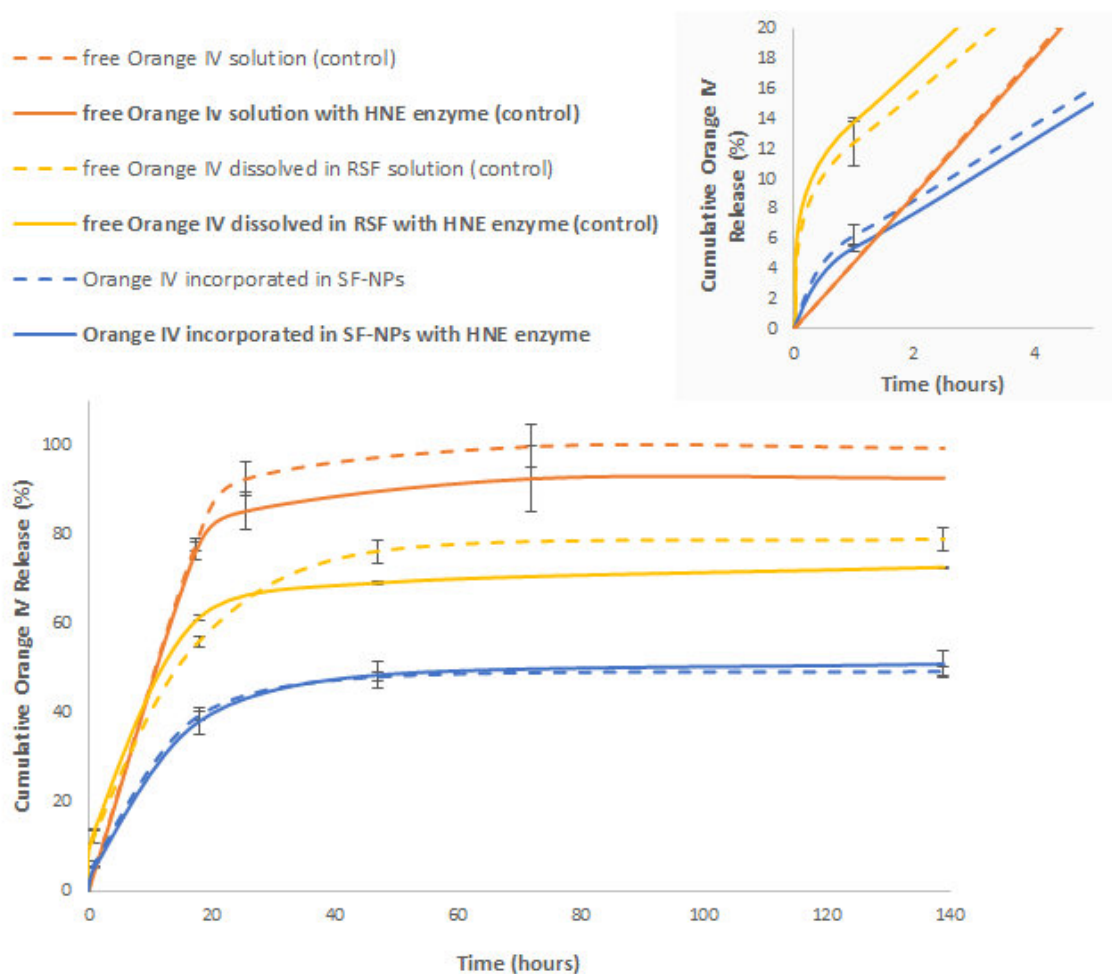
Figure V.5. *In vitro* model-drug cumulative Orange IV Release studies by dialysis bag method for silk fibroin nanoparticles incorporated with 100 µM of orange IV in absence and presence of human neutrophil (HNE) enzyme at 0.5 U/mL. As controls were used free orange IV dissolved in water and dissolved in RSF solution.

In Figure V.5, we can observe that when orange IV was incorporated in SF-NPs, their release was controlled at some extent. In fact, it showed a slower release than to the controls conditions. SF-NPs released nearly 40% of the entrapped orange IV at 20 hours while free orange IV (without being encapsulated) dissolved in water and in silk fibroin solution came out nearly 80% and 60% at this time, respectively.

This free orange IV exit to the outside solution differed according to the dissolved medium. More specifically, free orange IV dissolved in water showed a higher dispersion to the exterior than when dissolved in RSF solution. We suggest that this difference may be due to the possible interactions that orange IV may establishes with SF protein by their azo (N=N) and sulphonic groups (S=O) (Uddin *et al.*, 2010), as already discussed. In fact, these results also agree with the previous suggestions, in which orange IV might increase gelation in SF (Matsumoto *et al.*, 2006). Considering this, we hypothesized that SF association to

orange IV and further gelation, prevents the orange IV exit, slowing their exit rate; whereas in water, orange IV exits to the outside medium at a faster rate.

In general, the main challenges in developing proteinaceous particles is their incomplete release and initial burst release (Yeo *et al.*, 2004). Various authors suggested that the incomplete release is related to the protein instability since conformational and biological integrity of proteins are extensively affected by the involved particles production methods (Yeo *et al.*, 2004). In this case, as mentioned above, the severe disruptive forces involved in HPH emulsification process for SF-NPs production may lead to silk fibroin protein damage (Floury *et al.*, 2000).

According to Figure V.5, majority of the samples showed an incomplete orange IV release, in fact even for control conditions, we observed that free orange IV was not completely detected. In more detail, incorporated orange IV release from SF-NPs only achieved 50% of total release, while free orange IV dispersion when dissolved in water and in silk fibroin solution showed an ~90% and ~75%. This incomplete orange IV exit might be due to SF instability that could lead to SF protein aggregation and/or nonspecific adsorption within the nanoparticles (Yeo *et al.*, 2004;Crotts *et al.*, 1997;Crotts *et al.*, 1997;Kim, HK *et al.*, 1999), however it may also be related to the HNE enzyme action.

Since the aim of this study is for topically apply these SF-NPs in the skin as prevention of wrinkle formations by inhibiting the HNE enzyme, the release studies were carried out in absence and presence (at 0.5 U/mL) of this enzyme, in order to mimic the *in vivo* conditions. Comparing the behaviour of samples in absence and presence of HNE enzyme, we observed significant differences total exit of orange IV.

In general, orange IV total release is lower for samples with HNE enzyme. Considering the catalytic activity of HNE enzyme (Owen *et al.*, 1999), we suggest that this enzyme might cleave the orange IV dye compound, affecting their structure, for example their aromatic rings. Considering this, the orange IV absorbance might altered, preventing their detection by UV-Vis and lead to colourless of the orange IV.

In fact, the control of orange IV in solution suggests our hypothesis, since orange IV was completely detected in absence of HNE, while in presence of this enzyme, nearly 10% of orange IV was not detected. Moreover, orange IV when dissolved in RSF solution showed the same incomplete behaviour, in which we also suggest that 10% of orange IV was not detected due to the HNE action. To be noted, visual evaluation of the sample that showed an incomplete release were colourless, emphasizing this hypothesis.

Regarding the orange IV release from the SF-NPs, we suggested that the incomplete release is caused by the SF instability as described by other studies (Yeo *et al.*, 2004;Crotts *et al.*, 1997;Crotts *et al.*, 1997;Kim, HK *et al.*, 1999). In this case, results showed that HNE did not affect the orange IV release from the SF-NPs, which might be due to the fact that SF-NPs protect their content, in this case orange IV, against HNE activity.

To evaluate this hypothesis further studies had to be conducted, for example by assessing and measuring the human neutrophil elastase activity in various conditions, namely in RSF solution and when dissolved in orange IV solution. This could be achieved by a non-specific protease activity assay adapted for human neutrophil elastase.

Initial burst is defined as high release of a compound in the first hours of the release method, in which DDS possessing higher initial burst are considered as ineffective (Yeo *et al.*, 2004). Therefore, in order to assess the drug release profile of the DDS and their *in vivo* efficacy and safety is important to evaluate the onset and duration of burst (D'Souza *et al.*, 2006).

As observed in Figure V.5, the release profile of orange IV from SF-NPs showed a very low initial burst, in which only 5% of orange IV was released in the first hour and then was followed by a controlled release along time (plateau). Additionally, the control of orange IV dissolved in RSF solution presented a high initial burst, but we do not consider it relevant because it does not involve release *per se*, since orange IV is not encapsulated.

According to the literature, the initial burst can be associated to two events: first it can be caused by the diffusion of the non-entrapped drug molecules, dispersed around the particles surface (Muthu *et al.*, 2009;Yeo *et al.*, 2004); or due to the poor ability of encapsulation and stabilization of the compound inside of the particle (Yeo *et al.*, 2004).

Considering the first case, orange IV initial burst release may be due to the free orange IV dispersed in the nanosuspension and/or adsorbed on the SF-NPs (Muthu *et al.*, 2009). In this situation, the initial release can be reduced by improving the separation of the free drug (non-encapsulated) from the drug incorporated in the particles (Muthu *et al.*, 2009;Silva *et al.*, 2012;Yeo *et al.*, 2004).

According to the second possibility, the SF-NPs are not able to prevent the orange IV release which may be due to the particles instability and/or their morphology, in which the orange IV might be escaping through pores and cracks (Yeo *et al.*, 2004). Even so, this event is less likely since the observed initial release was minor, hence the initial release is mainly due to the dispersion of orange IV molecules near the SF-NPs (Silva *et al.*, 2012).

Even so, to better understand the mechanism involved in drug release from polymeric devices, it is important to analyse them by mathematical models (Ritger *et al.*, 1987;Ritger *et al.*, 1987;Siepmanm *et al.*, 2001;Silva *et al.*, 2012), being all based in Fickian diffusion equation, presented in Equation III.3 (Ritger *et al.*, 1987;Ritger *et al.*, 1987;Siepmanm *et al.*, 2001;Silva *et al.*, 2012). Considering this, evaluation of mechanism transport of the released orange IV to the exterior medium was assessed by determination of the *n* value (diffusional exponent). The *n* value was determined for orange IV release from SF-NPs, in absence and presence of HNE enzyme, being this presented in Table V.4. Additionally, in order to evaluate if the results are reliable, the correlation coefficient (r^2) of the linear equation of plot log (M_t/M_∞) *versus* log (t) used to determine *n* values was also determined.

Table V.4. Orange IV release kinetic data obtained from fitting into modified Ritger-Peppas equation (Equation III.4) from silk Fibroin nanoparticles incorporated with model-drug orange IV, in absence and presence of HNE enzyme (0.5 U/mL).

SF-NPs loaded with 100 μM Orange IV	*n*	R²
Without HNE enzyme	0.556	0.977
With 0.5 U/mL of HNE enzyme	0.593	0.980

The most important rate-controlling mechanism of DDS are diffusion, swelling and erosion (Siepmanm *et al.*, 2001), which can be defined by the *n* value. According to Ritger *et al.* and Siepmann *et al.* studies and considering our sample particles spherical, the diffusional exponent, *n*, can possess the following values: 0.43 indicates a Fickian diffusion of first order; between 0.43 and 0.85 indicates an anomalous transport; and above 0.85 indicates a Case II transport of zero-order release (Ritger *et al.*, 1987;Siepmanm *et al.*, 2001).

In detail, standard diffusion can be described by the Fickian diffusion while Case II-zero order nature indicates polymer relaxation and/or degradation of the particles causes the compound entrapped to be released (Ritger *et al.*, 1987;Siepmanm *et al.*, 2001;Silva *et al.*, 2012). The anomalous transport is the combination of both phenomena, being both contributing equally for the compound release (Ritger *et al.*, 1987;Siepmanm *et al.*, 2001;Silva *et al.*, 2012).

According to Table V.4, the correlation coefficient (r^2) for all *n* values was above the tolerable range (0.95), validating the obtained results. In absence and presence of HNE enzyme, the drug transport mechanism was considered as anomalous. In anomalous transport, also termed by non-Fickian diffusion, it is observed a coupling of Fickian diffusion (orange IV was released from the SF-NPs by simple diffusion) and polymer degradation (orange IV was released due to the SF structure relaxation/degradation), in which neither is predominant (Ritger *et al.*, 1987;Siepmanm *et al.*, 2001;Silva *et al.*, 2012).

The obtained *n* value was slightly larger in presence of HNE enzyme than in absence, however this difference is not significant, therefore the HNE presence only affects the diffusion coefficient but does not significantly influence the drug transport mechanism. Even so, to better evaluate this suggestion it is important to evaluate other HNE concentration.

In addition, in further studies we will assess the influence of the orange IV concentration in their release and drug transport mechanism.

Finally, we proceeded to HNE inhibitor sivelestat incorporation at 100 μM of concentration.

3.   Sivelestat Incorporation in SF-NPs and their HNE inhibition effect

Sivelestat incorporation into the SF-NPs and their HNE inhibition effect was evaluated in order to recognize these nanoparticles potential as an anti-wrinkling agent.

The initial characterization consisted in stability evaluation of the mean diameter and PDI over time, as presented in Figure V.6.
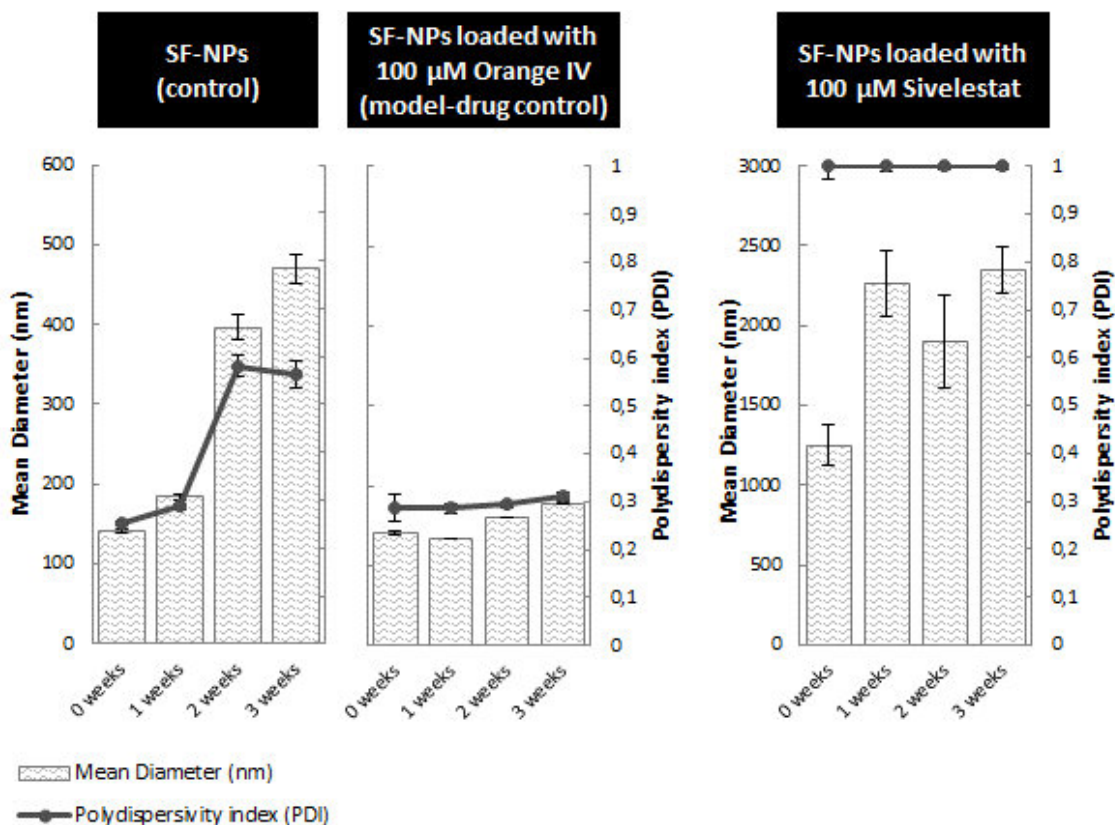
Figure V.6. Stability evaluation of silk fibroin nanoparticles incorporated with 100 µM of HNE inhibitor sivelestat, on mean diameter in nanometres (nm) and polydispersity index value (PDI) along several weeks.

According to previous evaluation of model-drug orange IV it was expected that the silk fibroin nanoparticles when loaded with sivelestat would present good stability of size and size distribution. However, results of Figure V.6 did not show this predictions.

In addition, emulsion with sivelestat presented an increase of the particles mean diameter. In fact, with sivelestat we were not able to obtain nanoparticles since the mean diameter of the resulting particles was higher than 1 µm, and also the obtained PDI values was 1, showing that the solution was very polydisperse.

To understand why this happen, we evaluate the surface charge of this sample at time of production (Figure V.7) and their formation and encapsulation efficiency (Table V.3).
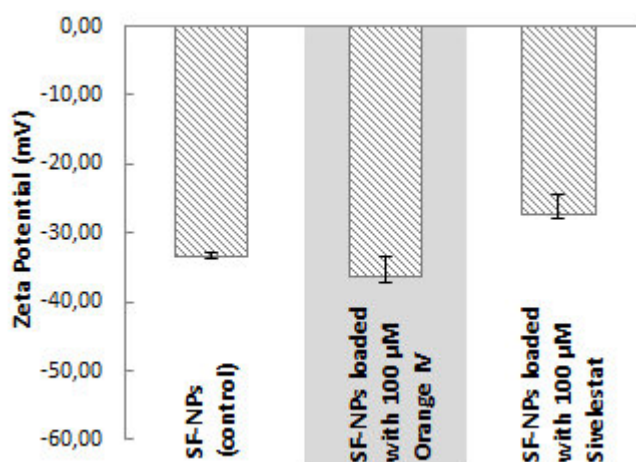
Figure V.7. Surface charge evaluation of silk fibroin nanoparticles incorporated with 100 µM of HNE inhibitor sivelestat by zeta-potential determination in millivolts (mV) at time of production.

The surface charge measurements highlight the stability difference between sivelestat and orange IV. In Figure V.7 it is possible to observe that SF-NPs with sivelestat present lower zeta-potential values than orange IV.

Considering what we already discussed, this stability difference may be due to the fact the differences between sivelestat and orange IV structures. As suggested, the stability of orange IV may be related to the establishment of strong interactions with SF protein by sulphonic and azo groups, which lead to a more stable conformation, thus, to the control of size and size distribution of the SF-NPs. Since sivelestat does not possess azo groups, it is understandable that his stability effect is lower.

Additionally, the formation and encapsulation efficiency of SF-NPs with sivelestat was also determined. In Table V.5, it is presented the obtained values for incorporation with sivelestat, without incorporation and with incorporation with the model-drug orange IV, to facilitate their comparison and further discussion.

Table V.5. Silk Fibroin Nanoparticles yield production (formation efficiency) and encapsulation efficiency for incorporation of 100 µM of sivelestat.

Sample	SF-NPs Yield Formation Efficiency (%)	SF-NPs Encapsulation Efficiency (%)
SF-NPs (control)	60.097 ± 3.033	-
SF-NPs loaded with 100 µM Orange IV	66.879 ± 2.147	91.446 ± 0.082
SF-NPs loaded with 100 µM Sivelestat	99.685 ± 0.224	~ 49.6 ± 5.6

Regarding the formation efficiency, the SF-NPs with sivelestat presented a higher value than without incorporation and with incorporated orange IV, which means that almost all SF molecules are being used in the nanoparticles formation.

Still, the encapsulation efficiency obtained for this condition is lower than the predicted by orange IV incorporation. However, the sivelestat concentration that was incorporated in the SF-NPs (> 50 µM) is enough to inhibit HNE enzyme since this HNE inhibitor is very potent (Kawabata *et al.*, 1991), which will be further proven in inhibition studies. In fact, according to Kawabata *et al.* studies, this drug showed an IC_{50} of 0.044 ± 0.003 µM, when using succinyl-Alanine-Alanine-proline-phenylanine-p-nitroanilide (suc-Ala-Ala-Pro-Phe-pNA) as substrate (Kawabata *et al.*, 1991).

It is also important to highlight that the method used to detect and quantify the free sivelestat (*i.e.* sivelestat not encapsulated in the SF-NPs) involved an extrapolation from the kinetic assays because sivelestat is very difficult to detection by simpler methods, like absorbance by UV-Vis. In this method, we detected the concentration of free sivelestat by measuring their inhibition effect on HNE enzyme, and then we determined sivelestat concentration by comparison and extrapolation with the standard HNE inhibition studies with sivelestat at various concentrations.

Besides, since the encapsulation efficiency determination methods for sivelestat and orange IV are different, this obtained values cannot be correctly compared. Hence, this results only served to have an idea of the final characteristics of the developed SF-NPs incorporating sivelestat.

In general, we have observed that the obtained results with sivelestat differ significantly from the predicted results with model-drug orange IV. As already discussed, this might be due to the differences between the orange IV and sivelestat structures, in which orange IV presented more stabilizing groups than sivelestat.

Although the formation and encapsulation efficiency values obtained for SF-NPs incorporated with sivelestat were considered good, the mean diameter and PDI values of this particles, after production and over time, were not. In fact, the obtained characteristic of size and size distribution and their stability along time were not adequate, being necessary to conduct more experiences. Considering this, we suggest to evaluate other model-drug with more similarities to sivelestat or even to use sivelestat in further production, being important to take into account the cost of these suggestions.

In addition, we also suggest that incorporation of stabilizers into the formulation would solve this instability problem, namely transcutol and SDS combination as previously proposed.

Even so, we considered the studies with SF-NPs incorporating orange IV to be relevant since the obtained results which showed that orange IV really stabilizes the SF-NPs (mean diameter and PDI values of the SF-NPs incorporated with orange IV showed to be persistent over time) could be applied in the textile industry. In fact, silk and orange IV are extensively used in textile, in which Uddin *et al.* describes silk dying with an acidic dye like orange IV (Sah *et al.*, 2010;Uddin *et al.*, 2010). Considering this and in agreement with others studies, we suggest that application of SF-NPs incorporated with dyes, like orange IV, would enable improvement of colourability and enhancement of bleaching resistance (Hegemann *et al.*, 2007;Mahltig *et al.*, 2005;Siegfried, 2007).

3.1. HNE Inhibition Studies of SF-NPs incorporated with Sivelestat

Although, the SF-NPs incorporated with sivelestat did not present good stability results, we continued their characterization, namely their HNE inhibition effect. For that, we first conducted standard assays of HNE inhibition effect of the drug sivelestat. In other words, we assessed the sivelestat effectiveness as an inhibitor of HNE and potential anti-wrinkling agent.

The inhibition studies consisted in measuring the HNE activity at various concentrations of sivelestat, namely 0, 0.1, 0.25, 0.5, 1, 1.5, 2, 2.5 and 5 µM of sivelestat. This results are presented below, in Figure V.8.
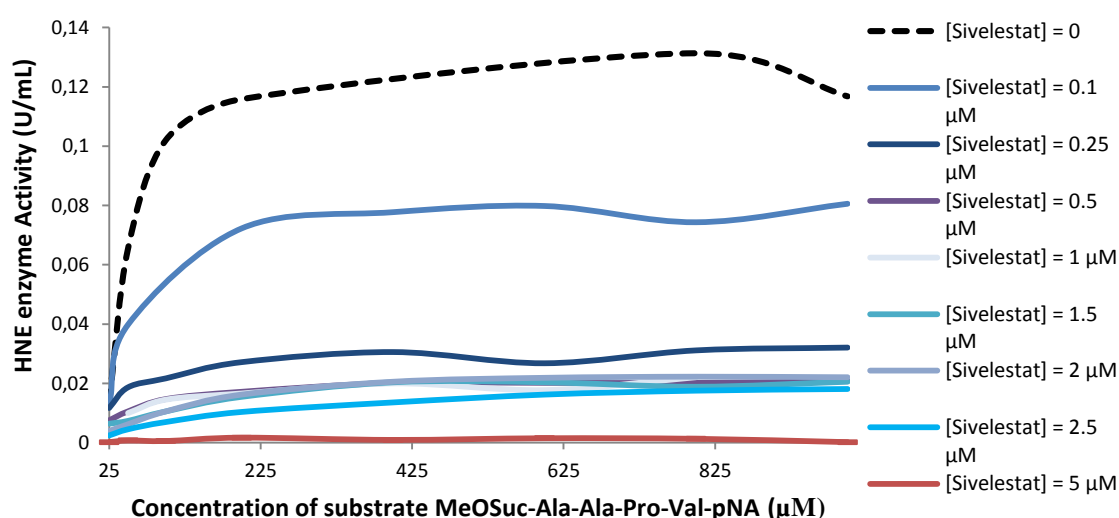
Figure V.8. Human Neutrophil Elastase (HNE) Inhibition studies with various concentration of the drug sivelestat (0.1, 0.25, 0.5, 1, 1.5, 2, 2.5 and 5 µM of sivelestat), at various concentrations of substrate *N*-methoxysuccinyl-Ala-Ala-Pro-Val-*p*-nitroanilide and at 0.5 U/mL of HNE.

The results of Figure V.8 highlight the effectiveness of sivelestat as a potent inhibitor of human neutrophil elastase, which agrees with previous publications (Aikawa *et al.*, 2011;Imokawa, 2008;Kawabata *et al.*, 1991;Tsuji *et al.*, 2001). In fact, it is possible to observe that at 5 µM of sivelestat, the HNE enzyme activity is completely inhibited. Hence, this shows the potential of sivelestat as an anti-wrinkling agent.

Finally, HNE inhibition studies of the SF-NPs incorporating sivelestat were performed. According to the encapsulation efficiency previously discussed, these developed particles possess sivelestat at a higher concentration than 50 µM, which has been shown in Figure V.8 to be enough to cause HNE inhibition.

In the following, we present the HNE inhibition studies of these developed particles with sivelestat incorporated, in Figure V.9. In this result, as controls we measured the HNE activity in buffer and in silk fibroin solution, being all in absence of sivelestat.

- - - Standard HNE kinetic (Buffer + Substrate + HNE)

——— HNE kinetic in silk fibroin solution (Buffer + Substrate + HNE + SF)

——— Silk Fibroin Nanoparticles incorporated with 100 µM of Sivelestat (Buffer + Substrate + HNE + SF-NPs loaded-Sivelestat sample)
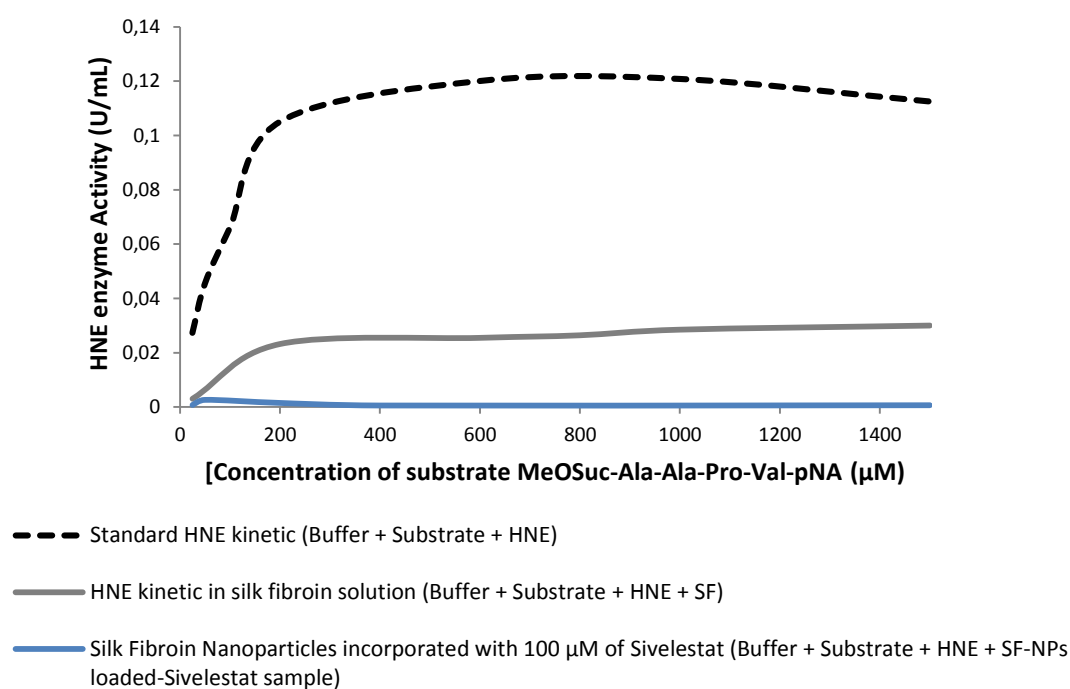
Figure V.9. Human Neutrophil Elastase (HNE) Inhibition studies with silk fibroin nanoparticles incorporated with 100 µM of sivelestat, at various concentrations of substrate *N*-methoxysuccinyl-Ala-Ala-Pro-Val-*p*-nitroanilide and at 0.5 U/mL of HNE.

According to Figure V.9, it is possible to observe the HNE inhibition effect that SF-NPs incorporating sivelestat possess. In fact, the SF-NPs with sivelestat incorporated were able to completely inhibit the HNE enzyme, indicating their potential as anti-wrinkling agents. So, even that the final characteristics of the developed SF-NPs with sivelestat were not ideal, we can conclude that this is a good approach.

In addition, Figure V.9 also showed that silk fibroin did reduce the HNE activity, when dissolved in solution. Taking into account the Wharram *et al.* studies, the authors showed that silk wound dressing effectively remove HNE from the wound site (Wharram *et al.*, 2010). We, then, suggest that silk fibroin may possess the capability of inhibit the HNE enzyme, which enhances their potential when applied as nanoparticles.

In conclusion, this results suggest that the silk fibroin nanoparticles incorporated with sivelestat can be used as anti-wrinkling agents since the developed particles were able to completely inhibit the HNE enzyme, which is extensively involved in wrinkle formation. by repeated UV irradiation and mild inflammation (Imokawa, 2008;Takeuchi *et al.*, 2010).

Chapter VI:

Structure Analysis of SF-NPs

by FTIR Spectroscopy
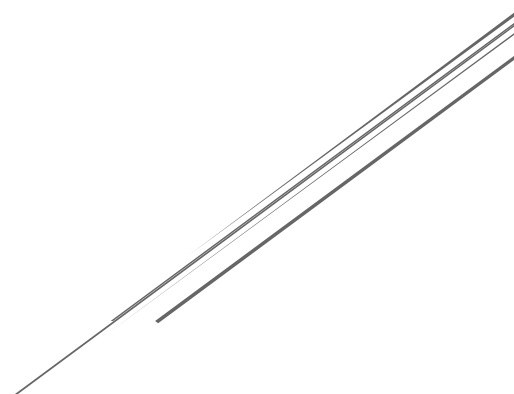
Chapter VI: Structure Analysis of SF-NPs by FTIR Spectroscopy

The silk fibroin nanoparticles (SF-NPs) were produced by high-energy emulsification using high-pressure homogenization (HPH) method. Briefly, in this process oil-in-water samples are submitted to disruptive forces, such as hydraulic shear, intense turbulence and cavitation (Lovelyn *et al.*, 2011). This forces break the oil and water initial phases, creating emulsion drops at nano range, which can ultimately lead to nanoparticles (Grebler *et al.*, 2010). Along this formation process, silk fibroin protein conformational changes may occur (Floury *et al.*, 2000;Silva *et al.*, 2012;Silva *et al.*, 2012). Hence, in order to better understand the HPH emulsification process, the secondary structure of the developed SF-NPs were evaluated by attenuated total reflectance Fourier transform infrared (ATR-FTIR) spectroscopy, being this technique further detailed in Annex X.

A range of conformations has been found in silk secondary structure, such as, random-coil, β-sheets, β-turns, α-helices and 3_{10} helices (Chen *et al.*, 2001)**.** The silk high conformational variability due to their high content of glycine, designating silk as a polymorphic protein (Wilson *et al.*, 2000). The dominant secondary structure of silk differs according to the environment of the protein, such as pH, temperature, ions presence and absence, energy involved, and others (Wilson *et al.*, 2000), being important to understand the conditions that lead to conformational changes of the secondary protein.

The unordered and rather unstable conformation, usually termed as random-coil, results from non-repetitive sequences (Kong *et al.*, 2007;Tsukada *et al.*, 1994), whereas the other structures are established due to the repetitive motifs (Rabotyagova *et al.*, 2010).

A more stable structure is β-sheet conformation, which is characterized by folded chains lied alongside of each other, in a parallel (sheets point in the same direction) or anti-parallel orientation (sheets point in opposite directions) (Chen *et al.*, 2001;Tsukada *et al.*, 1994). The β-sheet folding is nucleated and envisioned with reverse turn formations, the β-turns (Fuller *et al.*, 2009). This β-turns structures, also called by β-bends, are arranged end-to-end of each β-strand, enabling the β-sheets final conformation, connecting this two structures to the same conformation β-sheets (Vollrath *et al.*, 2001).

The α-helix conformation is also a stable structure, formed by winding the polypeptide backbone into a tightly packed right-handed helix, *i.e.* folded in clockwise direction (Rabotyagova *et al.*, 2010). Similar to α-helices conformation, there is the 3_{10} Helices, which are a more compact conformation, folded in counter clockwise direction (Vollrath *et al.*, 2001).

Silk in a natural source is composed by β-sheet crystalline segments with alternation with amorphous segments of random-coil (Rabotyagova *et al.*, 2010). Whereas silk fibroin particles prepared by mechanical mixing and self-assembly process is predominantly composed by β-sheets (Zhao *et al.*, 2013). In fact, their application as drug delivery systems is improved because of the crystalline β-sheets formation, since it increases encapsulation efficiency and enables control of the drug release kinetics (Tudora *et al.*, 2013).

There are a couple of normal modes of movements and vibration that proteins can achieve, which depends of the several internal coordinates of the protein, namely the bond lengths and bond angles (Barth *et al.*, 2002). Since there are a vast number of normal modes, the vibrational spectrum is complex in which many of the vibrational bands overlap, preventing accurate analysis (Barth *et al.*, 2002). As solution, it is possible to select a spectral region suitable for the information that we expect to extract (Barth *et al.*, 2002).

Mainly, these selected regions present a spectrum dominated by protein repeat units with the same kind of normal mode vibration (Barth *et al.*, 2002). The proteins repeat units can lead to nine characteristic IR absorption bands, namely amide A, B, and I to VII (Kong *et al.*, 2007).

As preliminary screening tool, the position of amide I, II and III bands of IR spectra was used identifying the prevailing structure taken by the silk fibroin. The amide I band is between 1600 cm^{-1} and 1700 cm^{-1} (Kong *et al.*, 2007) and is mainly dominated by signals of the backbone C=O stretching vibrations (Barth *et al.*, 2002; Kong *et al.*, 2007); amide II and III are attributed to the C-N stretching and N-H bending (Kong *et al.*, 2007), and are detected in 1480 to 1575 cm^{-1} and 1229 to 1301 cm^{-1}, respectively (Kong *et al.*, 2007).

The position of these bands can also specify the main conformation of the silk fibroin, namely for amide I, 1620-1638 cm^{-1} indicates β-sheets and 1639-1647 cm^{-1} indicates random-coil (Wilson *et al.*, 2000); for amide II, 1515-1530 cm^{-1} indicates β-sheets and 1534-1540 cm^{-1} indicates random-coil (Ha *et al.*, 2005; Miyazawa *et al.*, 1960); and for amide III, 1229-1244 cm^{-1} indicates random-coil and 1265-1270 cm^{-1} indicates β-sheets (Ha *et al.*, 2005; Tsukada *et al.*, 1994).

The obtained results of this initial analyse for silk fibroin solution (before emulsification process) and for silk fibroin nanoparticles with and without incorporation (after emulsification process) are presented in graph of Figure VI.1. For better elucidation, the respective band of amide I, II and III is also indicated.
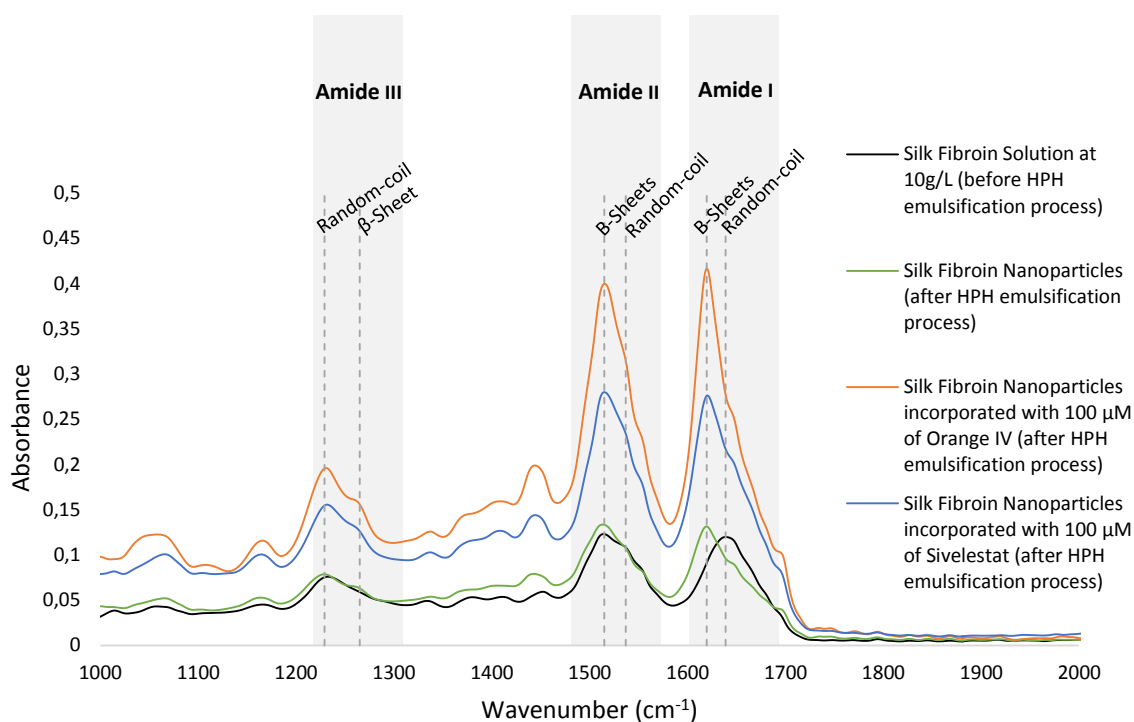
Figure VI.1. FTIR spectrum of the three principal amide (amide I, II and III) of silk fibroin protein before and after HPH emulsification process, in which the random-coil and β-sheets secondary structure is presented.

According to amide I and II, the silk fibroin nanoparticles (after HPH emulsification process) present higher signals for β-sheets, suggesting this secondary structure as dominant in these sample, wherein the silk fibroin solution (before HPH emulsification process) presents high signal for random-coil in amide I spectra. However according to amide II region, this sample presents minor signal for random-coil, presenting a higher signal for β-sheets structure. Regarding the amide III, all samples present higher signals for random-coil structure, which is discrepant to the amide I and II results.

As result of these discrepancies, further studies were conducted, in order to better understand the mechanisms involved in HPH emulsification and the conformational changes of the secondary structure that can occur.

Amide I band (1600 cm^{-1} and 1700 cm^{-1}) is considered the most prominent and sensitive vibrational bands (Kong *et al.*, 2007). This amide I is mainly dominated by signals of the backbone C=O stretch vibrations (Barth *et al.*, 2002), which indicates the peptide linkages and their frequencies components closely correlate to the secondary structure (Kong *et al.*, 2007). According to this and the fact that amide I spectrum is not significantly affected by side chain vibrations (Rabotyagova *et al.*, 2010), we selected the amide I spectral region for silk fibroin protein secondary structure deeper analyse by ATR-FTIR spectroscopy. For that, region between 1600 cm^{-1} and 1700 cm^{-1} was deconvulated into discreet components indicating the specific secondary structure. The assignment of the peaks to a respective secondary structure was based in Kong *et al.,* 2007 and Dong *et al.*, 1992 studies (Dong *et al.*, 1992;Dong *et al.*, 1992;Kong *et al.*, 2007)**.**

For amide I, peaks in the range of 1616-1643 cm^{-1} and 1689-1698 cm^{-1} were indicative of β-sheets structures, 1667-1688 cm^{-1} indicated β-turns, 1644-1650 cm^{-1} indicated presence of random-coil conformation, 1652-1657 were assigned to α-helices conformations, and 1658-1666 cm^{-1} were indicative of 3$_{10}$ Helix structure.

The results of deconvulation of amide I is presented in the following graph, Figure VI.2. In this figure, the secondary structures content (in percentage) of each sample (before and after HPH emulsification) is displayed. This result will allow us to better understand the mechanism and conformational changes that may occur during this nanoparticles formation process, and to compare the nanoparticles without and with incorporation of orange IV and sivelestat.
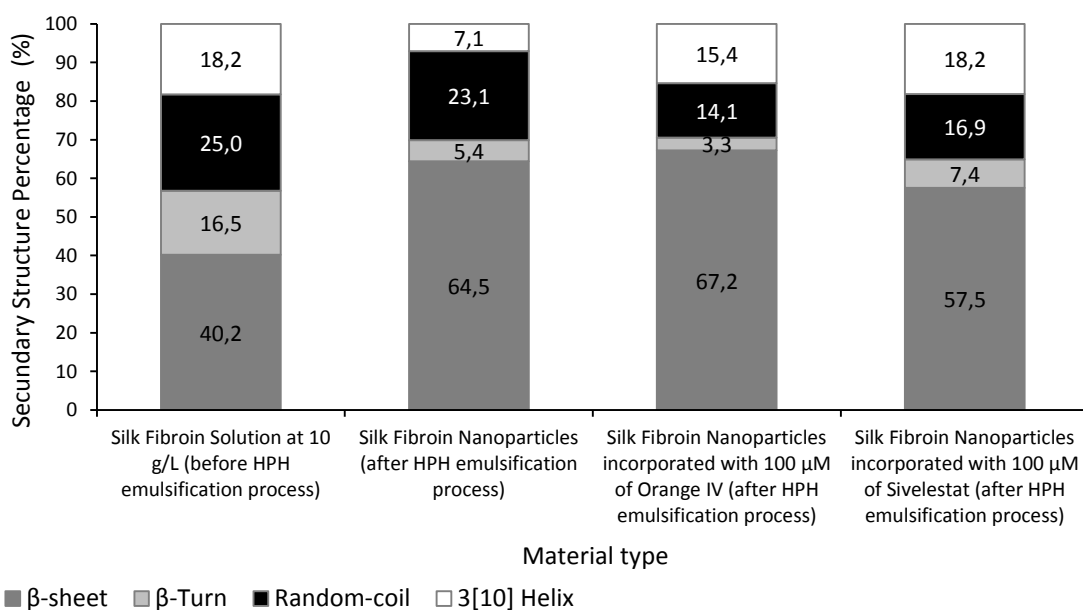

Figure VI.2. Results from the deconvulation of amide I region (1600 and 1700 cm^{-1}) of the FTIR spectrum of silk fibroin protein before and after HPH emulsification process.

As already mentioned above, forces involved in high-pressure homogenization (HPH) are very similar to the ones involved in ultrasonication, so we hypothesised that the silk fibroin behaviour in both methods is similar (Bang *et al.*, 2010;Lovelyn *et al.*, 2011). According to other studies, through nanoparticles formation by ultrasonic emulsification, silk fibroin protein acquire mainly β-sheets conformation (Silva *et al.*, 2012;Silva *et al.*, 2012). In detail, this sonochemical process increases the proximity of the molecular chains, which promotes crystallinity (Silva *et al.*, 2012;Silva *et al.*, 2012). Therefore, we hypothesized that crystalline conformation, namely β-sheets structure, increases along the nanoparticle formation by HPH emulsification process.

 In fact, results presented in Figure VI.2 agree with this hypothesize since the content of β-sheets increased with the high-pressure homogenization process. This is noticed because β-sheets content in silk fibroin solution (before HPH emulsification) to the silk fibroin nanoparticles (after HPH emulsification process), increased from ∼40% to 65%.

In addition, the same effect is observed for silk fibroin nanoparticles incorporated with a drug, in which, incorporation with orange IV and sivelestat presented β-sheets content of ∼67% and ∼57%, respectively. This difference might be related to the fact that orange IV possess a the capability to stabilize the SF by establishing hydrophobic interaction and van der Waals forces with the SF structure due to the azo (N=N) and sulphonate groups (S=O) whereas sivelestat only has the sulphonate group (Uddin *et al.*, 2010). Besides dissolution of orange IV in SF causes decrease of pH, since orange IV is an acid dye. This acidic environment causes protonation of the carboxyl groups on side chains of SF, decreasing repulsions and also leading to stronger hydrophobic interactions (Matsumoto *et al.*, 2006). According to this, orange IV is capable to stabilize the SF, and therefore promoting a higher crystallinity content.

Furthermore, the random-coil conformation decreased with the HPH emulsification process, from ∼25% of random-coil content in silk fibroin solution to ∼23% for silk fibroin nanoparticles without incorporation, and random-coil content of SF-NPs incorporated with orange IV and sivelestat was ∼14% and ∼16%, respectively. The random-coil opposite behaviour to the β-sheets content, suggested that random-coil may be conformational changing to β-sheets.

The same is applied to β-turns conformation, and since β-turns connect end-to-end the β-sheets, it may also imply that the β-sheets structures are becoming elongated and extended. Even so, the proximity of the peaks range of β-turns (1667-1688 cm^{-1}) to the range of β-sheets (1689-1698 cm^{-1}) can also lead to some difficulty in peaks assignment.

Finally, the 3_{10} Helix content decreased from silk fibroin solution ($\sim$18%) to silk fibroin nanoparticles ($\sim$7), which suggested a conformational change to a more stable structure, β-sheets. However, SF-NPs incorporated with orange IV and sivelestat showed a smaller decrease of 3_{10} Helix content, this may suggest that these structures are less stable than the SF-NPs without incorporation. The decrease of 3_{10} Helix content for SF-NPs incorporated with sivelestat was less significant than with orange IV because this last drug has a higher capability of stabilize the SF-NPs.

The FTIR spectroscopy results showed that the secondary structure of the silk fibroin changed during the high-pressure homogenization emulsification process, implying that this process possess the same behaviour of ultrasonication. The silk fibroin crystallinity content increased along the nanoparticle formation process by HPH, since the random-coil and other structures conformational changed to β-sheets after this emulsification process. Therefore, the silk fibroin associated in nanoparticles showed a more stable structure, which is very promising as drug delivery systems, specifically for the intended topical anti-wrinkling application.

Chapter VII:

General Conclusions and

Future Perspectives
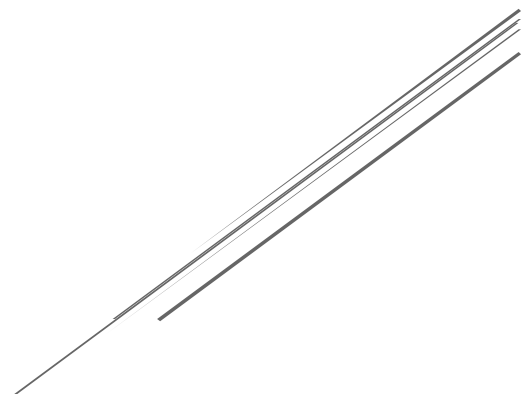
Chapter VII: General conclusions and future perspectives

The goal of this dissertation was the development and characterization of silk fibroin nanoparticles incorporated with a human neutrophil elastase inhibitor, sivelestat, for topical application as an anti-wrinkling agent. These SF-NPs are intended to effectively entrap sivelestat at a therapeutic concentration in order to successfully inhibit the HNE enzyme present in the skin, preventing wrinkles formation induced by UV radiation. Furthermore, these nanodevices should be able to penetrate the skin *stratum corneum*, in order to effectively inhibit the HNE degradation of the extracellular matrix, consequently preventing the wrinkles formation.

1. **Final Remarks**

To simplify, the final remarks of this dissertation work are summarized above.

For silk fibroin nanoparticles optimization process by the high-energy methods ultrasonication and high pressure homogenization (HPH) (chapter IV), the final remarks are the following:

❖ NPs production requires a large input of energy, in which we only effectively obtained uniform smaller NPs when the disruptive forced involved are sufficient to control the nanoemulsion and NPs formation.

❖ Increase of SF concentration and decrease of *n*-dodecane content allows better control of the NPs structure, which facilitates the emulsification process and enables production of smaller NPs with a uniform distribution.

❖ For HPH, the increase of number of cycles leads to uniform smaller NPs until a given cycle and pressure. At this point, it occur saturation-like behaviour where it negatively affects the emulsion and the NPs production.

❖ The best NPs characteristics was obtained when using 10 g/L of SF, at 20/80 of *n*-dodecane/RSF solution for 22 homogenization cycles with double-stage HPH emulsification (APV-2000™). At well-controlled conditions, the emulsification HPH method was considered reproducible.

❖ The origin of SF, namely the silkworm *Bombyx mori*, can extensively affect the obtained product and as consequence it produced different SF-NPs, being important to take all the methods variables into account.

Finally, the main conclusions obtained from silk fibroin nanoparticles incorporation studies at the optimized conditions (chapter V) and their structural analysis by FTIR (chapter VI) are presented above:

❖ Regarding incorporation of stabilizers into the formulation, transcutol showed to be more effective in stabilizing the size and size distribution over time and higher NPs yield (formation efficiency) was obtained for SDS.

❖ The model-drug orange IV showed to stabilize the size and size distribution over time, wherein incorporation of 100 μM of orange IV showed to be more effective. We considered this concentration as ideal for sivelestat incorporation in the SF-NPs.

❖ Orange IV releases from SF-NPs showed to be controlled at some extent. In this condition, we also observed incomplete release of orange IV, which could suggest instability of SF-NPs. However, results also suggest that HNE enzyme might cleave the orange IV, affecting their release detection.

❖ The drug transport mechanism involved in orange IV release from SF-NPs was considered to be anomalous (Fickian diffusion and polymer degradation/relaxation), in which it showed not to be affected by HNE enzyme at 0.5 U/mL.

❖ Incorporation of sivelestat in SF-NPs differed significantly from the predicted results using the model-drug orange IV, suggesting that orange IV was not the ideal model-drug for this project. Even so, results for orange IV could be applied in the textile industry to improve colourability and bleaching resistance.

❖ SF-NPs incorporated with sivelestat showed a good formation and encapsulation efficiency and successfully inhibit the HNE enzyme, enhancing their potential use as anti-wrinkling agents.

❖ During HPH emulsification process, the SF protein acquires mainly β-sheets content, due to probable shifting of random-coil conformation to more stable structures.

In conclusion, SF-NPs produced by HPH method showed to be a stable and effective drug delivery system, and when incorporating sivelestat showed to successfully inhibit HNE enzyme being very promising nanodevice for topical anti-wrinkling application.

2.   Future Work

Although the obtained results in the experimental work of this dissertation were satisfactory, further studies should be carried out for a more precise work evaluation. Those potential future studies are presented below:

❖   Evaluate the stabilizing effect when combining co-surfactant transcutol with surfactant SDS into the SF-NPs formulation.

❖   Measure and compare the HNE activity at various conditions (for example, in SF solution and in orange IV solution) to evaluate the possibility of HNE cleavage of orange IV.

❖   Study the developed SF-NPs morphology, for example by transmission electron microscopy (TEM) or scanning transmission electron microscopy (STEM).

❖   Optimize a better detection method for sivelestat, for example by high-performance liquid chromatography (HPLC).

❖   Optimize the production process of SF-NPs incorporated with sivelestat, namely the optimal concentration to incorporate.

❖   Evaluate the in vitro sivelestat release from SF-NPs at various parameters (such as pH, temperature and HNE concentration), for example by dialysis bag method and/or by confocal analysis, in which sivelestat could be associated to a fluorescent dye.

❖   Conduct molecular simulations of the behaviour of SF protein during HPH emulsification process and of sivelestat release from SF-NPs.

❖   Evaluate the in vitro cytotoxicity of the developed SF-NPs.

❖   Evaluate the transdermal delivery of the developed SF-NPs and their HNE inhibition effects by in vitro histological penetration studies

❖   Evaluate the developed SF-NPs as an anti-wrinkling agent by in vivo histological studies.

A number of valuable results were obtained in this dissertation, and hopefully may be further used in future investigations, taking into account that SF-NPs can be used for other applications.

Annexes
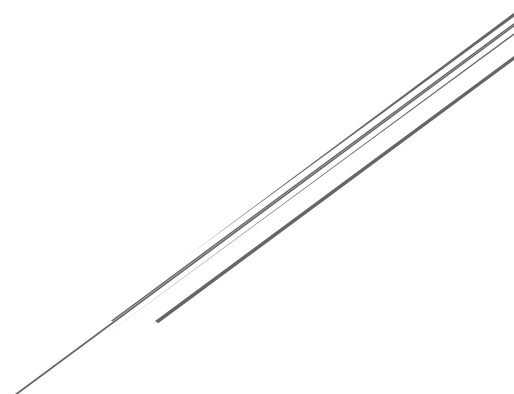
Annexes

Annex I. *Bombyx mori* Silk Fibroin Amino Acid Composition.

Table Annex.1. Amino acid composition expressed as mol % of *Bombyx mori* silk fibroin, quantified by High-performance liquid chromatography (HPLC) after acid hydrolytic treatment (24 hours of 6M HCl, at 105°C, under vacuum) and analysed according to the AccQ-Tag Method, published in Vasconcelos *et al.*, 2008.

Amino acid	Quantity in silk fibroin (mol %)
Aspartic acid (Asp)	1.67
Serine (Ser)	11.48
Glutamic Acid (Glu)	1.37
Glycine (Gly)	43.68
Histidine (His)	0.20
Arginine (Arg)	0.62
Threonine (Thr)	0.96
Alanine (Ala)	29.34
Proline (Pro)	0.67
Cysteine (Cys)	0.10
Tyrosine (Tyr)	5.30
Valine (Val)	2.23
Methionine (Met)	0.10
Lysine (Lys)	0.33
Isoleucine (Iso)	0.66
Leucine (Leu)	0.58
Phenylanine (Phe)	0.72

Annex II. Silk Fibroin Hydrogels formation.

SF hydrogels are determined by silk fibroin concentration, temperature, pH (Matsumoto *et al.*, 2006), presence of Ca^{2+} and K^+ (Kim, U *et al.*, 2004), and is even related to RSF preparation process (Ayub *et al.*, 1993). Briefly, Matsumoto studies showed that increasing SF concentration and temperature, the gelation time decreases, *i.e.* leads to gel formation (Matsumoto *et al.*, 2006); and Ayub and co-workers suggested that reduction of SF molecules movement and formation of hydrogen bonds increases and stabilizes β-sheets, leading to gel formation (Ayub *et al.*, 1993). In more detail, lower pH (2 to 4) and increasing pH (6 to 9) decreases gelation time, since lowering pH (2 to 4) causes protonation of the carboxyl groups on SF side chains, decreasing repulsions and consequently stronger hydrophobic interactions are established, leading to gel formation; and increasing pH (6 to 9) triggers electrostatic interactions between charged amino and carboxylic groups, also leading to gelation but at a lower rate (Matsumoto *et al.*, 2006). Lastly, Ca^{2+} also increases these interactions, also leading to gel formation (Kim, U *et al.*, 2004).

SF gels can also be formed by vortexing, sonication, by applying electrical current (Rockwood *et al.*, 2011), or induced by supplementation with poly(ethylene oxide) (PEO) (Jin *et al.*, 2004) or poly(ethylene glycol)-*block*-poly(propylene glycol)-*block*-poly(ethylene glycol (commonly named as poloxamer 407) (Vepari *et al.*, 2007), or sodium dodecyl sulphate (SDS) (Wu, X *et al.*, 2012). In particular, PEO is a biocompatible polymer, which reassembles to a surfactant (Jin *et al.*, 2004), and facilitates interactions among SF protein and increasing β-sheets content (Kim, U *et al.*, 2004); and poloxamer 407 and SDS also increases these interactions, also leading to gel formation (Wu, X *et al.*, 2012). However, poloxamer 407 is non-biodegradable and presents minor effect in gel formation, hence is not considered as an ideal gel inducer, whereas SDS is approved by FDA and highly recommended (Wu, X *et al.*, 2012).

Annex III. Equipment's used in this work.

Table Annex.2. List of equipment used through the experimental work of this dissertation with their basic description, such supplier, the method which was associated with and its use in the experimental work.

Name of the equipment	Supplier	Associated-method	Use
20 kHz Vibrocell ™ CV 33 - Probe type ultrasound source fitted with a 3 mm diameter titanium micro-tip	Sonics and Materials Inc., Connecticut, USA	Ultrasonic emulsification	Nanoemulsion and NP production
EmulsiFlex™-C3	Avestin, Ottawa, Canada	High Pressure Homogenization (single-stage system)	Nanoemulsion and NP production
APV-2000™	SPX Flow Technology, APV Manufacturing, Poland	High Pressure Homogenization (double-stage system)	Nanoemulsion and NP production
ZetaSizer Nano ZS (with ZetaSizer software version 7.01)	Malvern Instruments Ltd., Worcestershire, United Kingdom	Dynamic Light Scattering (DLS); Laser Doppler Anemometry (LDA)	NPs characterization
SynergyMx with Gen5™ Microplate Data Collector and Analysis Software	Bio-Tek Instruments, Inc., Vermont, USA	Ultraviolet-Visible (UV-Vis) Spectrophotometry	HNE studies and inhibition; Calibration curves; NPs Characterization
Jasco FT/IR 4100 spectrometer equipped with attenuated total reflectance (ATR) accessory	Jasco, Inc., Easton, EUA.	Fourier Transform Infrared (FTIR) Spectroscopy	NPs characterization
Allegra® X-15R Centrifuge with an FX6100 rotor	Beckman Coulter, Inc., California, EUA.	Ultracentrifugation	NPs characterization

Annex IV. Calibration curve of Regenerated Silk Fibroin by Bradford method.
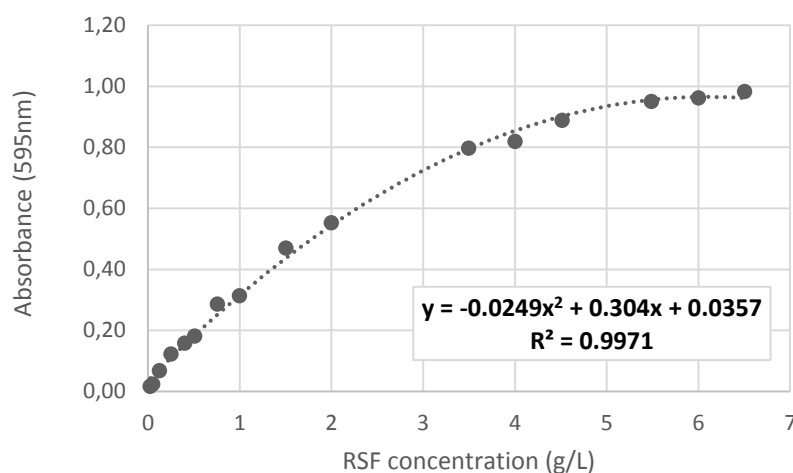
Figure Annex. 1. Calibration the curve of regenerated silk fibroin by Bradford method, used in further quantification of this protein along this work. The determined equation is $y = -0.0249x^2 + 0.304x + 0.0357$, with r^2 of 0.9971.

Annex V. Information of the Stabilizers used in this work.

Table Annex.3. Chemical basic information (molecular weight, molecular formula and structure) of the stabilizers used along this work, namely poloxamer 407, transcutol, tween 80 and SDS, retrieved from the suppliers document sheet.

Name	Molecular Weight	Molecular Formula	Structure
Poloxamer 407	(9,840 to 14,600) $\sim$ 1,260 g/mol	$(C_3H_6O.C_2H_4O)_n$	
Transcutol	134.17 g/mol	$C_6H_{14}O_3$	
Tween 80	$M_n \sim$1,310 Da	$C_{64}H_{124}O_{26}$	
SDS	288.38 g/mol	$CH_3(CH_2)_{11}OSO_3Na$	

Annex VI. Information of Orange IV and Sivelestat used in this work.

Table Annex.4. Chemical basic information (molecular weight, molecular formula and structure) of orange IV and sivelestat, retrieved from the suppliers document sheet.

Name	Molecular Weight (g/mol)	Molecular Formula	Structure
Orange IV	375.38	$NaC_{18}H_{14}SN_3O_3$	
Sivelestat sodium salt hydrate	434.46	$C_{20}H_{22}N_2O_7S$	

Annex VII. Dynamic Light Scattering (DLS) Method.

In this experimental work, the developed nanoparticles characterization according to size and size distribution was determined by dynamic light scattering (DLS), also known as photonic correlation spectroscopy (PCS), which measures the Brownian motion of the particles, and the diffusion coefficient is determined by Stokes-Einstein equation (Bunjes, 2005), presented above.

$$D = \frac{K.T}{3.\pi.d}$$

Equation Annex.1. Stokes-Einstein equation used to determinate the diameter of the particles, where D, d, K and T represent the diffusion coefficient, the diameter of the particles, the Botlzman constant and the temperature in Kelvin, respectively. Based in Bunjes, 2005 publication.

Annex VIII. Laser Doppler Anemometry (LDA) Method.

In this experimental work, the developed nanoparticles surface charge characterization was determined by laser Doppler anemometry method according to zeta-potential. In this method, the particles are submitted to weak electric field (Malvern, 2005), resulting in frequency (Doppler) shift, then their electrophoretic mobility is indirectly determined according to Henry equation (Bunjes, 2005), presented above**.**

$$\mu_e = \frac{2.\,\varepsilon.\,\zeta-.\,f(Ka)}{3.\,\eta}$$

Equation Annex.2. Henry equation used to determinate the electrophoretic mobility of the particles, where μ_e, ε, ζ, η and $f(Ka)$ represent the electrophoretic mobility, dielectric potential, zeta-potential, role of Henry and viscosity of the medium, respectively. Based in Bunjes, 2005 publication.

Annex IX. Calibration curve of compound Orange IV.
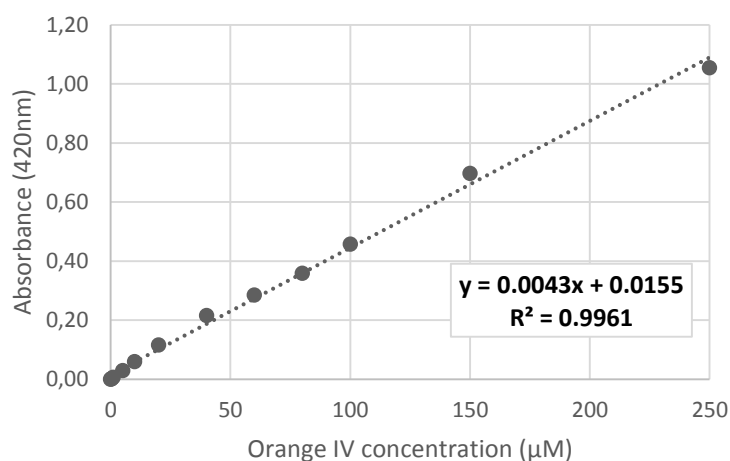
Figure Annex. 2. Calibration the curve of orange IV, used in further quantification of this compound along this work. The determined equation is y=-0.0043x + 0.0155, with r^2 of 0.9961.

Annex X. Fourier transform infrared (FTIR) Spectroscopy Method.

Being one of the oldest and well established experimental techniques for protein secondary structure analysis (Hsu, 1997;Kong *et al.*, 2007), infrared (IR) spectroscopy is based in the fact that each molecule absorbs distinct wavelength (Kong *et al.*, 2007). In IR spectroscopy samples are submitted to infrared radiation, causing molecular vibration, which can be detected (Barth *et al.*, 2002). Emerge of Fourier transform infrared (FTIR) spectroscopy revolutionised the IR technique by enabling wavenumber detection simultaneously and massive data acquisition, making it a faster and reliable technique (Barth *et al.*, 2002;Kong *et al.*, 2007). Coupling of attenuated total reflectance (ATR) accessory to FTIR allows IR radiation deeper penetration, being used for thick or highly absorbing solid and liquid materials (Hsu, 1997). In ATR method a thin protein film (portion of the lyophilized sample) was deposited on an internal reflection element (IRE), a crystal (Barth *et al.*, 2002;Kong *et al.*, 2007), then the IR radiation passes through the IRE material, and interacts with the sample material at the interface of these two materials (Hsu, 1997).

References
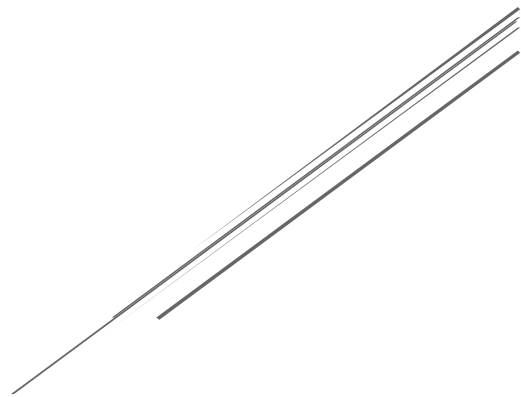
References

Aikawa, N; Ishizaka, A; Hirasawa, H; Shimazaki, S; Yamamoto, Y; Sugimoto, H; Shinozaki, M; Taenaka, N; Endo, S; Ikeda, T; and Kawasaki, Y (2011). "Reevaluation of the ef fi cacy and safety of the neutrophil elastase inhibitor, Sivelestat, for the treatment of acute lung injury associated with systemic inflammatory response syndrome; a phase IV study." Pulmonary Pharmacology & Therapeutics **24**: 549-554.

Altman, G; Diaz, F; Jakuba, C; Calabro, T; Horan, R; Chen, J; Lu, H; Richmond, J; and Kaplan, D (2003). "Silk-based biomaterials." Biomaterials **24**: 401-416.

Anton, N; Benoit, J; and Saulnier, P (2008). "Design and production of nanoparticles formulated from nano-emulsion templates- A review." Journal of Controlled Release **128**: 185-199.

Arakama, T; and Kita, Y (2000). "Protection of Bovine Serum Albumin from Aggregation by Tween 80." Journal of Pharmaceutical Sciences **89**(5): 646-651.

Asasutjarit, R; Sorrachaitawatwong, C; Tipchuwong, N; and Pouthai, S (2013). "Effect of Formulation Compositions on Particle Size and Zeta Potential of Diclofenac Sodium-Loaded Chitosan Nanoparticles " International Journal of Pharmaceutical Sciences **7**(9): 454-456.

Ayub, ZH; Arai, M; and Hirabayashi, K (1993). "Mechanism of the Gelation of Fibroin Solution." Bioscience, Biotechnology, and Biochemistry **57**(11): 1910-1912.

Bang, JH; and Suslick, KS (2010). "Applications of Ultrasound to the Synthesis of Nanostructured Materials." Advanced Materials **22**: 1039-1059.

Barnadas-Rodríguez, R; and Sabés, M (2001). "Factors involves in the production of liposomes with a high-pressure homogenizer." International Journal of Pharmaceutics **213**: 175-186.

Barth, A; and Zscherp, C (2002). "What vibrations tell us about proteins." Quarterly Reviews of Biophysics **35**(4): 369-430.

Brandl, M; Bachmann, D; Drechsler, M; and Bauer, KH (1990). "Liposome preparation by a new high-pressure homogenizer Gaulin Micron LAB 40." Drug Development and Industrial Pharmacy **16**(4): 2167-2191.

Bunjes, H (2005). Characterization of Solid Lipid Nanoparticles and Microparticle. Lipospheres in Drug Targets and Delivery Approaches, Methods and Applications. Nastruzzi, C. Boca Raton, Florida, CRC Press LLC**:** 41-66.

Buzea, C; Blandino, IP; and Robbie, K (2007). "Nanomaterials and nanoparticles: Sources and toxicity." Biointerphases **2**(4): MR17-MR172.

Caligur, V (2008). "Detergents and Solubilization Reagents." BioFiles for File Science Research **3**(3): 1-36.

Cao, Y; and Wang, B (2009). "Biodegradation of silk biomaterials." International journal of molecular sciences **10**(4): 1514-1524.

Cao, Z; Chen, X; Yao, J; Huang, L; and Shao, Z (2007). "The preparation of regenerated silk fibroin microspheres." Soft Matter **3**(7): 910.

Chen, X; Shao, Z; Marinkovic, NS; Miller, LM; Zhou, P; and Chance, MR (2001). "Conformation transition kinetics of regenerated Bombyx mori silk fibroin membrane monitored by time-resolved FTIR spectroscopy." Biophysical Chemistry **89**: 25-34.

Crotts, G; and Park, TG (1997). "Stability and release of bovine serum albumin encapsulated within poly(D,L-lactide-co-glycolide) microparticles." <u>Journal of Controlled Release</u> **44**: 123-134.

Crotts, G; Sah, H; and Park, TG (1997). "Adsorption determines *in-vitro* protein release rate from biodegradable microspheres: quantitative analysis of surface area during degradation." <u>Journal of Controlled Release</u> **47**: 101-111.

D'Souza, SS; and DeLuca, PP (2006). "Methods to Asssess *in vitro* Drug Release from Injectable Polymeric Particulate Systems." <u>Pharmaceutical Research</u> **23**(3): 460-474.

Darrell, RT (1973). Method of compacting silk sutures by stretching. United States, Ethicon, Inc. **US4014973A**.

De Jong, WH; and Borm, PJA (2008). "Drug delivery and nanoparticles: Applications and hazards." <u>International Journal of Nanomedicine</u> **3**(2): 133-149.

DeLauder, S; and Kidwell, DA (2000). "The incorporation of dyes into hair as a model for drug binding." <u>Forensic Science International</u> **107**: 93-104.

Dong, A; Caughey, B; Caughey, WS; Bhat, KS; and Coe, JE (1992). "Secondary structure of the pentraxin female protein in water determined by infrared spectroscopy: Effects of calcium and phosphorylcholine." <u>Biochemistry</u> **31**(9364-9370).

Dong, A; Huang, P; and Caughey, WS (1992). "Redox-dependent in β-extended chain and turn structures of cytochrome c in water solution determined by second derivative amide I infrared spectra." <u>Biochemistry</u> **31**: 182-189.

Dumortier, G; Grossiord, JL; Agnely, F; and Chaumeil, JC (2006). "A Review of Poloxamer 407 Pharmaceutical and Pharmacological Characteristics." <u>Pharmaceutical Research</u> **23**(12): 2709-2728.

Edwards, JV; Howley, P; and Cohen, IK (2004). "In vitro inhibition of human neutrophil elastase by oleic acid albumin formulations from derivatized cotton wound dressings." <u>International Journal of Pharmaceutics</u> **284**: 1-12.

Floury, J; Desrumaux, A; and Lardières, J (2000). "Effect of high-pressure homogenization on droplet size distributions and rheological properties of model oil-in-water emulsions." <u>Innovative Food Science & Emerging Technologies</u> **1**: 127-134.

Fuller, AA; Du, D; Liu, F; Davoren, JE; Bhabha, G; Kroon, G; Case, DA; Dyson, HJ; Powers, ET; Wipf, P; Gruebele, M; and Kelly, JW (2009). "Evaluating β-turn mimics as β-sheet folding nucleators." <u>Proceedings of the National Academy of Sciences</u> **106**(27): 11067-11072.

Gonçalves, I; Martins, M; Loureiro, A; Gomes, A; and Cavaco-Paulo, A (2013). "Sonochemical and hydrodynamic cavitation reactors for laccase/hydrogen peroxide cotton bleaching." <u>Ultrasonics Sonochemistry</u>.

Grebler, S; Gazso, A; Simkó, M; Friedeler, U; and Nentwitch, M (2010). "Nanotechnology in Cosmetics." <u>NanoTrust Dossiers</u> **008en**: 1-6.

Greenwood, R; and Kendall, K (1999). "Selection of Suitable Dispersants for Aqueous Suspensions of Zirconia and Titania Powders using Acoustophoresis." <u>Journal of the European Ceramic Society</u> **19**: 479-488.

Ha, S; Tonelli, E; and Hudson, SM (2005). "Structural Studies of Bombyx mori Silk Fibroin during Regeneration from Solutions and Wet Fiber Spinning." <u>Biomacromolecules</u> **6**(3): 1722-1731.

Häggström, M (2010). Layers of the epidermis. <u>WVSOM Meissner's corpuslce.JPG, based on Wbensmith</u>. layers.png, Epidermal.

Hajjar, E; Broemstrup, T; Kantari, C; and Witko-Sarsat, V (2010). "Structures of human proteinase 3 and neutrophil elastase – so similar yet so different." The Federation of European Biochemical Societies Journal **277**: 2238-2254.

Hanaor, D; Michelazzi, M; Leonelli, C; and Sorrell, CC (2012). "The effects of carboxylic acids on the aqueous dispersion and electrophoretic deposition of ZrO_2." Journal of the European Ceramic Society **32**: 325-244.

Hans, ML; and Lowman, AM (2002). "Biodegradable nanoparticles for drug delivery and targeting." Current Opinion in Solid State and Materials Science **6**: 319-327.

Hegemann, D; Hossain, MM; and Balazs, DJ (2007). "Nanostructured plasma coatings to obtain multifunctional textile surfaces." Progress in Organic Coatings **58**(2-3): 237-240.

Hofmann, S; Wong Po Foo, CT; Rossetei, F; Textor, M; Vunjak-Novakovic, G; Kaplan, DL; Merkle, HP; and Meinel, L (2006). "Silk fibroin as an organic polymer for controlled drug delivery." Journal of Controlled Release **111**: 219-227.

Hsu, CPS (1997). Infrared Spectroscopy. Handbook of Instrumental Techniques for Analytical Chemistry. Settle, FA. New Jersey, Prentice Hall PTR**:** 247-283.

Hyde, AJ; and Wippler, C (1962). "Molecular weight of silk fibroin." Journal of Polymer Science **58**(166): 1083-1088.

Iizuka, E; and Yang, JT (1968). "The disordered and β-conformations of silk fibroin in solution." Biochemistry **7**(6): 2218-2228.

Imokawa, G (2008). "Recent advances in characterizing biological mechanisms underlying UV-induced wrinkles: a pivotal role of fibrobrast-derived elastase." Archives of Dermatological Research **300**(1): S7-S20.

Jin, H; Park, J; Valluzi, R; Cebe, P; and Kaplan, D (2004). "Biomaterial films of *Bombyx mori* Silk Fibroin with Poly(ethylene oxide)." Biomacromolecules **5**(3): 711-717.

Kaplan, D (1994). Silk : Biology , Structure , Properties , and Genetics. Silk Polymers. Kaplan, David; Adams, W Wade; Farmer, Barry; Viney, Christopher. Charlottesville, Virginia, American Chemical Society**:** 2-16.

Kawabata, K; Suzuki, M; Sugitani, M; Imaki, K; Toda, M; and Miyamoto, T (1991). "ONO-5046, A Novel Inhibitor of Human Neutrophil Elastase." Biochemical and Biophysical Research Communications **177**(2): 814-820.

Kearns, V; MacIntosh, AC; Crawford, A; and Hatton, PV (2008). Silk-based biomaterials for tissue engineering. Topics in Tissue Engineering. Expertissues, Eds. N. Ashammakhi, R Reis, & F Chiellini. **4:** 1-19.

Kim, HK; and Park, TG (1999). "Microencapsulation of Human Growth Hormone within Biodegradable Polyester Microspheres: Protein Aggregation Stability and Incomplete Release Mechanism." Biotechnology and Bioengineering **65**(6): 659-667.

Kim, S; Fernandes, MM; Matamá, T; Loureiro, A; and Cavaco-Paulo, A (2013). "Chitosan-lignosulfonates sono-chemically prepared nanoparticles: Characterization and potential applications." Colloids and Surface B: Biointerfaces **103**: 1-8.

Kim, U; Park, J; Li, C; Jin, U ; Valluzi, R; and Kaplan, D (2004). "Structure and Properties of Silk Hydrogels." Biomacromolecules **5**(3): 786-792.

Kitamura, M; Endo, S; Sato, N; Yamada, Y; Makabe, H; Abe, H; Imai, S; Shioya, N; Takahashi, G; Mori, K; Inoue, H; Miyata, M; and Ito, Y (2003). "Effect of Sivelestat Sodium Hydrate in Three Patients with Septic ARDS." <u>Critical Care and Shock</u> **6**(3): 172-176.

Kloet, JV; and Schramm, LL (2002). "The Effect of Shear and Oil/Water Ratio on the Required Hydrophile-Lipophile Balance for Emulsification." <u>Journal of Surfactants and Detergents</u> **5**(1): 19-24.

Kong, J; and Shaoning, YU (2007). "Fourier Tranform Infrared Spectroscopic Analysis of Protein Secondary Structures." <u>Acta Biochimica et Biophysica Sinica</u> **39**(8): 549-559.

Korkmaz, B; Moreau, T; and Gauthier, F (2008). "Neutrophil elastase, proteinase 3 and cathepsin G: Physicochemical properties, activity and physiopathological functions." <u>Biochimie</u> **90**: 227-242.

Krowarsch, D; Cierpicki, T; Jelen, F; and Otlewski, J (2003). "Canonical protein inhibitors of serine proteases." <u>Cellular and Molecular Life Sciences</u> **60**: 2427-2444.

Kumar, KPS; Bhowmik, D; and Chandira, CB (2010). "Transdermal drug delivery system - a novel drug delivery system and its market scope and opportunities." <u>International Journal of Pharma and Bio Sciences</u> **1**(2): 1-21.

Kundu, J; Chung, Y; Kim, YH; Tae, G; and Kundu, SC (2010). "Silk fibroin nanoparticles for cellular uptake and control release." <u>International journal of pharmaceutics</u> **388**(1-2): 242-250.

Lo, Y (2003). "Relationships between the hydrophilic–lipophilic balance values of pharmaceutical excipients and their multidrug resistance modulating effect in Caco-2 cells and rat intestines." <u>Journal of Controlled Release</u> **90**: 37-48.

Lovelyn, C; and Attama, AA (2011). "Current State of Nanoemulsions in Drug Delivery." <u>Journal of Biomaterials and Nanobiotechnology</u> **2**: 626-639.

Mahltig, B; Haufe, H; and Bottcher, H (2005). "Functionalisation of textiles by inorganic sol-gel coatings." <u>Journal of Materials Chemistry</u> **15**(41): 4385-4398.

Malay, Ö (2005). <u>Formation and characterization of silk fibroin / Hyaluronic acid complexes and their use in iontophoretic drug delivery</u>. Master Thesis, İzmir Institute of Technology.

Malvern, I (2005). Zeta-potential Theory. <u>Zetasizer Nano Series</u>. Worcestershire, Malvern Instruments, Ltd.

Mandal, BB; Mann, JK; and Kundu, SC (2009). "Silk fibroin/gelatin multilayered films as a model system for controlled drug release." <u>European Journal of Pharmaceutical Sciences</u> **37**(2): 160-171.

Mandal, S; and Mandal, SS (2011). "Microemulsion Drug Delivery System: A Platform for Improving Dissolution Rate of Poorlt Water Soluble Drug." <u>International Journal of Pharmaceutical Sciences and Nanotechnology</u> **3**(4): 1214-1219.

Mason, TG; Graves, SM; Wilking, JN; and Lin, MY (2006). "Extreme emulsification: formation and structure of nanoemulsions." <u>Condensed Matter Physics</u> **9**(1): 193-199.

Mason, TG; Wilking, JN; Meleson, K; Chang, CB; and Graves, SM (2006). "Nanoemulsions: formation, structure, and physical properties." <u>Journal of physics: condensed matter</u> **18**: R635-R666.

Matsumoto, A; Chen, J; Collette, AL; Kim, U; Altman, GH; Cebe, P; and Kaplan, D (2006). "Mechanisms of Silk Fibroin Sol - Gel Transitions." <u>The Journal of Physical Chemistry B</u> **110**: 21630-21638.

Meinel, L; Fajardo, R; S, Hofmann; Langer, R; Chen, J; Snyder, B; Vunjak-Novakovic, G; and Kaplan, D (2005). "Silk implants for the healing of critical size bone defects." Bone **37**(5): 688-698.

Middelberg, APJ (2000). 2. Microbial Cell Disruption by High-Pressure Homogenization. Downstream Processing of Proteins: Methods and Protocols. Desai, MA. Totowa, New Jersey, Humana Press. **9:** 11-21.

Miyazaki, Y; Inoue, T; Kyi, Min; Sawada, M; Miyake, S; and Yoshizawa, Y (1998). "Effects of a Neutrophil Elastase Inhibitor (ONO-5046) on Acute Pulmonary Injury Induced by Tumor Necrosis

Factor Alpha (TNFa) and Activated Neutrophils in Isolated Perfused Rabbit Lungs." American Journal of Respiratory and Critical Care Medicine **157**: 89-94.

Miyazawa, T; and Blout, ER (1960). "Infrared Spectra of Polypeptides in Various Conformations : Amide I and II Bands." Jounal of the American Chemical Society **83**(3): 712-719.

Mohanraj, VJ; and Chen, Y (2006). "Nanoparticles – A Review." Tropical Journal of Pharmaceutical Research **5**(1): 561.

Mondal, M; Trivedy, K; and Kumar, SN (2007). "The silk proteins, sericin and fibroin in silkworm, *Bombyx mori* Linn - a review." Caspian Jounal of Environmental Sciences **5**(2): 63-76.

Monteiro-Riviere, NA; Nemanich, RJ; Inman, AO; Wang, YY; and Riviere, JE (2005). "Multi-walled carbon nanotube interactions with human epidermal keratynocytes." Toxicology Letters **155**: 377-384.

Moreau, T; Baranger, K; Dadé, S; Dallet-Choisy, S; Guyot, N; and Zani, M (2008). "Multifaceted roles of human elafin and secretory leukocyte proteinase inhibitor (SLPI), two serine protease inhibitors of the chelonianin family." Biochimie **90**: 284-295.

Morganti, P (2010). "Use and potential of nanotechnology in cosmetic dermatology." Clinical, Cosmetic and Investigational Dermatology **3**: 5-13.

Mura, P; Faucci, MT; Bramanti, G; and Corti, P (2000). "Evaluation of transcutol as a clonazepam transdermal permeation enhancer from hydrophilic gel formulations." European Journal of Pharmaceutical Sciences **9**: 365-372.

Muthu, MS; and Singh, S (2009). "Poly (D, L-Lactide) Nanosuspensions of Risperidone for Parenteral Delivery: Formulation and *in vitro* Evaluation." Current Drug Delivery **6**(1): 62-68.

Nagarkar, SP (2010). Gelation of regenerated fibroin solution. Doctor of Philosophy Thesis, Indian Institute of Technology.

Nagavarma, BVN; Hemant, KSY; Ayaz, A; Vasudha, LS; and Shivakumar, HG (2012). "Different techniques for preparation of polymeric nanoparticles - a review." Asian Journal of Pharmaceutical and Clinical Research **5**(3): 16-23.

Naik, JB; Lokhande, AB; Mishra, S; and Kulkarni, RD (2012). "Development of sustained release micro/nano particles using different solvent emulsification techniques: a review." International Journal of Pharma and Bio Sciences **3**(4): 573-590.

Nawa, M; Osada, S; Morimitsu, K; Nonaka, K; Futamura, M; Kawaguchi, Y; and Yoshida, K (2012). "Growth Effect of Neutrophil Elastase on Breast Cancer: Favorable Action of Sivelestat and Application to Anti-HER2 Therapy." Anticancer Research **32**: 13-20.

Nogueira, E; Loureiro, A; Nogueira, P; Freitas, J; Almeida, CR; Härmark, J; Hebert, H; Moreira, A; Carmo, AM; Preto, A; Gomes, A; and Cavaco-Paulo, A (2013). "Liposome and protein based stealth." The Royal Society of Chemistry.

Nounou, MM; El-Khordagui, LK; Khalafallah, N; and Khalil, SA (2006). "In vitro release of hydrophilic and hydrophobic drugs from liposomal dispersions and gels." Acta Pharmaceutica **56**: 311-324.

Orive, G; Anitua, E; Pedraz, JL; and Emerich, DF (2009). "Biomaterials for promoting brain protection, repair and regeneration." Nature Reviews Neuroscience **10**: 682-692.

Owen, C; and Campbell, E (1999). "The cell biology of leukocyte-mediated proteolysis." Journal of Leukocyte Biology **65**: 137-150.

Pandolfe, WD (1995). "Effect of premix condition, surfactant concentration, and oil level on the formation of oil-in-water emulsions by homogenization." Journal of Dispersion Science and Technology **16**(7): 633-650.

Pankaj, M; Patidar, A; Harsoliya, MS; and Pathan, JK (2011). "A Review: Development of Transdermal Drug Delivery System By Using Different

Modified Chitosan." International Journal of Pharmaceutical & Biological Archives **2**(3): 837-839.

Park, K (2007). "Nanotechnology: What it can do for drug delivery." Journal Control Release **120**(1-2): 1-3.

Patel, A; Prajapati, P; and Boghra, R (2011). "Overview on application of nanoparticles in cosmetics." Asian Journal of Pharmaceutical and Clinical Research **1**(2): 40-55.

Pathak, Y; and Thassu, D (2009). Drug Delivery Nanoparticles Formulation and Characterization. New York, Informa Healthcare USA, inc.

Prow, TW; Grice, JE; Lin, LL; Faye, R; Butler, MB; Becker, W; Wurm, EMT; Yoong, C; Robertson, TA; Soyer, HP; and Roberts, MS (2011). "Nanoparticles and microparticles for skin drug delivery." Advanced Drug Delivery Reviews **63**: 470-491.

Qiang, C; and McClements, DJ (2011). "Formation of nanoemulsions stabilized by model food-grade emulsifiers using high-pressure homogenization: Factors affecting particle size." Food Hydrocolloids **25**: 1000-1008.

Rabotyagova, OS; Cebe, P; and Kaplan, D (2010). "Role of Polyalanine Domains in β-Sheet Formation in Spider Silk Block Copolymers." Macromolecular Bioscience **10**: 49-59.

Rahmathulla, VK; Mathur, VB; and Devi, RGG (2004). "Growth and Dietary Efficiency of Mulberry Silkworm (*Bombyx mori L.*) Under Various Nutritional and Environmental Stress Conditions." Philippine Journal of Science **133**(1): 39-43.

Reis, CP; Neufeld, RJ; Ribeiro, AJ; and Veiga, FV (2006). "Nanoencapsulation I. Methods for preparation of drug-loaded polymeric nanoparticles." Nanomedicine **2**(1): 8-21.

Rijken, F (2011). Pathophysiology and prevention of photoaging: the role of melanin, reactive oxygen species and infiltrating neutrophil. Doctoral Thesis, University Medical Center Utrecht.

Ritger, PL; and Peppas, NA (1987). "A simple equation for description of solute release. I. Fickian and non-Fickian release from non-swellable devices in the form of stabs spheres, cylindres or discs." Journal of Controlled Release **5**: 23.

Ritger, PL; and Peppas, NA (1987). "A Simple Equation for Description of Solute Release. II. Fickian and Anomalous Release from Swellable Devices." Journal of Controlled Release **5**: 37-42.

Rockwood, DN; Preda, RC; Yücel, T; Wang, X; Lovett, ML; and Kaplan, D (2011). "Materials fabrication from *Bombyx mori* silk fibroin." Nature protocols **6**(10): 1612-1631.

Roy, A; Sahu, RK; and Dwivedi, J (2012). "*In vitro* methods to evaluate the efficiency of skin care cosmetic formulations: A Review." <u>Asian Pacific Journal of Tropical Biomedicine</u>: 1-9.

Sah, MK; Kumar, A; and Pramanik, K (2010). "The extraction of fibroin protein from *Bombyx mori* silk cocoon: Optimization of process parameters." <u>International Journal of Bioinformatics Research</u> **2**(2): 33-41.

Sah, MK; Pramanik, K; and Materials, A (2010). "Regenerated Silk Fibroin from *B. mori* Silk Cocoon for Tissue Engineering Applications." <u>International Journal of Environmental Science and Development</u> **1**(5): 404-408.

Satardekar, KV; and Deodhar, MA (2010). "Anti-Ageing Ability of *Terminalia* Species with Special Reference to Hyaluronidase, Elastase Inhibition and Collagen Synthesis *In Vitro*." <u>International Journal of Pharmacognosy and Phytochemical Research</u> **2**(3): 30-34.

Schiffelers, RM; Metselaar, JM; Fens, MHAM; Janssen, APCA; Molema, G; and Storm, G (2005). "Liposome-Encapsulated Prednisolone Phosphate Inhibits Growth of Established Tumors in Mice." <u>Neoplasia</u> **7**(2): 118-127.

Sharma, K; Singh, V; and Arora, A (2011). "Natural biodegradable polymers as matrices in transdermal drug delivery." <u>International Journal of Drug Developments & Research</u> **3**(2): 85-103.

Shazly, G; Nawroth, T; and Langguth, P (2008). "Comparison of Dialysis and Dispersion Methods for *in vitro* release Determination of Drugs from Multilamellar Liposomes." <u>Dissolution Technologies</u> **15**(2): 7-10.

Shu, XZ; and Zhu, KJ (2000). "A novel approach to prepare tripolyphosphate: chitosan complex beads for controlled release drug delivery." <u>International Journal of Pharmaceutics</u> **201**: 51-58.

Siedle, B; Hrenn, A; and Merfort, I (2007). "Natural Compounds as Inhibitors of Human Neutrophil Elastase." <u>Planta Medica</u> **73**(5): 401-420.

Siegfried, B (2007). <u>NanoTextiles: Functions, nanoparticles and commercial applications</u>. Graduation Thesis, Empa Materials Science & Technology.

Siepmanm, J; and Peppas, NA (2001). "Modeling of drug release from delivery systems based on hydroxypropyl methylcellulose (HPMC)." <u>Advanced Drug Delivery Reviews</u> **48**: 139-157.

Silva, R; Ferreira, H; Azoia, NG; Shimanovich, U; Freddi, G; Gedanken, A; and Cavaco-Paulo, A (2012). "Insights on the Mechanism of Formation of Protein Microspheres in Biphasic System." <u>Molecular pharmaceutics</u> **9**(11): 3079-3088.

Silva, R; Ferreira, H; Carvalho, AC; Gomes, AC; and Cavaco-Paulo, A (2012). "Protein microspheres as suitable devices for piroxicam release." <u>Colloids and Surface B: Biointerfaces</u> **92**: 277-285.

Silva, R; Ferreira, H; Vasconcelos, A; Gomes, AC; and Cavaco-Paulo, A (2012). "Sonochemical proteinaceous microspheres for wound healing." <u>Advances in Experimental Medicine and Biology</u> **733**(155-164).

Solanki, SS; Sarkar, B; and Dhanwani, RK (2012). "Microemulsion Drug Delivery System: For Bioavailability Enhancement of Ampelopsin." <u>International Scholarly Research Network</u> **2012**: 1-4.

Soppimath, KS; Aminabhavi, TM; AR, Kulkarni.; and Rudzinski, WE (2001). "Biodegradable polymeric nanoparticles as drug delivery devices." <u>Journal of Controlled Release</u> **70**(1-2): 1-20.

Stevanovic, M; and Uskokovic, D (2009). "Poly(lactide-co-glycolide)-based Micro and Nanoparticles for the Controlled Drug Delivery of Vitamins " <u>Current Nanoscience</u> **5**(1): 1-15.

Su, J (2008). <u>Formation and Stability of Foog-Grade Water-in-Oil-in-Water Emulsions</u>. Doctor of Philosophy Thesis, Massey University.

Sugihara, A; Sugiura, K; Morita, H; Ninagawa, T; Tubouchi, K; and Tobe, R (2000). "Promotive effects of a silk film on epidermal recovery from full-thickness skin wounds." <u>Proceedings of the Society for Experimental Biology and Medicine</u> **225**(1): 58-64.

Sundar, S; Kundu, J; and Kundu, S (2010). "Biopolymeric nanoparticles." <u>Science and Technology of Advanced Materials</u> **11**(1): 1-13.

Tadros, TF (2011). Colloid Aspects of Cosmetic Formulations with Particular Reference to Polymeric Surfactants. <u>Colloids in Cosmetics and Personal Care</u>. Tadros, TF. Weinheim, Germany, Wiley-VCH Verlag GmbH & Co. **4**.

Takada, A; and Sudoh, M (2003). Solution of N-[O-(P-Pivaloyloxybenzenesulfonylamino)benzoyl]Glycine monosodium salt tetrahydrate and drug product thereof. Japan, Ono Pharmaceutical Co., Ltd. **US006552082B2**.

Takeuchi, H; Gomi, T; Shishido, M; Watanabe, H; and Suenobu, N (2010). "Neutrophil elastase contributes to extracellular matrix damage induced by chronic low-dose UV irradiation in a hairless mouse photoaging model." <u>Journal of Dermatological Science</u> **60**: 151-158.

Taniguch, N (1983). "Current Status in, and Future Trends of, Ultraprecision Machining and Ultrafine Materials Processing." <u>Annals of the CIRP</u> **32**(2): 573-582.

Teichmann, A; Heuschkel, S; Jacobi, U; Presse, G; Neubert, RHH; Sterry, W; and Lademann, J (2007). "Comparison of stratum corneum penetration and localization of a lipophilic model drug applied in an o/w microemulsion and an amphiphilic cream." <u>European Journal of Pharmaceutics and Biopharmaceutics</u> **67**: 699-706.

Toll, R; Jacobi, U; Richter, H; Lademann, J; Schaefer, H; and Blume-Peytavi, U (2004). "Penetration Profile of Microspheres in Follicular Targeting of Terminal Hair Follicles." <u>The Journal of Investigative Dermatology</u> **123**: 168-176.

Tsioris, K; Raja, WK; Pritchard, EM; Panilaitis, B; Kaplan, D; and Omenetto, FG (2012). "Fabrication of Silk Microneedles for Controlled-Release Drug Delivery." <u>Advanced Functional Materials</u> **22**: 310-335.

Tsuji, N; Moriwaki, S; Suzuki, Y; Takema, Y; and Imokawa, G (2001). "The Role of Elastases Secreted by Fibroblasts in Wrinkle Formation: Implication Through Selective Inhibition of Elastase Activity." <u>Photochemistry and Photobiology</u> **74**(2): 283-290.

Tsukada, M; Gotoh, Y; Nagura, M; Minoura, N; Kasai, N; and Giuliano, F (1994). "Structural Changes of Silk Fibroin Membranes Induced by Immersion in Methanol Aqueous Solutions." <u>Journal of Polymer Science, Part B: Polymer Physics</u> **32**(5): 961-968.

Tudora, M; Zaharia, C; Stancu, I; Vasile, E; Trusca, R; and Cincu, C (2013). "Natural Silk Fibroin Micro- and Nanoparticles with potential uses in Drug Delivery Systems." <u>UPB Scientific Bulletin, Series B: Chemistry and Materials Science</u> **75**(1): 43-52.

Uddin, K; and Hossain, S (2010). "A comparative study on silk dyeing with acid dye and reactive dye." <u>International Journal Engineering & Technology</u> **10**(6): 21-26.

Valluzzi, R; Gido, S P; Muller, W; and Kaplan, D L (1999). "Orientation of silk III at the air-water interface." <u>International Journal of Biological Macromolecules</u> **2-3**: 237-242.

Vasconcelos, A; Freddi, G; and Cavaco-Paulo, A (2008). "Biodegradable materials based on silk fibroin and keratin." <u>Biomacromolecules</u> **9**(4): 1299-1305.

Vasconcelos, A; Gomes, AC; and Cavaco-Paulo, A (2012). "Novel silk fibroin/elastin wound dressings." Acta Biomaterialia **8**: 3049-3060.

Vepari, C; and Kaplan, D (2007). "Silk as a biomaterial." Progress in Polymer Science **32**(8-9): 991-1007.

Vollrath, F; and Knight, DP (2001). "Liquid crystalline spinning of spider silk." Nature **410**: 541-548.

Wagner, JG; and Roth, RA (1999). "Neutrophil migration during endotoxemia." Journal of Leukocyte Biology **66**: 10-24.

Wang, HY; Han, J; Feng, XG; and Pang, YL (2006). "Study of inclusion complex formation between tropaeolin OO and β-cyclodextrin by spectrophotometry and Infrared spectroscopy." Spectrochimica Acta Part A **65**(100-105).

Wang, X; Wenk, E; Matsumoto, A; Meinel, L; Li, C; and Kaplan, D (2007). "Silk microspheres for encapsulation and controlled release." Journal of Controlled Release **117**: 360-370.

Weedon, D (2002). The demis and subcutis. Weedon's Skin Phatology. Strutton, Geoffrey. London, Churchill Livingstone Elsevier**:** 275-316.

Weitz, JI; Landman, SL; Crowley, KA; Birken, S; and Morgan, FJ (1986). "Development of an Assay for *In Vivo* Human Neutrophil Elastase Activity." The American Society for Clinical Investigation, Inc. **78**: 155-162.

Wen, CM; Ye, ST; Zhou, LX; and Yu, Y (1990). "Silk-induced asthma in children: a report of 64 cases." Annals of Allergy **65**: 375-378.

Wharram, SE; Zhang, X; Kaplan, DL; and McCarthy, SP (2010). "Electrospun Silk Material Systems for Wound Healing." Macromolecular Bioscience **10**(3): 246-257.

Wilson, D; Valluzi, R; and Kaplan, D (2000). "Conformational Transitions in Model Silk Peptides." Biophysical Jounal **78**(5): 2690-2701.

Winiarski, L; Oleksyszyn, J; and Siénczyk, M (2012). "Human Neutrophil Elastase Phosphonic Inhibitors with Improved Potency of Action." Journal of Medicinal Chemistry **55**: 6541-6553.

Woodman, RC; Reinhardt, PH; S, Kanwar; Johnston, FL; and Kubes, P (1993). "Effects oh human neutrophil elastase (HNE) on neutrophil function *in vitro* in inflamed microvessels." Blood **82**: 2188-2195.

Wray, LS; Hu, X; Gallego, J; Georgakoudi, I; Omenetto, FG; Schmidt, D; and Kaplan, D (2011). "Effect of processing on silk-based biomaterials: reproducibility and biocompatibility." Journal of biomedical materials research (Part B, Applied biomaterials) **99**(1): 89-101.

Wu, BM; Borland, SW; Giordano, RA; Cima, LG; Sachs, EM; and Cima, MJ (1996). "Solid free-form fabrication of drug delivery devices." Journal of Controlled Release **40**: 77-87.

Wu, X; Hou, J; Li, M; Wang, J; Kaplan, D; and Lu, S (2012). "Sodium dodecyl sulfate-induced rapid gelation of silk fibroin." Acta Biomaterialia **8**(2185-2192).

Yampolskaya, GP; Tarasevich, BN; and Elenskii, AA (2005). "Secondary Structure of Globular Proteins in Adsorption Layers at the Solution-Air Interface by the Data of Fourier Transform IR Spectroscopy." Colloid Journal **67**(3): 385-391.

Yang, M; Shuai, Y; He, W; Min, S; and Zhu, L (2012). "Preparation of Porous Scaffolds from Silk Fibroin Extracted from the Silk Gland of *Bombyx mori* (*B. mori*) " International Journal of Molecular Sciences **13**: 7762-7775.

Yeo, Y; and Park, K (2004). "Control of Encapsulation Efficiency and Initial Burst in Polymeric Microparticle Systems." Archives of Pharmacal Research **27**(1): 1-12.

Zhang, Q; Yan, S; and Li, M (2009). "Silk Fibroin Based Porous Materials." Materials **2**: 2276-2295.

Zhang, X; Tsukada, M; Morikawa, H; Aojima, K; Zhang, G; and Miura, M (2011). "Production of silk sericin/silk fibroin blend nanofibers." Nanoscale Research Letters **5**(510): 1-8.

Zhao, Z; Li, Y; Chen, A; Zheng, Z; Hu, J; Li, J; and Li, G (2013). "Generation of Silk Fibroin Nanoparticles via Solution-Enhanced Dispersion by Supercritical CO_2." Industrial & Engineering Chemistry Research **52**: 3752-3761.

Zhou, CZ; Confalonieri, F; Jacquet, M; Perasso, R; Li, ZG; and Janin, J (2001). "Silk fibroin: structural implications of a remarkable amino acid sequence." Proteins **44**(2): 119-122.

Zhou, CZ; Confalonieri, F; Medina, N; Zivanovic, Y; Esnault, C; Yang, T; Jacquet, M; Janin, J; Duguet, M; Perasso, R; and Li, ZG (2000). "Fine organization of *Bombyx mori* fibroin heavy chain gene." Nucleic acids research **28**(12): 2418-2419.